THE STRUCTURE AND EXCITATIONS OF AMORPHOUS SOLIDS AND SURFACES

by

ROBERT B. LAUGHLIN

A.B., University of California at Berkeley
(1972)

Submitted in Partial Fullfillment of the

Requirements for the Degree of

DOCTOR OF PHILOSOPHY

at the

MASSACHUSETTS INSTITUTE OF TECHNOLOGY

June 1979

Signature of Author..
Department of Physics, May 20, 1979

Certified by..
Thesis Supervisor

Accepted by..
Chairman, Departmental Committee on Graduate Studies

THE STRUCTURE AND EXCITATIONS OF AMORPHOUS

SOLIDS AND SURFACES

by

Robert B. Laughlin

Submitted to the Department of Physics on May 20, 1979 in partial fulfillment of the requirements for the degree of Doctor of Philosophy.

ABSTRACT

Atomic vibrations and electronic states of amorphous solids and surfaces are investigated using silicon dioxide as a prototype. A new theory of the lattice vibrations in amorphous SiO_2 is presented in which the randomness in the solid is treated separately from its chemistry. The theory attributes all measurable properties of phonons in silica to the nearly crystalline nearest-neighbor geometry of the lattice and the disruptive effects of bond-angle disorder. Neutron, infrared and Raman spectra are calculated and compared with experiment. A new theoretical approach to studying surface vibrations in amorphous solids is then developed. The method entails modeling the surface as a Bethe lattice with a dangling bond, and treating the two-dimensional nature of the surface and the surface topography as small perturbations. The theory successfully describes the nature and origin of the surface states, as well as their relative intensities as observed in recent infrared reflectivity and Raman scattering experiments. Both intrinsic surface effects and those caused by the presence of adsorbates are discussed. The electronic structures of crystalline and amorphous SiO_2 are then examined via the tight-binding method. A realistic description of the electronic structure of α-quartz, consistent with experiment and with the pseudopotential band structure and charge densities, is developed. An important aspect of this description is the identification of oxygen 2s states as the prime cause of the large gap in SiO_2. The cluster-Bethe-lattice method is used to examine the energy distribution and character of the electronic states for non-periodic systems. It is found that most of the features in the density of states of SiO_2 are insensitive to topology, and are thus universal among all allotropes in which the integrity of the SiO_4 tetrahedra is preserved. This universality is shown to lead to a dipole selection rule forbidding the lowest energy optical transitions. The effects of topological and bond-angle disorder in the glass are discussed. Bond-angle fluctuations are shown to induce approximately 0.5 eV band tailing at the conduction band edge. A new method for studying interfaces theoretically which allows one to deal directly with disorder at the interface is then discussed. Using tight-binding Hamiltonians which give good descriptions of the valence and conduction states of α-quartz and silicon, Bethe lattices are constructed for each material and then bonded together in a variety of configurations. The method enables one to avoid the problem of lattice mismatch and to deal individually with the effects of different bonding configurations. The principal result of the theory is that there are no interface states in the silicon gap for an interface which is perfectly bonded and undistorted. Bond-angle distortions induce a tail of gap states near the bottom of the SiO_2 conduction band, an effect which occurs in bulk SiO_2 as well. Broken-bond defects, on the other hand, lead to distinct interface states in the gap. We specifically identify a state observed experimentally as being due to a silicon dangling-bond defect at the interface.

Thesis Supervisor: John D. Joannopoulos

Title: Associate Professor of Physics

ACKNOWLEDGEMENTS

I would like to thank IBM for providing my financial support during two of the years I was at MIT. I would also like to thank the Xerox Corporation for the use of their computing facilities in the electron work, and the U.S. Navy for supporting the SiO_2 work as a whole.

Special thanks are in order for my collaborators on this project: Cherry Murray, Professor Thomas Greytak and Kevin Hartnett, who performed the Vycor experiements and whose cooperation was essential to the development of the surface phonon work; Jim Chadi, who provided the first one-electron Hamiltonian for SiO_2 and whose unbridaled enthusiasm stimulated us all.

I would also like to acknowledge the members of my group, who provided the ambience necessary for good theory to be produced: Gene Mele, Bill Pollard and David Vanderbilt. I would also like to thank Professor Marc Kastner and his group for poignant criticism and helpful suggestions.

The greatest thanks of all, however, goes to my thesis advisor, Professor John Joannopoulos. Professor Joannopoulos literally took me off the street as a first-year graduate student. Four years later, he has provided me with legitimacy as a scientist. He has been the kind of teacher one dreams of finding: sharp, demanding, competent and fair. And like one's parents, a teacher of his quality gives something of himself which can never be repaid, but only passed on.

TABLE OF CONTENTS

Page

LIST OF FIGURES

LIST OF TABLES

INTRODUCTION

Surfaces and amorphous materials are active sub-fields of physics which are similar in a number of respects. Both deal with systems which are nonperiodic but infinite -- systems to which Bloch's theorem cannot be applied except in a contrived manner, yet which are still, for the most part, weakly correlated fermi systems described in the one-electron picture. Both deal with systems which can be structurally complex or indeterminate yet have measurable properties which are fairly well defined. Both deal with systems in which localized and extended states can coexist. Both present the same computational difficulties.

Although in principle the two-dimensionality of surfaces sets them apart from the amorphous bulk, in practice the questions usually asked about surfaces (e.g. What are the surface states? What is the effect of chemisorbtion? etc.) are not sensitive to dimensionality. This experimentally verified fact embodies the spirit of the main tenet of this work: that virtually all the measurable properties of these systems can be traced to local atomic structure. The experimental significance of a point of view in which the differences between surfaces, crystals and amorphous materials are subtle is that results from one type of system may be brought to bear on another. The theoretical significance is that the ability to draw analogies between systems is a sign one understands them.

The theoretical approach appropriate to these systems is that of modeling and extrapolating, rather than first-principles calculation. While the latter (self-consistent pseudopotential) has been performed for both types of system in the past, it has proved equivalent in most respects to simpler, less expensive methods, such as emperical tight binding. Furthermore, first-principles calculations are not possible for many of these systems. Aside from the use of model Hamiltonians, the theoretical technique binding this work together is the cluster-Bethe-lattice method. This is a procedure for approximating the structure of amorphous solids and surfaces which relates to the more precise random-network approach as tight-binding relates to pseudopotential.

All the results presented in this work involve silicon dioxide. SiO_2 is the archtypal amorphous material, it is of enormous technological importance, and it is in every way adequate for demonstrating the principles just mentioned. Two main problems are dealt with: (i) the atomic vibrations at SiO_2 surfaces and (ii) the electronic structure of the Si-SiO_2 interface. Chapters I and III provide the groundwork for these by describing phonons and electrons in bulk amorphous SiO_2. Chapters II and IV deal with the surface and the interface, respectively.

CHAPTER I

BULK PHONONS IN AMORPHOUS SILICA

The cluster-Bethe lattice method[1,2] is a powerful new tool for studying the electronic and vibrational properties of amorphous solids. Its basic precept is that embedding a cluster of atoms in a solid is nearly equivalent to applying to the cluster a simple dynamic boundary condition characterizing the chemical composition of the host. It has significantly improved our understanding of amorphous solids by simplifying the mathematics used to study them theoretically.

Amorphous silicon dioxide has attracted considerable attention recently in its capacity as a medium for surface studies.[3] Silica is transparent, which means that its phonons are accessible by means of light scattering, and it is also available in a very porous state -- porous enough that the contribution to the scattering intensity from the vibrations of the surfaces of the pores can be detected. Light scattering studies of surface chemistry are practical in silica, and this practicality has stimulated substantial experimental activity.

As yet, no simple theory has arisen to compliment these experiments which can address the dynamic interaction between the surface and the substances adsorbed on it. Such a theory is needed to interpret and clarify the experimental results for heavy, weakly-bonded adsorbates, especially those whose vibrational bands coincide with those of the substrate. We propose to use the cluster-Bethe lattice method to synthesize a suitable theory, capitalizing on the similarity between pores in the solid and structural defects. The cluster-Bethe lattice method was developed for the express purpose of investigating structural defects and is ideally suited to constructing a theory of surface vibrations based on them.

In this chapter, we will be concerned primarily with the preliminary aspects of the synthesis: constructing the Bethe lattice, obtaining its solution and testing its predictions for bulk amorphous silicon dioxide against experiment. Since the behavior of surfaces is so closely tied to the behavior of the bulk, we will also concentrate in this chapter on improving our understanding of the bulk, particularly the relative importance of the various kinds of disorder. In addition to spelling out how the Bethe lattice is constructed, we wish to establish the following:

1. What in the Hamiltonian causes the features in the vibrational density of states to be where they are?
2. How are the atoms moving?
3. What causes the matrix elements associated with a given measurement to assume the values they do?

The plan of presentation is as follows. We will first describe the Bethe lattice and explain how it functions as a boundary condition for clusters. We will then show that if it is constructed using sensible interaction parameters, the Bethe lattice possesses a vibrational density of states similar enough to that of the actual solid to imply that local geometry is primarily responsible for the character of the vibrations. We will provide evidence that most of the disparity between the two densities of states is due to bond-angle disorder. To establish how the atoms are moving, we will calculate local densities of states, and use them to establish how the displacements of nearby atoms correlate at low temperatures. We will then use the correlation functions to calculate neutron, infrared and raman spectra directly, rather than multiplying the density of states by the square of the appropriate matrix element, in order to explain from a local point of view why the spectra look as they do. We conclude with a summary.

1.1. The Bethe Lattice

Silicon dioxide is a bonded solid. It is approximately true in bonded solids that the bonds provide the springs which connect the atoms together, in the sense that two atoms are connected if the displacement of one produces a force on the other. The rules by which atoms are connected in a lattice is referred to as the lattice topology.

A Bethe lattice is a bonded network of atoms which has the topology of a tree. Every atom interacts with its nearest neighbors by virtue of being bonded to them, just as would occur in the actual solid, but the ordinary necessity of having rings of bonds in the structure and fluctuations in the interaction parameters due to disorder is arbitrarily abolished. The Bethe lattice itself is a poor model for the structure of the actual amorphous solid, except in cases where lattice topology is unimportant. Its virtue lies in its exceptional simplicity and in the "transfer matrix" feature of its solution, this transfer matrix being identical to the simple boundary condition mentioned previously. The tree-like topology characterizes the Bethe lattice and is responsible for its simplicity and usefulness.

The transfer matrix feature of the Bethe lattice is best illustrated with an example. We consider a tetrahedrally bonded crystal, such as Germanium, which we will transform into a Bethe lattice axiomatically. We postulate that each bond may be characterized by a 3 x 3 matrix of spring constants D_ν which connects the atoms at either end of the bond. The index ν runs from 1 to 4 and indicates into which of the four possible directions the bond points. D_ν is to be a symmetric matrix.

We now label the atoms. We pick any atom and label it 0. We label its 1st nearest neighbors by 1 and ν_1, where ν_1 runs from 1 to 4 and indicates the direction from the central atom to the one addressed. We label the 2nd nearest neighbors by 2, ν_1 and ν_2, where ν_1 and ν_2 now indicate the <u>sequence</u> of directions used in going from the central atom to the one in question. The 3rd nearest neighbors are labeled by 3, ν_1, ν_2 and ν_3, and so on. In the actual solid, this labeling scheme eventually becomes redundant, as it specifies a particular path of bonds leading to the labeled atom, which cannot be unique. However, we can conveniently convert the solid into a Bethe lattice simply by <u>declaring every atom indexed in this manner distinct</u>. If this is done, the vibrational Green's function of the new tree-like lattice satisfies a simple, repeating set of equations.

If we let G_{00} denote the part of the Green's function connecting atom 0 to itself, $G_{01}{}^{\nu_1}$ the part connecting to a 1^{st} nearest neighbor, and so on, then we have

$$(\omega^2 - A)G_{00} = \sum_{\nu_1} D_{\nu_1} G_{01}{}^{\nu_1} + 1 \tag{1}$$

$$(\omega^2 - A)G_{01}{}^{\nu_1} = D_{\nu_1} G_{00} + \sum_{\nu_2 \neq \nu_1} D_{\nu_2} G_{02}{}^{\nu_1,\nu_2} \tag{2}$$

$$(\omega^2 - A)G_{02}{}^{\nu_1,\nu_2} = D_{\nu_2} G_{01}{}^{\nu_1} + \sum_{\nu_3 \neq \nu_2} D_{\nu_3} G_{03}{}^{\nu_1,\nu_2,\nu_3} \tag{3}$$

$$\vdots \qquad\qquad\qquad\qquad \vdots$$

where A is the matrix of spring constants connecting an atom with itself, given from translational invariance of the Hamiltonian by

$$A = -\sum_{\nu} D_{\nu} \tag{4}$$

We have set the masses of the atoms to 1. These equations have a solution of the form

$$G_{01}{}^{\nu_1} = \Phi_{\nu_1} G_{00} \tag{5}$$

$$G_{02}{}^{\nu_1,\nu_2} = \Phi_{\nu_2} G_{01}{}^{\nu_1} \tag{6}$$

$$\vdots$$

provided that the four <u>transfer matrices</u> Φ_{ν} satisfy

$$(\omega^2 - A)\Phi_\nu = D_\nu + \sum_{\mu \neq \nu} D_\mu \Phi_\mu \Phi_\nu \tag{7}$$

Finding the transfer matrices is a difficult task, but once they are found, the Green's function is relatively easy to construct. For example, from equation (1) we obtain the diagonal term

$$G_{00} = [\omega^2 - A - \sum_\mu D_\mu \Phi_\mu]^{-1} \tag{8}$$

from which the remainder of the Green's function may be constructed by repeatedly applying the transfer matrices.

Possessing the vibrational Green's function of any large mechanical system greatly simplifies determining the vibrational behavior of molecules when they are bonded to the system. The Green's function connecting the i^{th} atom to the j^{th} may be thought of as the response of the i^{th} atom to an harmonic force applied to the j^{th}. Suppose an extra atom is bonded to the j^{th} atom with a spring having a force constant k. If we denote the displacement of this atom by x_0 and that of the j^{th} atom by x_j, then we have

$$M \ddot{x}_0 = F_0 = -k\, x_0 + k\, x_j \tag{9}$$

and if the motion is harmonic, then

$$(\omega_0^2 - \omega^2)\, x_0 = \omega_0^2\, x_j \tag{10}$$

However, since G_{jj} describes the response of the j^{th} atom to forces, we have

$$x_j = G_{jj} F_j/M = G_{jj}\omega_0^2[x_0 - x_j] \qquad (11)$$

so that ω must satisfy the equation

$$\left[\omega_0^2 - \frac{\omega_0^2}{1 + \omega_0^2 G_{jj}}\right] x_0 = 0 \qquad (12)$$

If we want to calculate the Green's function of the new system, the analysis proceeds along the same lines and leads to

$$G_{00} = \left[\omega^2 - \frac{\omega_0^2}{1 + \omega_0^2 G_{jj}}\right]^{-1} \qquad (13)$$

The "molecule" in this example has vibrations which are shifted and broadened with respect to the natural vibration at $\omega = 0$ because the lattice "loads" the harmonic oscillator as though it were a transmission line. The diagonal Green's function matrix element G_{jj} corresponds to the impedance of the line.

The loading of a molecule by the solid becomes more complicated when the molecule bonds to the solid in more than one place. If the molecule is connected to both atoms j and j', then the off-diagonal Green's function matrix elements $G_{jj'}$ must be taken into account, and this necessitates inverting a matrix of rank two in this case, and of rank equal to the number of connections between the molecule and its host generally. The spirit of the cluster-Bethe lattice method is that these off-diagonal matrix elements are relatively unimportant, so that each connection can be loaded independently of the others, and that the Bethe lattice Green's function, which is much simpler to calculate than that of the actual solid, models the impedance of the solid adequately. The validity of these approximations has been borne out in numerous theoretical investigations of electronic and vibrational states in amorphous solids.[1]

The silicon dioxide Bethe lattice we have constructed differs from the elementary one just described only in that it is made up of two different kinds of atoms. Its topology is illustrated in figure 1. Its solution is conceptually the same as that of the monatomic Bethe lattice, but is sufficiently complicated that we have elected to address its details in Appendix A.

We have used a Born model[4] Hamiltonian in our calculation because it was used previously with great success by Bell and Dean[5] in their random-network calculation for silicon dioxide. The Born Hamiltonian assigns to each bond a potential energy of the form

$$U = \frac{\alpha}{2}\,|\vec{x} - \vec{y}|^2 + \frac{(\beta - \alpha)}{2}\,|(\vec{x} - \vec{y})\cdot\hat{r}|^2 \qquad (14)$$

where $\vec{x}$ and $\vec{y}$ are the displacements of the atoms at either end of the bond, and $\hat{r}$ is a unit vector pointing along the bond. α and β are respectively 4×10^5 dynes/cm and $.7 \times 10^5$ dynes/cm. We have also employed bond angles and bond lengths approximately the same as those

Figure 1: Topology of the Bethe lattice. Every pair of atoms is connected by one and one path of bonds.

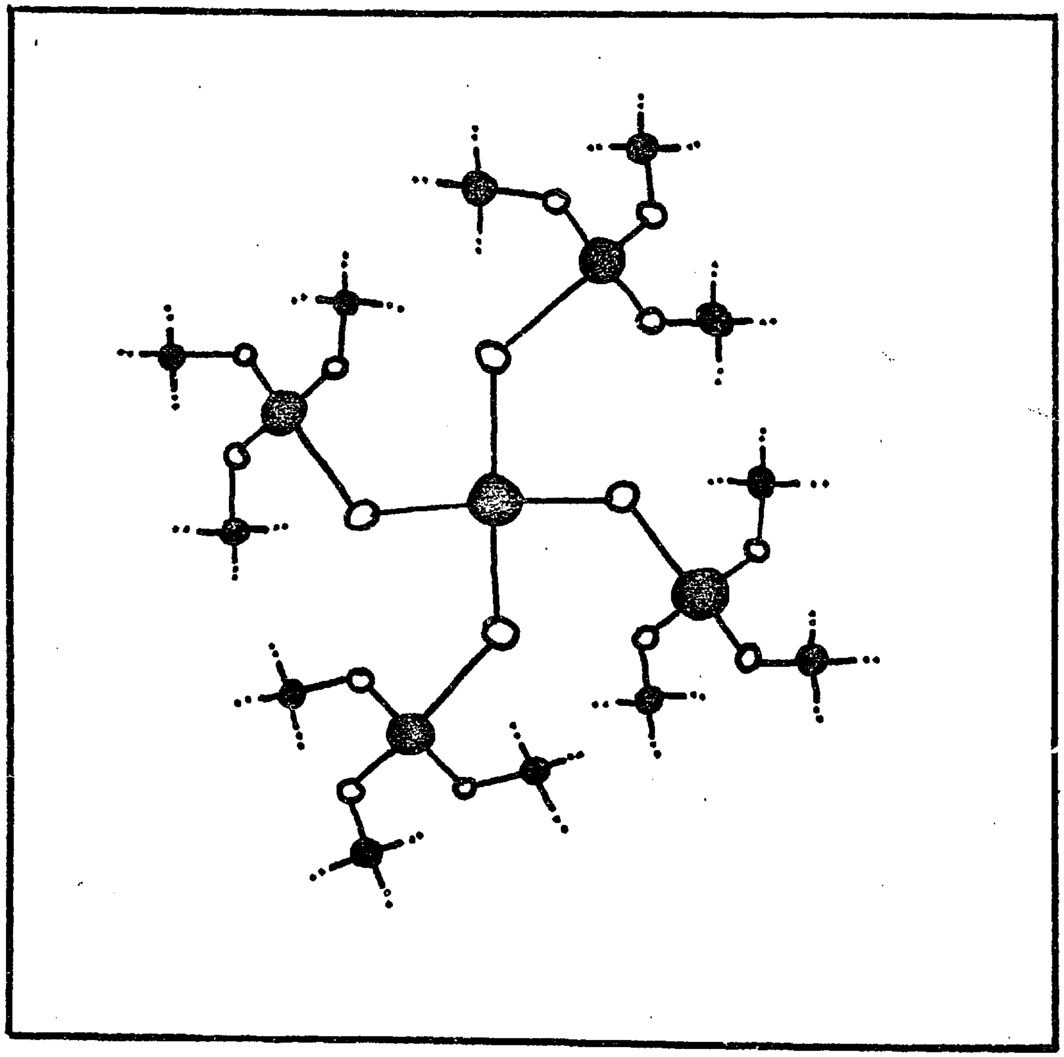

found in quartz. The practice of incorporating crystal parameters into Bethe lattices is well established,[1] the philosophy being that the amorphous solid is very similar to the crystal over short distances.

1.2. Properties of the SiO_2 Bethe Lattice: Densities of States

We generate the density of states of the Bethe lattice from the transfer matrices using the relation[1]

$$\rho(\omega) = - \sum_{j} \frac{2\omega}{\pi} \mathrm{Im}[G_{jj}(\omega)] \tag{15}$$

where G_{jj} is the diagonal Green's function matrix element associated with the j^{th} degree of freedom. Each term in the sum is referred to as a "local density of states" because it represents the actual density of states weighted according to how much the particular degree of freedom participates in the state. We rely heavily upon local state calculations because they give us an excellent feel for the nature of the atomic motions while being relatively easy to perform.

In our silicon dioxide Bethe lattice, atoms of a given species are all equivalent, so that there exist only six independent elementary degrees of freedom. Of these, the three associated with the oxygen atoms are particularly important because they are customarily used to identify the major features in the infrared absorbtion spectrum. In their early work on silicon dioxide, Bell and Dean[5] suggested that the three primary features in the density of states could be characterized as bond-rocking, bond-bending or bond-stretching, according to whether the oxygen atoms were moving primarily so as not to compress bonds, so as to bisect the Si-O-Si angle, and parallel to a line joining the two silicon neighbors respectively. Their classification, though correct, has never been supported quantitatively, and for this reason we are particularly interested in the bond-rocking, bond-bending and bond-stretching local densities of states.

In figure 2, we show the calculated local densities of states, comparing the three characteristic oxygen local densities of states with that of a silicon atom and with the total density of states. The three features at 450 cm^{-1}, 800 cm^{-1} and 1080 cm^{-1} are each enhanced in the appropriate oxygen spectrum, except for the bending peak, which is accompanied by spurious features in the "bending" spectrum. The peak at 800 cm^{-1} was found by Bell and Dean[5] to correspond to a complex vibration involving substantial silicon motion in addition to "bending" oxygen motion, a behavior reflected in the Bethe lattice results. This feature is accompanied by a smaller triangle-shaped band peaking at 550 cm^{-1} which is also predominantly "bending" in character but which does <u>not</u> involve substantial silicon motion. It is important that this latter band is the only one which is exclusively bond-bending in character.

The bond-bending local density of states also manifests large features in the "rocking" bands at 450 cm^{-1}. This is most easily understood from the standpoint that "rocking" and "bending" are distinguished from one another only by the presence of the Si-O-Si "bend", which in silicon dioxide has an angle of about 140°. The "bend" is a perturbation to the 180° Bethe lattice previously solved by Thorpe[6],

Figure 2: Local densities of states in the silicon dioxide Bethe lattice.

(a) Average of local densities of states associated with the three degrees of freedom on a silicon atom.

(b) Average of local densities of states associated with the three degrees of freedom on an oxygen atom.

(c) Average density of states.

(d) "Bond-rocking" local density of states.

(e) "Bond-bending" local density of states.

(f) "Bond-stretching" local density of states.

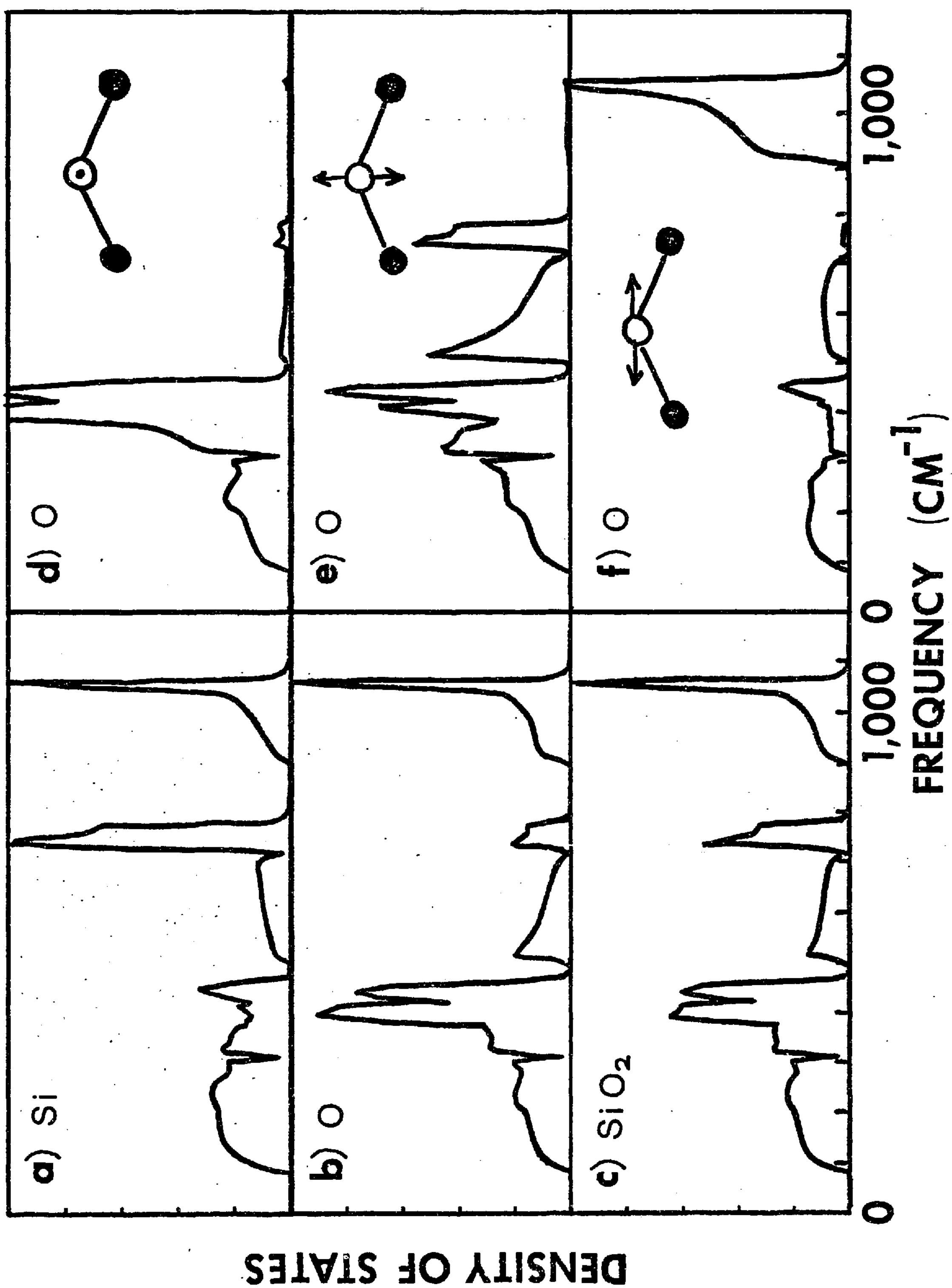

a) Si
b) O
c) Si O2
d) O
e) O
f) O
0
1,000
0
1,000
FREQUENCY (CM-1)
DENSITY OF STATES

in which "rocking" and "bending" are degenerate. The bend causes part of the "rocking" bands to split off and become the 550 cm^{-1} feature, while it mixes the 800 cm^{-1} silicon-silicon motion with "bending" oxygen motion, causing this feature to show up in the "bending" spectrum. At 180° this feature has no oxygen character. The rocking features in the bending spectrum are the states left behind when the 550 cm^{-1} bands split off.

In figure 3, we compare the Bethe lattice density of states with experiment. The neutron data shown in the figure, that of Leadbetter and Stringfellow[7], represents the density of states of amorphous silicon dioxide modulated by a fairly uniform matrix element. In order to obtain good agreement with experiment, we have artificially broadened the Bethe lattice density of states by convolving it with a gaussian of width 75 cm^{-1}. The amount of broadening was determined from disorder considerations. For completeness we have also included in figure 3 the density of states calculated by Bell and Dean[5] for their random network. The agreement of the Bethe lattice density of states with experiment is tolerably good, except for the feature at 1233 cm^{-1} in the experiment. There are three oxygen features with proper widths and intensities, and a low-frequency shoulder coinciding with the acoustic-like bands of the Bethe lattice. Galeener and Lucovsky[8] have pointed out that the 1233 cm^{-1} feature results from a Lyddane-Sachs-Teller splitting of the band at 1080 cm^{-1} which, since it is due to long-range coulomb interactions, we expect to be absent in the theory.

In addition to Bell and Dean's classification scheme, there

Figure 3: Comparison of calculated density of states with neutron measurement.

(a) Neutron data of Leadbetter and Stringfellow, showing density of states of silica modulated by a fairly uniform matrix element.

(b) Solid curve: calculated average density of states of silicon dioxide Bethe lattice broadened by 75 cm^{-1}. Dotted curve: density of states of silicon dioxide weighted as discussed in the text for comparison with neutron data.

(c) Theoretical density of states for silica from random network model of Bell and Dean.

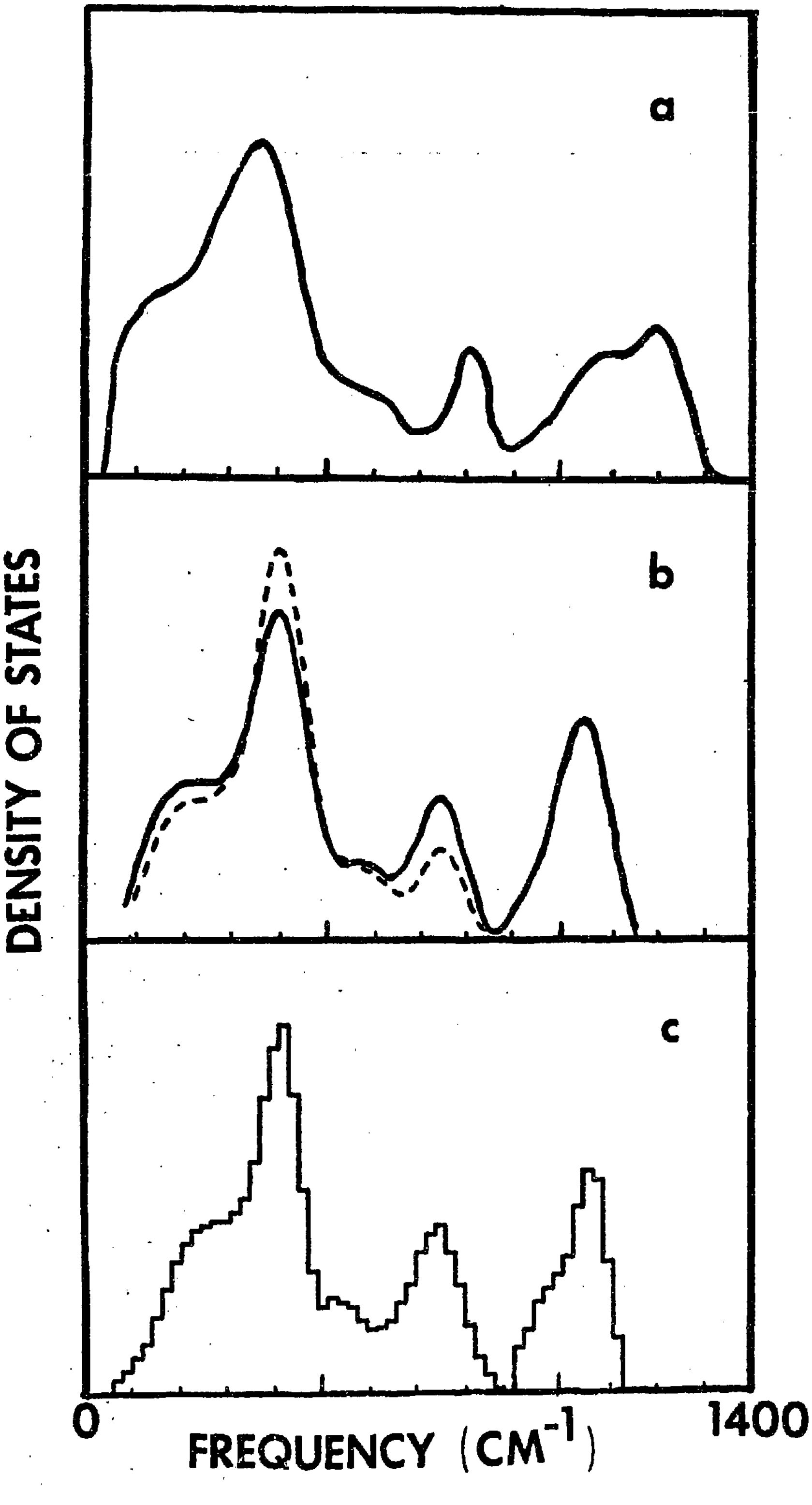
a
b
c
DENSITY OF STATES
0
1400
FREQUENCY (CM^{-1})

exists a scheme recently proposed by Galeener and Lucovsky[8] in which the vibrational bands in amorphous silicon dioxide can be viewed as dispersively broadened vibrational modes of SiO_4 molecules. Since the normal modes of an SiO_4 tetrahedron are as acceptable degrees of freedom for the Bethe lattice as the atomic displacements, we can investigate the SiO_4-nature of the vibrations by calculating the local densities of states associated with the four fundamental vibrations of a SiO_4 molecule.[9] In figure 4 we show the results of such a calculation, in which we use theoretical normal modes deriving from the same Born Hamiltonian used in constructing the Bethe lattice. The SiO_4 local densities of states do not emphasize the major features in the density of states. The high-frequency mode sees no rocking, but leaves the high-frequency part of the density of states intact. The symmetric-stretch mode is similarly insensitive to rocking, but it is insensitive to silicon motion as well, causing the 800 cm^{-1} peak to disappear and the 1080 cm^{-1} peak to undergo distortion. The two low-frequency modes select out the rocking motions, but are distinct from one another only in which half of the peak at 450 cm^{-1} they suppress. It is clear that the vibrations of the Bethe lattice are not well characterized as SiO_4 normal modes.

A "molecular" model more in keeping with Bell and Dean's[5] already successful classification scheme is that of triatomic Si_2O units. Triatomic "bent" molecules such as H_2O have three fundamental vibrations which correspond crudely to rocking, bending and stretching oxygen motions. The local densities of states of the Bethe lattice

Figure 4: Bethe lattice density of states projected onto normal modes of SiO_4 molecule. The modes are identified in ref. 9 in order (a) through (d) as ν_3 ν_1 ν_4 ν_2. Averages were performed over the degenerate modes.

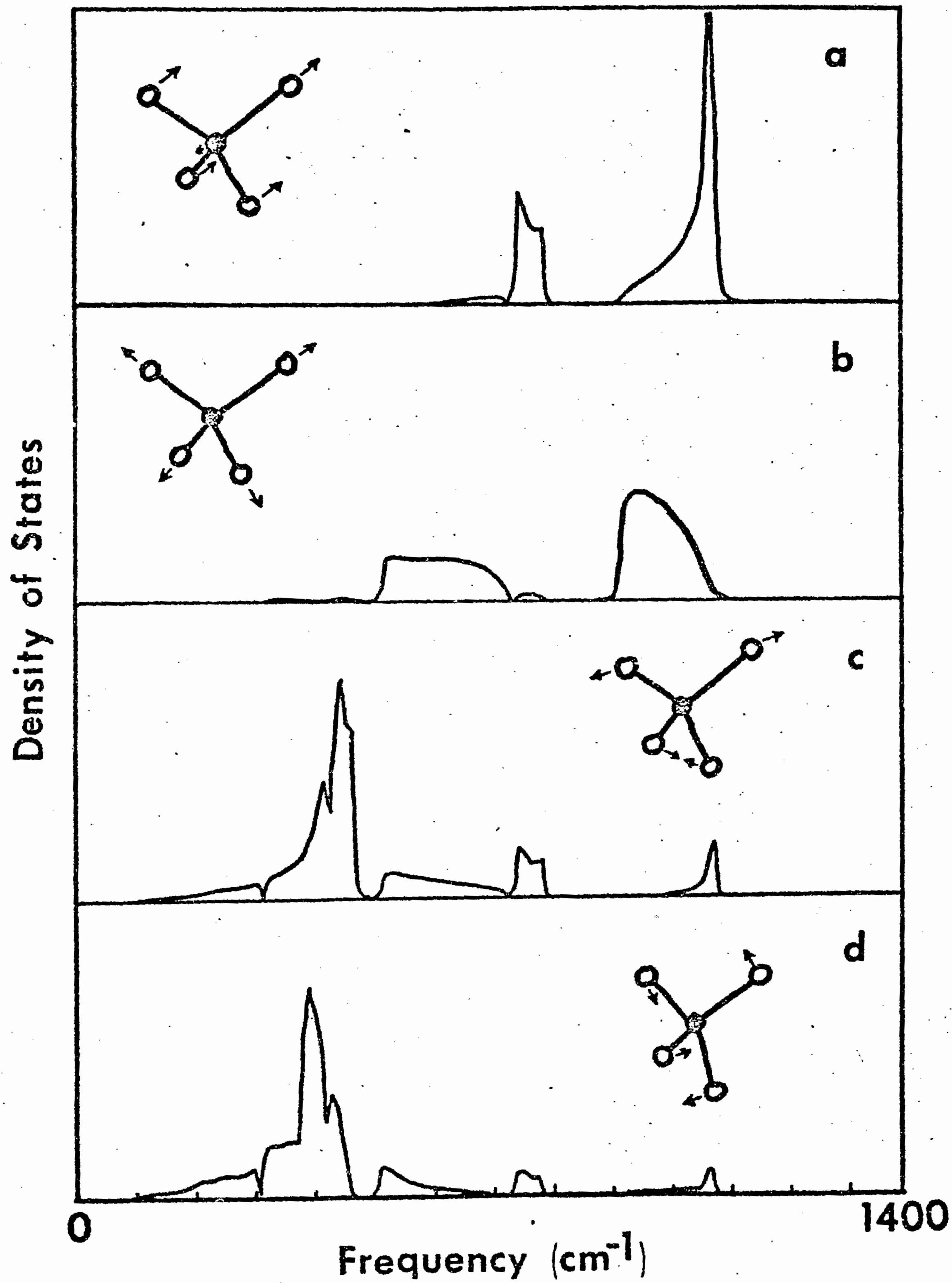
a
b
c
d
Density of States
0
1400
Frequency (cm^{-1})

Figure 5: Bethe lattice density of states projected onto normal modes of Si_2O molecule. The modes are identified in ref. 9 in order (a) through (c) as ν_3, ν_2, ν_1.

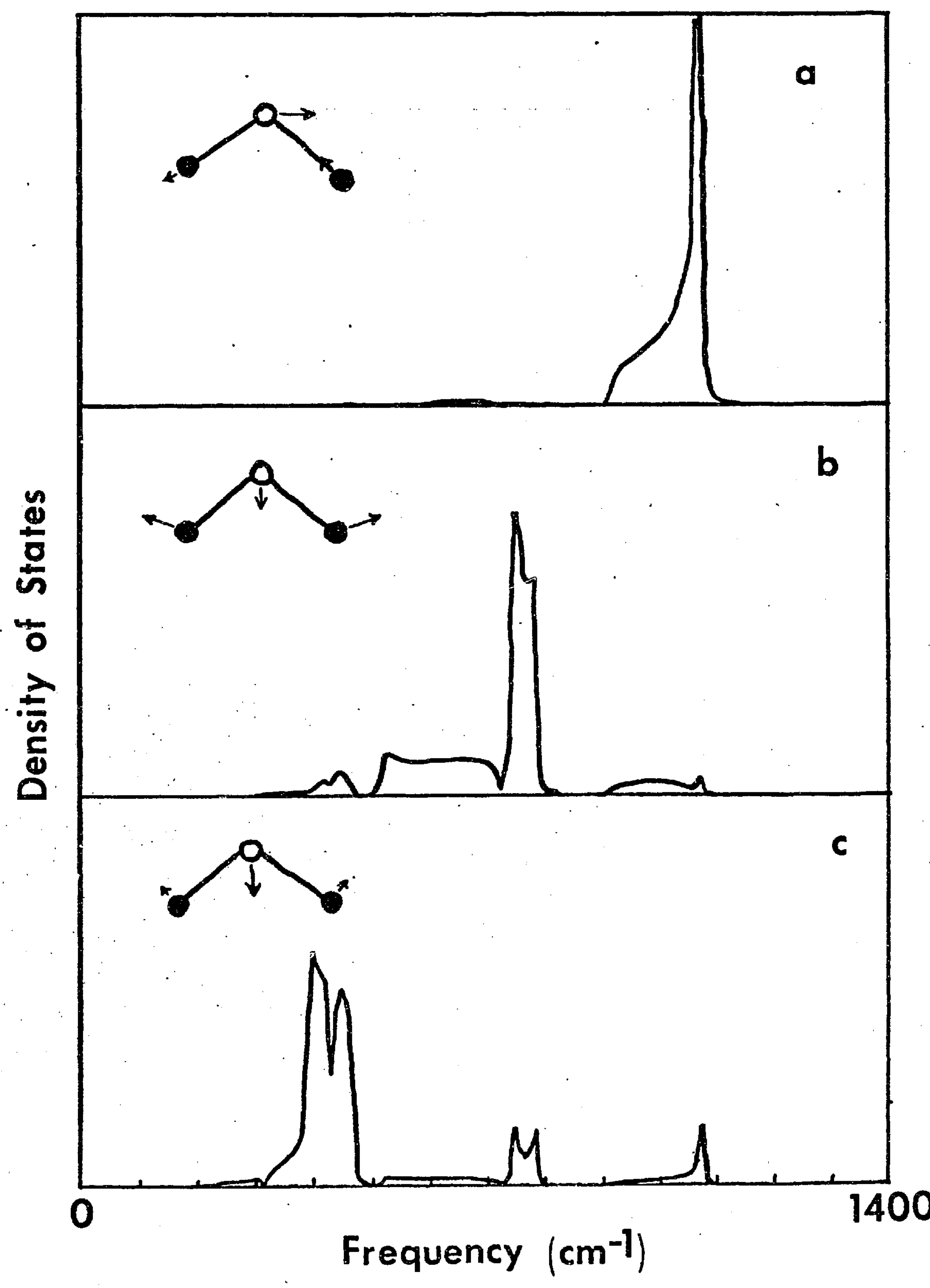
a
b
c
Density of States
0
1400
Frequency (cm-1)

corresponding to these modes of an Si_2O molecule are shown in figure 5. The projections are much more systematic for these molecules than for SiO_4 units. Each local density of states properly emphasizes one of the three major features in the density of states, and the agreement is good enough to indicate that silica may possibly be thought of as an array of weakly-interacting Si_2O molecules.

1.3. Disorder

In a bonded amorphous solid, such as silicon dioxide, we expect to find two kinds of structural disorder: topological and angular. Bond-length variations are forbidden because the distortion energies are too large, whereas bond-angle and connectivity variations are expected and observed experimentally in x-ray data.[10] Si-O-Si bond angle fluctuations of about 10° are typical for amorphous silicon dioxide,[10] and are particularly important because the positions of the features in the spectrum, especially the silicon-silicon and bond-stretching peaks, are very sensitive to this angle. In figure 6 we show the effect on the Bethe lattice density of states of increasing or decreasing every Si-O-Si angle by 10°. The most important change induced in the spectrum by this distortion is lateral dispersion of the silicon-silicon and bond-stretching peaks by about 75 cm^{-1}. This displacement of the states by bond angle fluctuations should cause a smearing of the density of states in the actual amorphous solid, and was our basis for broadening the Bethe lattice density of states by 75 cm^{-1} when comparing it with experiment in figure 3. The sensitivity of the density of states to very

Figure 6: Density of states of silicon dioxide Bethe lattice with every Si-O-Si angle (a) closed or (b) opened by 10° with respect to the nominal value of 138°.

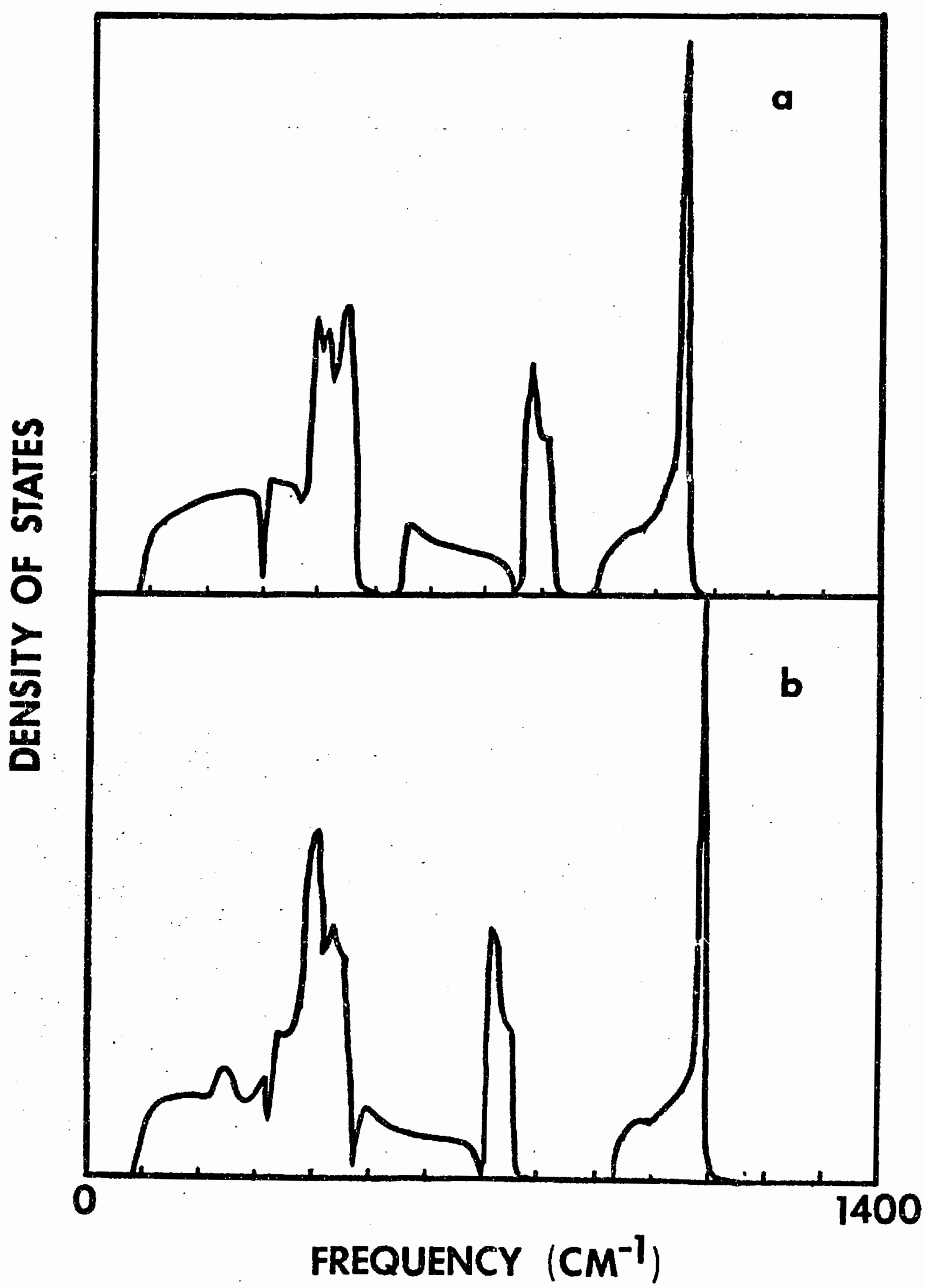
a
b
DENSITY OF STATES
0
1400
FREQUENCY (CM^{-1})

large Si-O-Si bond angle distortions has recently been investigated by Sen and Thorpe[11]. In figure 7 we show the effect on the Bethe lattice density of states of increasing or decreasing the dihedral angles by 10°. Dihedral angles have smaller distortion energies than the Si-O-Si angle and are consequently more likely to fluctuate in the amorphous solid, but the density of states is relatively insensitive to these fluctuations, so that the most important angle disorder still resides in the Si-O-Si angles.

In figure 8 we compare the Bethe lattice density of states with that of quartz calculated using the same Hamiltonian. Quartz has a predominance of 12-fold rings of bonds in its structure which is responsible for the disparity between the two spectra. Since the types of rings of bonds most likely to form in the amorphous solid are those which form in the crystal, we expect topology to introduce features in regions, such as that between 100 cm^{-1} and 400 cm^{-1}, where large disparities occur. However, we expect the features to be smaller than those induced by the crystal topology, as it is known[1] that the effect of topological <u>disorder</u> is generally to make the density of states more closely resemble that of the Bethe lattice.

The most important aspect of the features induced by the crystal topology is that they are sharp and narrow, so that when the spectrum is broadened to account for bond-angle disorder, they disappear completely, causing the spectrum to be indistinguishable from the broadened Bethe lattice density of states. As can be seen from figure 3, however, the broadened Bethe lattice density of states is itself

Figure 7: Density of states of silicon dioxide Bethe lattice with every dihedral angle (a) closed or (b) opened by 10° with respect to the nominal value of 22°.

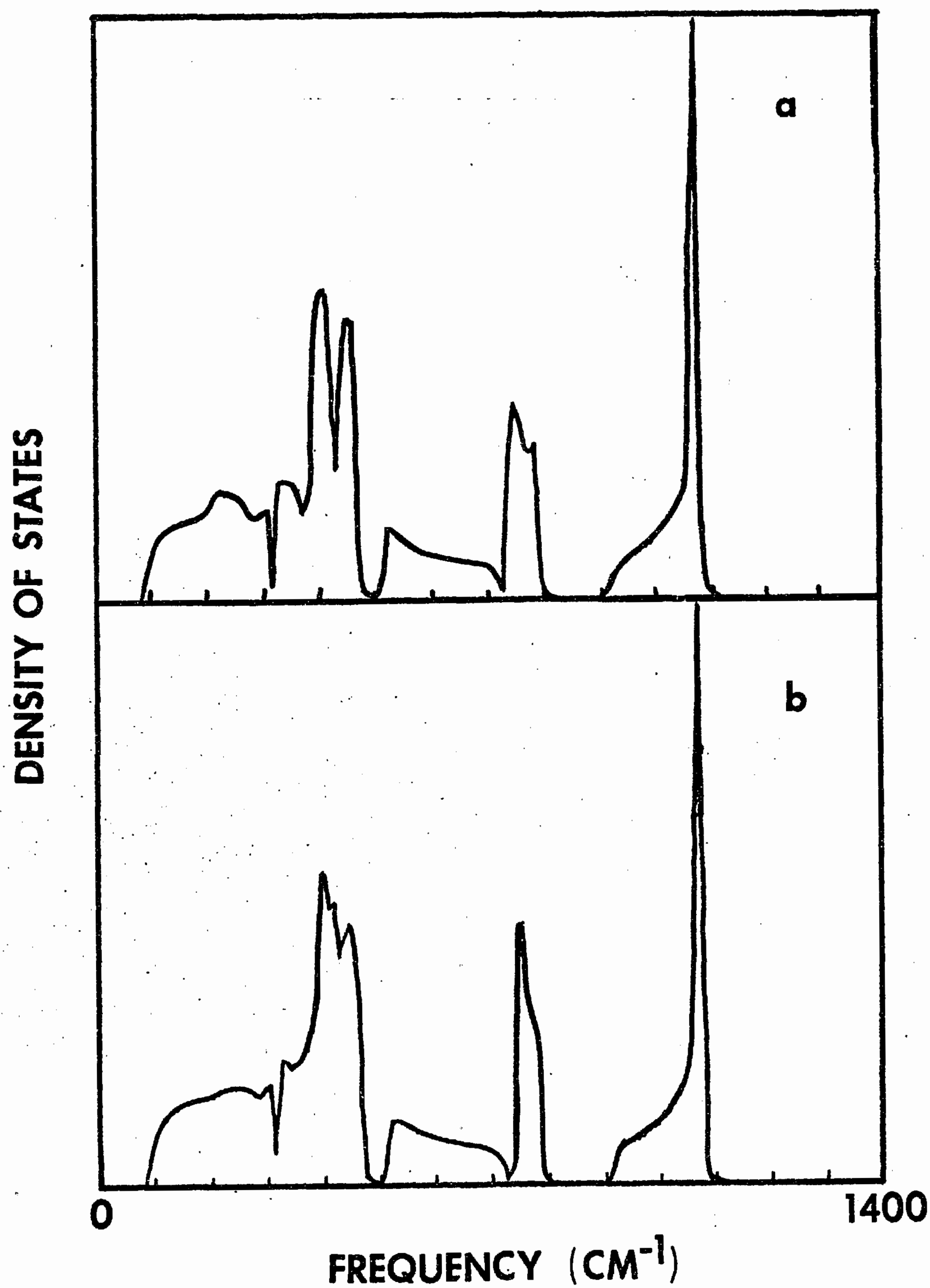
a
b
DENSITY OF STATES
0
1400
FREQUENCY (CM^{-1})

Figure 8: Comparison of Bethe lattice density of states with that of quartz calculated using the same Hamiltonian.

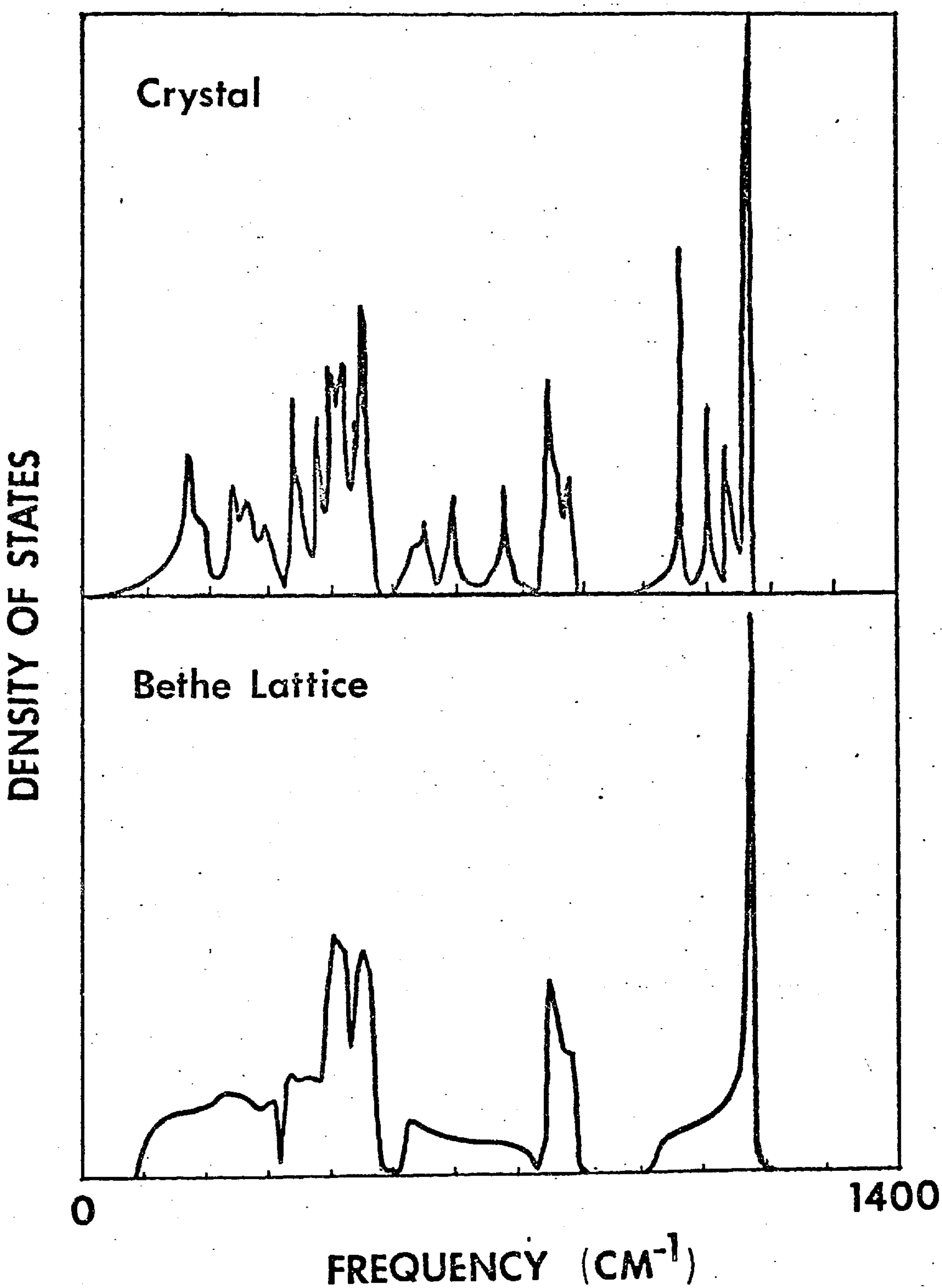
Crystal
Bethe Lattice
DENSITY OF STATES
0
1400
FREQUENCY (CM^{-1})

virtually indistinguishable from that of the random network of Bell and Dean[5], so we have established the important principle that bond angle disorder destroys any explicit manifestations of the network topology in the density of states of amorphous silica. This might alternatively be viewed as a consequence of the absence of small rings of bonds in the solid.

1.4. Infrared and Raman Spectra

The other two phonon-sensitive experiments for which data on amorphous silicon dioxide are readily available are infrared absorbtion and raman scattering. Neither of these is a particularly good measure of the density of states. We will test theory against these experiments by calculating theoretical spectra using the mechanisms for these processes presumed to be valid for quartz.

The usual procedure of obtaining the normal modes of the lattice and evaluting the matrix elements directly is impractical in the Bethe lattice because the normal modes are highly degenerate and difficult to orthogonalize. We surmount this problem by calculating spectra directly from the Green's function, using a simple relation between the Green's function and the displacement-displacement correlation function.

The Green's function is a sum over the normal modes of the form

$$G_{ij}(\omega) = \sum_n \frac{\vec{x}_i^{(n)} \vec{x}_j^{(n)}}{\omega^2 - \omega_n^2} \tag{16}$$

where $\vec{x}_i^{(n)}$ is the displacement of the i^{th} atom when the lattice oscillates in its n^{th} normal mode. ω_n is the frequency of this mode. G_{ij} is again a 3 x 3 matrix which operates on a force at j to produce a displacement at i:

$$\vec{x}_i = G_{ij}\cdot\vec{F}_j = \sum_n \vec{x}_i^{(n)}\left\{\frac{\vec{x}_j^{(n)}\cdot\vec{F}_j}{\omega^2 - \omega_n^2}\right\} \tag{17}$$

Since any displacement can be expanded in terms of the normal modes

$$\vec{x}_i = \sum_n a_n\vec{x}_i^{(n)} \tag{18}$$

we have

$$<\vec{x}_i\vec{x}_j^*> = \sum_{n,m} <a_n a_m^*> \vec{x}_i^{(n)}\vec{x}_j^{(m)} = \sum_n <|a_n|^2> \vec{x}_i^{(n)}\vec{x}_j^{(n)} \tag{19}$$

therefore

$$\frac{1}{2\pi}\int <\vec{x}_i(0)\vec{x}_j^*(t)>e^{i\omega t}\,dt = \sum_n\left\{\frac{1}{2\pi}\int <a_n(0)a_n^*(t)>e^{i\omega t}\right\}dt\ \cdot\vec{x}_i^{(n)}\vec{x}_j^{(n)}$$

$$= \sum_n f(\omega)\delta(\omega - \omega_n)\ \vec{x}_i^{(n)}\vec{x}_j^{(n)} \tag{20}$$

where $f(\omega)$ is a function of frequency which depends on the temperature. However, the imaginary part of the Green's function also takes this form

$$\mathrm{Im}\{G_{ij}(\omega)\} = -\frac{\pi}{2\omega}\sum_n \delta(\omega - \omega_n)\ \vec{x}_i^{(n)}\vec{x}_j^{(n)} \tag{21}$$

so we have

$$\frac{1}{2\pi}\int \langle \vec{x}_i(0)\vec{x}_j^*(t)\rangle\, e^{i\omega t}\, dt = -\frac{2\omega f(\omega)}{\pi}\,\mathrm{Im}\,\{G_{ij}(\omega)\} \tag{22}$$

Referring back to figure 2, we see that the diagonal correlations of the Bethe lattice are already quite different from one another, these differences being associated with the slight enhancement of the 450 cm^{-1} peak in the neutron spectrum of figure 3 over the theoretical value. Inelastic neutron scattering measures the dynamical structure factor $S(\vec{q},\omega)$,[12] which is related to the correlation function by

$$S(\vec{q},\omega) \propto \sum_{i,j}\left\{\frac{1}{2\pi}\int \langle \vec{q}\cdot\vec{x}_i(0)\vec{x}_j(t)\cdot\vec{q}\rangle\, e^{i\omega t}\, dt\right\} e^{iq\cdot(\vec{R}_i - \vec{R}_j)} \tag{23}$$

where $\vec{R}_i$ is the position vector of the i^{th} atom. This may also be written in terms of the Green's function

$$S(\vec{q},\omega) \propto -\,\mathrm{Im}\left\{\sum_{i,j} \vec{q}\cdot G_{ij}\cdot\vec{q}\; e^{iq\cdot(\vec{R}_i - \vec{R}_j)}\right\} \tag{24}$$

The particular experiment we have referenced evaluates $S(\vec{q},\omega)$ at high momentum transfers $\vec{q}$, in the so-called "incoherent limit", where configurational fluctuations in nearest-neighbor distance cause the off-diagonal correlations to contribute nothing to the scattering cross-section. Since the local densities of states derive from the reduced Green's function, they are converted to mean square displacements by dividing by the mass of the atom. This implies that the oxygen local densities of states are weighted more in the neutron spectrum than they are in the total density of states. The difference in the neutron cross-sections for the different nuclei enters in as well, the net result being to overemphasize the oxygen local density of states by about a factor of two. The dotted curve in figure 3 is a theoretical neutron spectrum.

While the off-diagonal correlations do not contribute to the neutron spectrum, they are extremely important in the other two experiments. For example, in figure 9(a) the trace of the nearest-neighbor correlation matrix reveals strong negative correlations between silicon and oxygen displacements at 450 cm^{-1}, 800 cm^{-1} and 1080 cm^{-1}, which causes the infrared activity of these bands. Modes of heteropolar solids are infrared active when dissimilar atoms vibrate out of phase. The strong positive correlation at 200 cm^{-1} is associated with the acoustic-like bands of the Bethe lattice and suppresses their infrared activity. In figure 10(c) we see very strong "bending-bending" correlation at 500 cm^{-1} associated with a very intense raman band. The proposed mechanism for raman scattering[13] in quartz is the dialation of the electronic polarizability by the oxygen atoms when they move in the "bending" direction.

The infrared experiment measures the phonon contribution to the dielectric function in a solid. We evaluate this theoretically by means of the formula

Figure 9: Nearest-neighbor correlation functions in the Bethe lattice.

(a) Trace of the correlation matrix, showing negative correlation in the infrared-active bands.

(b) Silicon motion along the bond correlated with "bending" oxygen motion, showing tendency at 800 cm^{-1} for silicon atoms to squeeze oxygen atoms in the bending direction.

(c) Silicon motion along the bond correlated with "stretching" oxygen motion, showing tendency of atoms to move together in the acoustic-like bands.

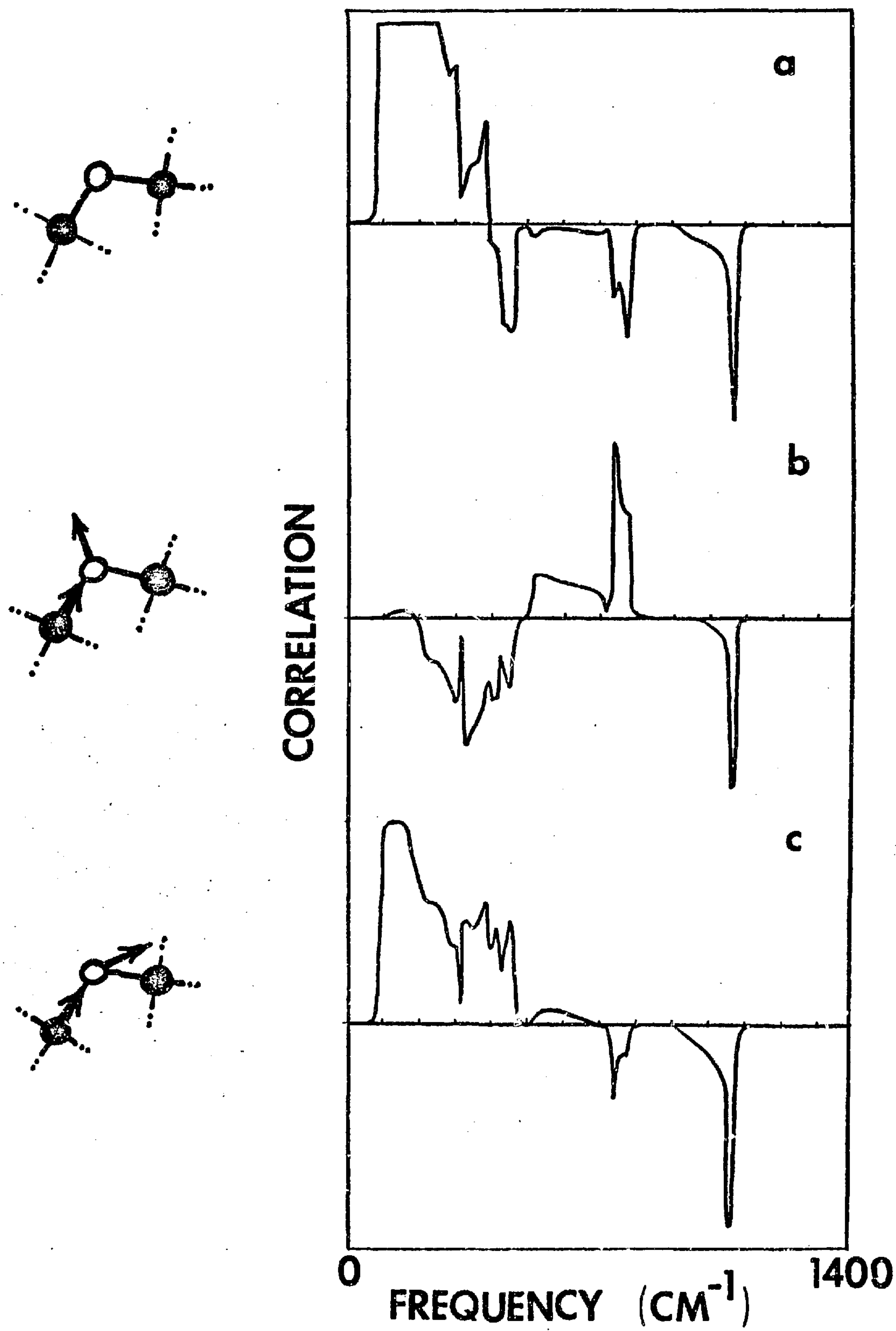
a
b
c
CORRELATION
0
1400
FREQUENCY (CM-1)

Figure 10: Second-nearest neighbor correlation functions in the Bethe lattice.

(a) Silicon-silicon correlation showing squeezing effect at 800 cm^{-1}.

(b) Stretching-stretching correlation.

(c) Bending-bending correlation showing strong positive value at 550 cm^{-1} associated with Raman activity.

(d) Rocking-rocking correlation.

All oxygen-oxygen correlations are between "1" and "2" atoms as defined in the text.

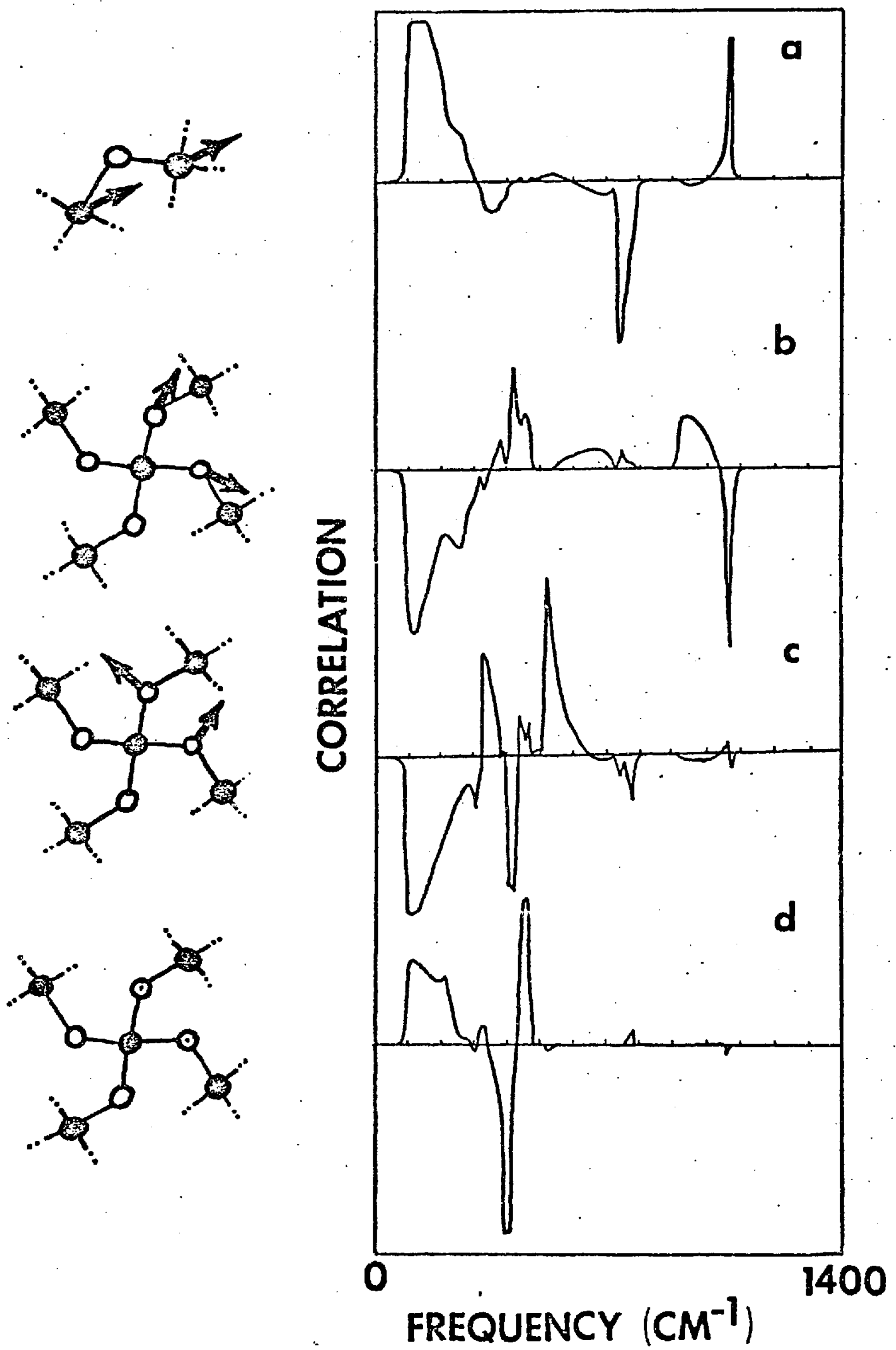
a
b
c
d
CORRELATION
0
1400
FREQUENCY (CM^{-1})

$$\varepsilon = 1 + \frac{4\pi}{v} \sum_{i,j} Q_i G_{ij} Q_j + 4\pi\chi_{electrons} \qquad (25)$$

where v is the volume of the solid and Q_i is the charge on the i^{th} atom. Rather than viewing G as a correlation function in this expression, it is convenient to think of it as describing the dipole moment induced on atom i resulting from applying a force $Q_j\vec{E}$ to atom j.

In figure 11 we compare with experiment the imaginary part of the phonon contribution in (25) summed not over the entire solid, but over a 33-atom nucleus in the Bethe lattice. The Bethe lattice is topologically identical to quartz up to fifth nearest neighbors, due to the absence of rings of bonds in quartz smaller than 12-fold. If we assume that the same holds true for the amorphous solid, we can approximate the actual Green's function with the Bethe lattice Green's function for fifth nearest neighbors and closer. The 33-atom cluster just includes fifth nearest neighbors of the central atom. Restricting the sum (25) to such a cluster in the actual solid would lead to large errors; however, the trends would be right. If the cluster were diminished to one atom, the sum would produce a local density of states. If it were extended to the whole solid, the sum would produce the correct spectrum. If we discover how the density of states is weighted when the sum is taken over an immediate system, we can infer how it will be weighted when the sum is done correctly. In the calculation we use the effective charge tensors Q_i bound by Kleinman and Spitzer to be appropriate for quartz.[13] The theory has been artificially broadened

Figure 11: Theoretical versus experimental values for the phonon contribution to $\varepsilon_2(\omega)$ silica.

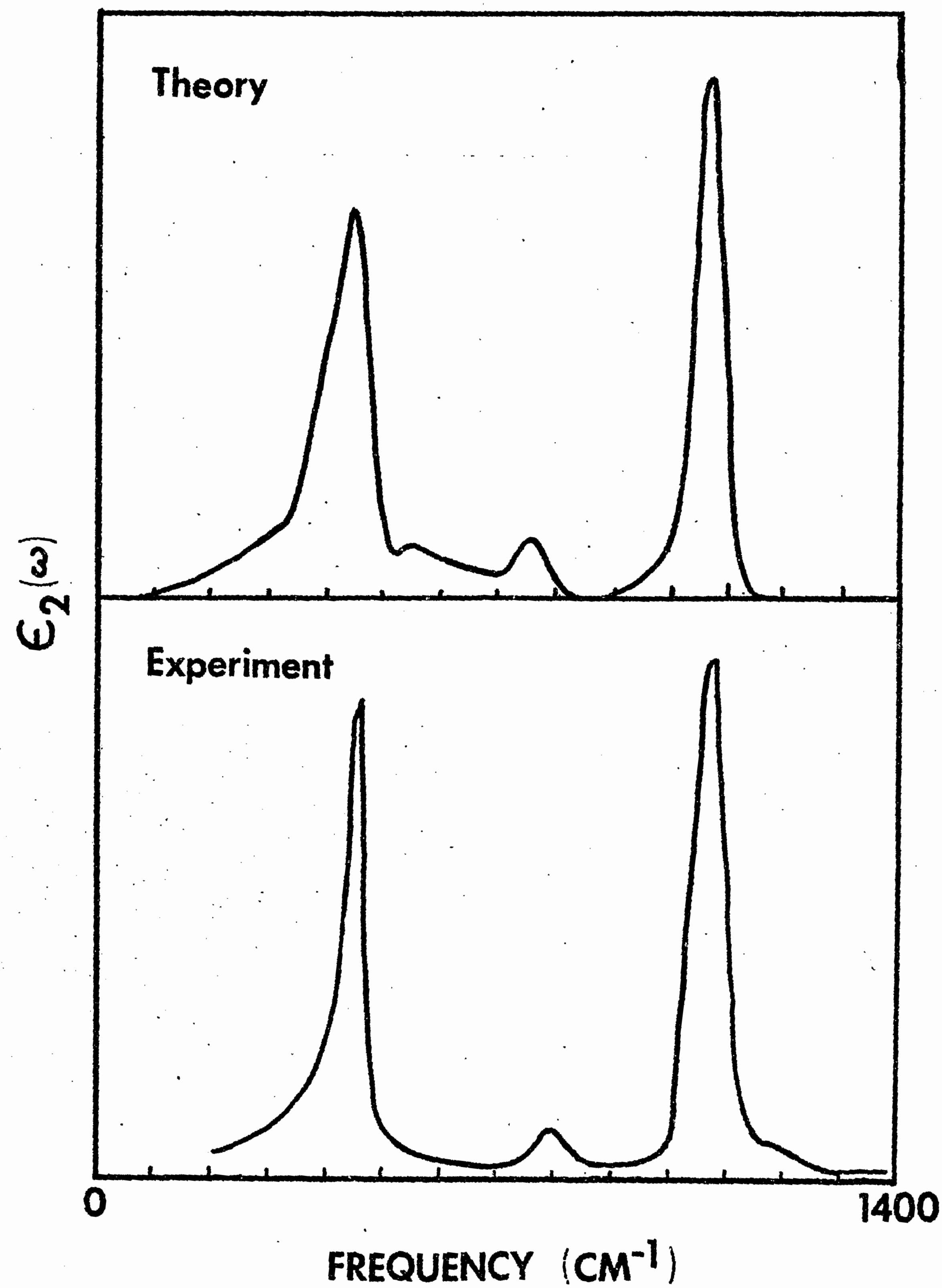
Theory
Experiment
$\epsilon_2^{(\omega)}$
0
1400
FREQUENCY (CM^{-1})

by 75 cm^{-1}. The experimental spectrum is that of Galeener and Lucovsky.[8] The agreement between theory and experiment is excellent, except for the excessive width of the peak at 450 cm^{-1}, which we believe to be due to the small size of the cluster over which the sum was taken. We conclude that the Bethe lattice is consistent with the infrared data.

Agreement of the Bethe lattice with existing raman data is less good. The mechanism used with moderate success by Kleinman and Spitzer[13] to account for the intensities of the four A_1 raman lines in quartz involves an isotropic dialation of a scalar polarizability by the atoms when they move so as to compress bonds. Kleinman and Spitzer observed that the raman intensities were harder to fit than the infrared intensities. They did not address the eight E lines in the raman spectrum.

The raman cross-section is given by[14]

$$\frac{d\sigma}{d\Omega} \propto \sum_{i,j} \left\{ \int <\delta\alpha_i(0)\delta\alpha_j(t)> e^{i\omega t}\, dt \right\} e^{i\vec{q}\cdot(\vec{R}_i - \vec{R}_j)} \tag{26}$$

where $\delta\alpha_i$ is the change in the electronic polarizability at atom i. If we let $(\vec{\nabla}\alpha_i)$ denote the gradient of α_i with respect to $\vec{x}_i$, we obtain for the small momentum transfers $\vec{q}$ of light scattering

$$\frac{d\sigma}{d\Omega} \propto \sum_{i,j} (\vec{\nabla}\alpha_i) \cdot \left\{ \int <x_i(0)x_j(t)> e^{i\omega t}\, dt \right\} \cdot (\vec{\nabla}\alpha_j)$$

$$= -\frac{2\omega f(\omega)}{\pi} \sum_{i,j} (\vec{\nabla}\alpha_i)\ \mathrm{Im}\ \{G_{ij}(\omega)\} \cdot (\vec{\nabla}\alpha_j) \tag{27}$$

We approximate this expression as before by summing over a 33-atom cluster in the Bethe lattice.

In figure 12 we compare our results with the experimental spectrum of Galeener and Lucovsky.[8] The theory has again been artificially broadened by 75 cm^{-1}. The agreement is terrible. The intense peak at 550 cm^{-1} in the theory is probably the feature at 500 cm^{-1} in the experiment. It is too strong and in the wrong place in the theory. The band between 100 cm^{-1} and 400 cm^{-1} is shifted upward and is too weak in the theory. We can rectify this problem by adopting the more sophisticated Keating[15] Hamiltonian -- however, the 550 cm^{-1} peak seems to be a property of bond-oriented Hamiltonians. The rest of the features in the experimental spectrum, except for one at 600 cm^{-1}, may be reproduced by adopting an additional small <u>depolarizing</u> mechanism for the raman effect. It has been suggested[8] that this feature at 600 cm^{-1} is a defect state. We have not been able to identify it as such. We conclude from the raman calculation that the Bethe lattice is somewhat inaccurate in the region of 200 cm^{-1} and very inaccurate at 550 cm^{-1} because it is constructed using nearest-neighbor interactions only.

1.5. Summary

The Bethe lattice provides a simple means of investigating explicitly the effects of local geometry, topology and disorder on the vibrational spectrum of an amorphous solid. Using Born model interactions and the configurations of nearest neighbors found in quartz, we have constructed a Bethe lattice for silicon dioxide and have used it both

Figure 12: Theoretical versus experimental values for the reduced Raman spectrum of silica. The dotted curve is the H-V spectrum, which is identically zero in the theory. The solid curve is the V-V spectrum.

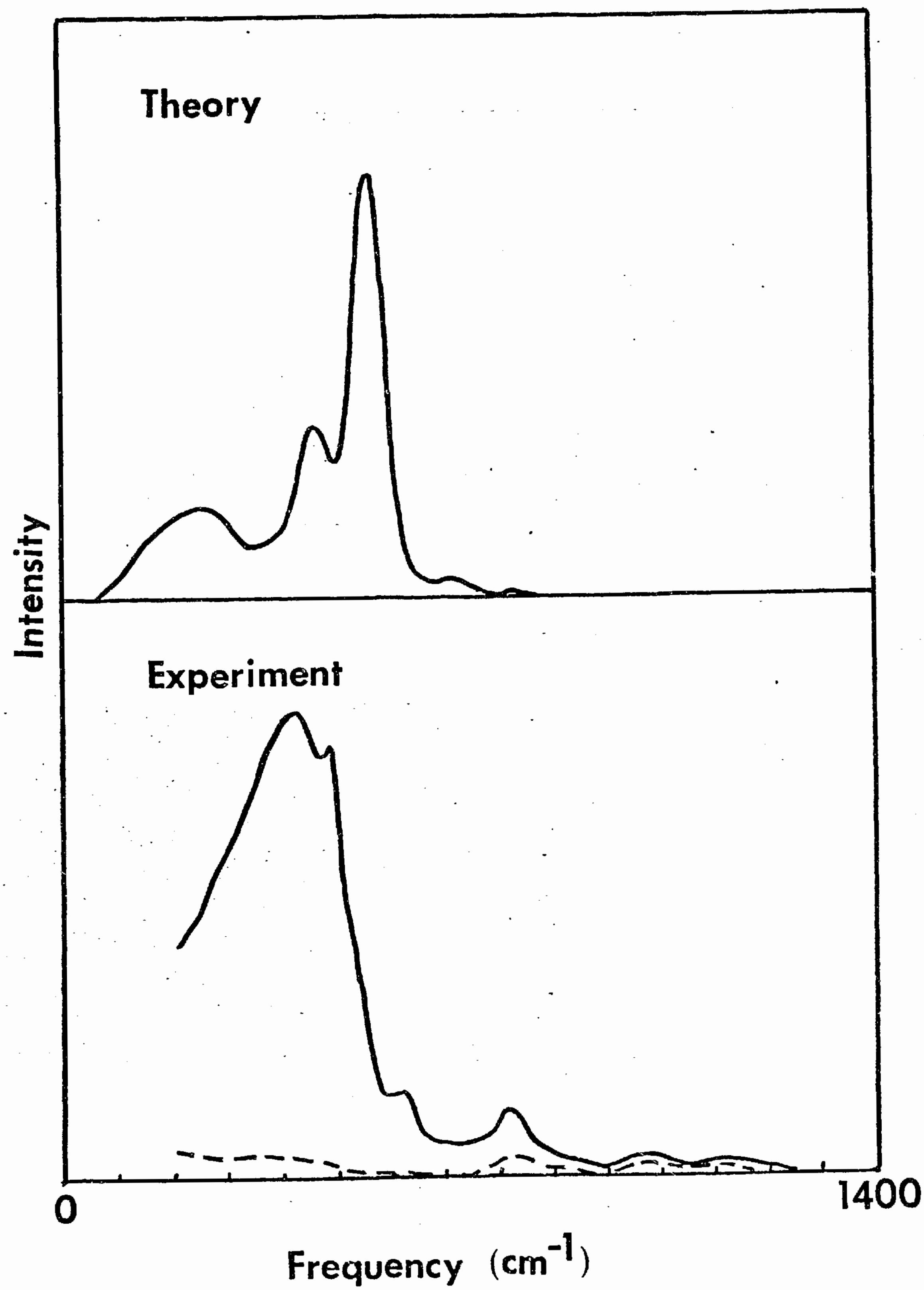
Theory
Experiment
Intensity
0
1400
Frequency (cm-1)

to analyze neutron, infrared and Raman experiments, and to investigate the effects of disorder. From this study several new facts about amorphous silica have emerged, the most important of which may be summarized as follows:

1. The vibrational properties of amorphous silica are completely dominated by local effects, particularly the values of the bond angles in the immediate vicinity of an atom.
2. Bond angle fluctuations are important only in that they broaden features in the spectra that would otherwise be sharp.
3. The topology of amorphous silica is not manifested in any available data.
4. Phonons in amorphous silica are not characteristically SiO_4-like.
5. Matrix element effects in neutron, infrared and raman experiments are <u>local</u> phenomena.

CHAPTER II

SURFACE PHONONS IN AMORPHOUS SILICA

The current widespread interest in solid surface is due, in part, to the development of a number of new analytical tools adapted specifically to surface studies and distinct from those applied successfully in the past to studies of the bulk. While studies of surface vibrations have always had enormous potential for improving our understanding of the surface, the difficulty of the experiments has discouraged their use in surface analysis. Unlike surface electrons, surface phonons are extremely difficult to measure. Photons and neutrons, the probes traditionally used to detect phonons, are weakly-interacting particles which tend to penetrate deeply into the material and sample its interior. Surface phonons represent a rich, untapped source of information about the surface which is just beginning to be exploited.[16]

Recently,[17,18] several experiments have been performed which overcome the problem of inherent bulk-sensitivity of the probe by substituting an extremely porous sample for an ordinary homogeneous one. A sufficiently large fraction of the atoms <u>inside</u> the sample are surface atoms that the surface phonon spectrum, superimposed on that of the bulk, may be detected using conventional spectroscopic techniques. The principal disadvantage of the approach is that the surfaces are poorly characterized, in that they are irregular and disoriented as a consequence both of the preparation methods and of the amorphous nature of the substrate. Feasible surface-phonon-sensitive experiments are so rare, however, that these experiments are important despite the poor surface characterization.

Stimulated by the experimental situation, we have developed a theory of surface phonons in amorphous solids. The theory is constructed using methods recently developed for describing bulk amorphous solids,[19] and is based on the idea that the first- and second-nearest-neighbor environment of the surface atoms and the presence of an infinite substrate alone can account for the behavior of most of the surface phonons regardless of the surface topography. The theory is relatively simple, is realistic, and can be compared readily with experiment.

In this chapter, we present a detailed discussion of the theory using silicon dioxide as a prototype. We have chosen silicon dioxide because of its technological importance and because of the relative abundance of experimental information on porous glass. The methods and ideas we discuss, however, are applicable to any amorphous material. The chapter is organized as follows. In the first section, we discuss what problems are involved in constructing a theory of surface phonons in amorphous silica, what approximations are appropriate and what we expect the theory to do. In the second section we deal with mathematical aspects of the theory. In the third section, we investigate the behavior of the surface predicted by the theory and compare this behavior with experiment. In the fourth section, we study a chemisorption which drastically changes the surface behavior. We conclude with a summary.

2.1. Preliminary Considerations

The approach we follow in trying to understand a disordered silicon dioxide surface is motivated by our understanding of the effects of disorder in the bulk. In bonded solids, the two fundamental types of disorder, bond-angle fluctuations and topological disorder, disrupt the long-range order of the solid while leaving its local structure intact. As a consequence, the behavior of the amorphous and crystalline phases of bonded solids tend to be very similarly locally.[20] Both kinds of disorder tend to broaden the crystal density of states somewhat and to perturb the character of states within the first few neighbors of an atom only slightly. In addition, topological disorder can introduce rings of bonds of various sizes into the material whose effects can be traced to the occurrence of resonances about the rings.[20] It has been shown in Chapter 1, however, that phonons in bulk amorphous silica are adequately described when the structure of the material is modeled as a Bethe lattice, a bonded network of atoms which has the same local geometry as the crystal but which has no rings of bonds. The Bethe lattice is effective in this function, despite the fact that it lacks the rings of bonds which any real material must have, because it is similar to the actual solid locally.

The two major problems impeding a simple view of the disordered surface are the poorly defined relationship of adjacent atomic sites on the surface and the disorder of the substrate itself. Since disorder in the substrate is essentially disorder in the bulk, it follows that the substrate can be understood, like the bulk, in terms of the bonding arrangement of the atoms locally. The approach we use to overcome the remaining problem, that of intrasurface interactions, relies on the observed[21] tendency in bonded solids for the surface effects to be highly localized. The high degree of localization causes the effect of adjacent surface sites on one another to be small, and the states induced by the presence of the surface to be characteristic of an isolated site bonded to an infinite substrate. The principal approximation of our theory is that the surface sites do not interact _at all_ -- that the surface can be accurately modeled as _one_ site, so long as the infinity of the substrate is accounted for.

The aspect of the material with which we are primarily concerned is the nature and origin of the localized surface states. We want to know why surface states occur, how the structure of the surface affects them and what they tell us about the surface. In order to build a theory which is tractable and at the same time capable of describing the surface states realistically, we need approximations for both the structure and the Hamiltonian of the surface which are suited to the question we are asking.

Because of the localization of the surface states and the established[21] realtive unimportance of intra-surface interactions, we need not deal initially with the effects of surface two-dimensionality. To obtain a suitable structural model for the surface, therefore, we need only break a bond in the Bethe lattice. The atom with the dangling bond becomes the site, while the structure to which it is attached becomes the substrate. The bond-breaking procedure is illustrated in Fig. 13. The scission of a bond produces two fundamental types of surface, one terminating on a silicon atom, and a similar surface with an oxygen atom attached. Since native silicon dioxide surfaces are presently thought to terminate in hydroxyl groups,[22] the oxygen-terminated surface is most likely more representative of real materials. However, both kinds of surface site should be formed when a sample is broken or cut.

The Hamiltonian appropriate for the theory is the one we have used for studying the nature and origin of phonons in the bulk. The primary disadvantages of the Born[4] Hamiltonian are that it does not properly account for the ionicity of the atoms and that it is not rotationally invariant. While neither of these problems prevents the bulk from being described qualitatively, they do introduce up to 30% inaccuracy in the frequencies of the states. A more sophisticated Hamiltonian can eliminate this inaccuracy; however, the correct Hamiltonian is not known and the physically reasonable Born Hamiltonian is the simplest one which suits our purpose. It should be emphasized that the only adjustable parameters in theory are the two which characterize the Born Hamiltonian in the bulk.

Figure 13: Transformation of Bethe lattice from model for the bulk to model for the surface. Breaking a bond generates two fundamental kinds of surface.

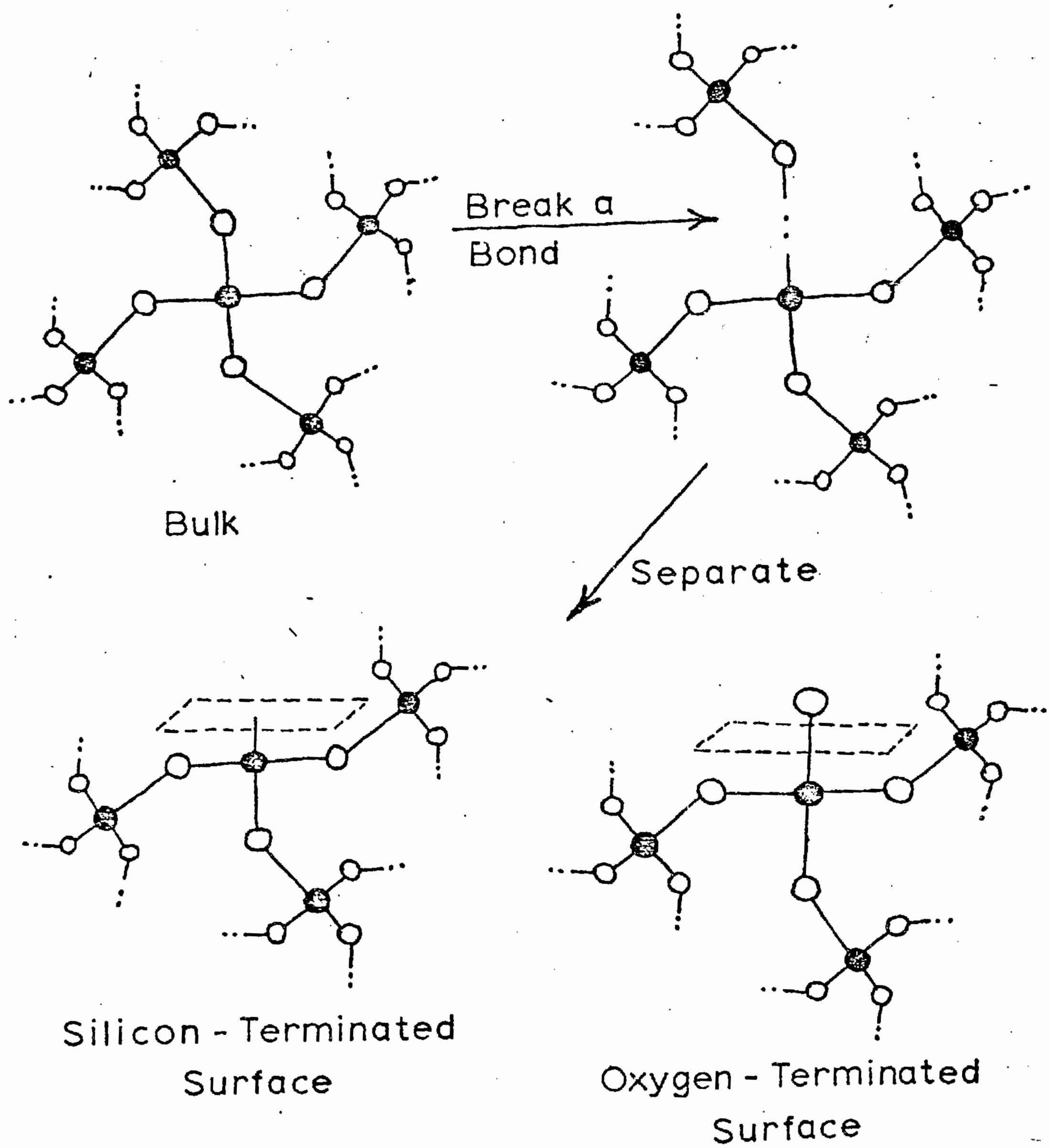
Break a
Bond
Bulk
Separate
Silicon - Terminated
Surface
Oxygen - Terminated
Surface

2.2. Manipulating the Bethe Lattice

Modeling the surface as a Bethe lattice with a broken bond has the great advantage that the solution of the bulk problem is also the solution of the surface problem. Both rely on the existence of a set of transfer matrices Φ_ν, which must be calculated before the density of states of the bulk can be obtained. As has been discussed previously, the transfer matrix is basically the mechanical impedance of the atom at the base of a broken-bond Bethe lattice when the restoring forces on the atom itself are artificially maintained at their bulk values. Ordinarily, removing a neighbor diminishes these restoring forces. The transfer matrix is obtained by satisfying a self-consistency relation, which is the mathematical equivalent of requiring that bonding three broken-bond Bethe lattices to a silicon atom creates a new broken-bond Bethe lattice. The transfer matrices are used to invert the dynamical matrix and produce the vibrational Green's function of the system. The imaginary part of the diagonal Green's function matrix elements are proportional to the local densities of states of the problem.

The notation we use is the same used to discuss the bulk. If we let

$$\tilde{A} = \omega^2 - A - \sum_\nu D_\nu(\omega^2 - B_\nu)^{-1}D_\nu \ , \tag{28}$$

and

$$\tilde{D}_\nu = D_\nu(\omega^2 - B_\nu)^{-1} M_\nu D_{\sigma(\nu)} \ . \tag{29}$$

then the transfer matrices Φ_ν are given by

$$\Phi_\nu = \left[\tilde{A} - \sum_{\mu\neq\sigma(\nu)} \tilde{D}_\mu \Phi_\mu\right]^{-1} \tilde{D}_\nu^t , \tag{30}$$

and the Green's function confined to a silicon atom in the bulk by

$$G_0 = \left[\tilde{A} - \sum_\mu D_\mu \Phi_\mu\right]^{-1} \tag{31}$$

If we define additional transfer matrices ψ_ν in the manner

$$\psi_\nu = (\omega^2 - B_\nu)^{-1}\left\{D_\nu + M_\nu D_{\sigma(\nu)}\Phi_\nu\right\} \tag{32}$$

then we have equivalently for the Green's function confined to silicon in the bulk

$$G_0 = \left[\omega^2 - A - \sum_\nu D_\nu \psi_\nu\right]^{-1} \tag{33}$$

To determine the analogous quantity for the silicon atom at a silicon-terminated <u>surface</u>, we first construct the reduced restoring force matrix A_0 on the surface atom

$$A_0 = -\sqrt{\frac{m}{M}} \sum_{\nu\neq\mu} D_\nu = A + \sqrt{\frac{m}{M}}\, D_\mu \tag{34}$$

where m and M are the oxygen and silicon masses respectively. μ denotes the direction of the dangling bond. We then have

$$G_0^S = \left(\omega^2 - A_0 - \sum_{\nu\neq\mu} D_\nu\psi_\mu\right)^{-1} \tag{35}$$

for the surface Green's function submatrix.

To determine the Green's function submatrix connecting a neighbor oxygen atom with itself, we make use of the fact that the Green's function is its own transpose. If we let

$$\eta_\nu = \Phi_\nu\psi_\nu^{-1} \tag{36}$$

then the Green's function confined to the oxygen neighbor in the ρ^{th} direction is given by

$$\begin{aligned} g_0^\rho &= \left(\omega^2 - B_\rho - M_\rho D_{\sigma(\rho)}\eta_\rho\right)^{-1}\left\{1 + D_\rho[\psi_\rho G_0^S]^t\right\} \\ &= b_\rho + \psi_\rho G_0^S\psi_\rho^t \end{aligned} \tag{37}$$

where

$$b_\rho = \left(\omega^2 - B_\rho - M_\rho D_{\sigma(\rho)}\eta_\rho\right)^{-1} \tag{38}$$

Similarly, the Green's function confined to the next silicon atom down is given by

$$\begin{aligned} G_0^\rho &= \left(\omega^2 - A - \sum_{\nu\neq\sigma(\rho)} D_\nu\psi_\nu\right)^{-1}\left\{1 + D_{\sigma(\rho)}M^t[\eta_\rho g_0^\rho]^t\right\} \\ &= A_\rho + \eta_\rho g_0^\rho \eta_\rho^t \end{aligned} \tag{39}$$

where

$$A_{\rho} = \left[\omega^2 - A - \sum_{\nu \neq \sigma(\rho)} D_{\nu}\psi_{\nu}\right]^{-1} \qquad (40)$$

and so on. In this manner, the Green's function confined to a layer beneath the surface is generated in terms of its value on the previous layer.

If we now chemisorb an atom onto the surface, for example, an oxygen atom to form an oxygen-terminated surface, the Green's function may be propagated into the bulk exactly as before. It remains only to calculate it for the first two atoms. If we define the dynamical matrix confined to the adsorbate as B', we then construct its interaction D' with the surface silicon atom

$$D' = -\sqrt{\frac{m'}{M}}\, B' \qquad (41)$$

and the new restoring force matrix for the silicon atom

$$A' = A_0 - \sqrt{\frac{m'}{M}}\, B' \qquad (42)$$

where m' denotes the mass of the adsorbate. We then have for the surface silicon atom

$$G_0^S = \left[\omega^2 - A' - D'(\omega^2 - B')^{-1}D' - \sum_{\nu \neq \mu} D_{\nu}\psi_{\nu}\right]^{-1} \qquad (43)$$

and for the adsorbate

$$g = (\omega^2 - B')^{-1}\left\{1 + D'[(\omega^2 - B')^{-1}D'G_0^S]^t\right\} \qquad (44)$$

2.3. Results

In Fig. 14 we show local densities of states for both a silicon-terminated and an oxygen-terminated surface. The top frame in each case refers to the surface atom, the next frame to the atom below, and so on, layer-by-layer into the bulk.

As we approach the silicon-terminated surface from below we see two major changes in the local density of states: a buildup of low-frequency states around 200 cm^{-1} and a sharp surface state at the upper edge of the band peaking at 450 cm^{-1}. The first effect is the consequence of the presence of acoustic-like surface states. The gap from 0 to 100 cm^{-1} is a pathology of the Bethe lattice which stems from its unphysical long-range behavior. Low-frequency acoustic phonons are long-wavelength excitations which the Bethe lattice cannot describe. Short-wavelength acoustic phonons have frequencies around 100 cm^{-1} and are described correctly by the Bethe lattice. We call these vibrations acoustic-like because the distinction between acoustic and optic phonons is ill-defined in a material with no periodicity. The presence of these low-frequency vibrations may also be viewed as a consequence of the reduction of the restoring forces acting on the surface silicon atom. Removing an oxygen neighbor to make the surface diminishes these forces, which causes the atom to tend to vibrate

Figure 14: Local densities of states versus frequency for silicon-terminated (left) and oxygen-terminated (right) surfaces, starting from the surface atom and proceeding layer-by-layer down into the bulk. The features caused by the surface are marked with arrows.

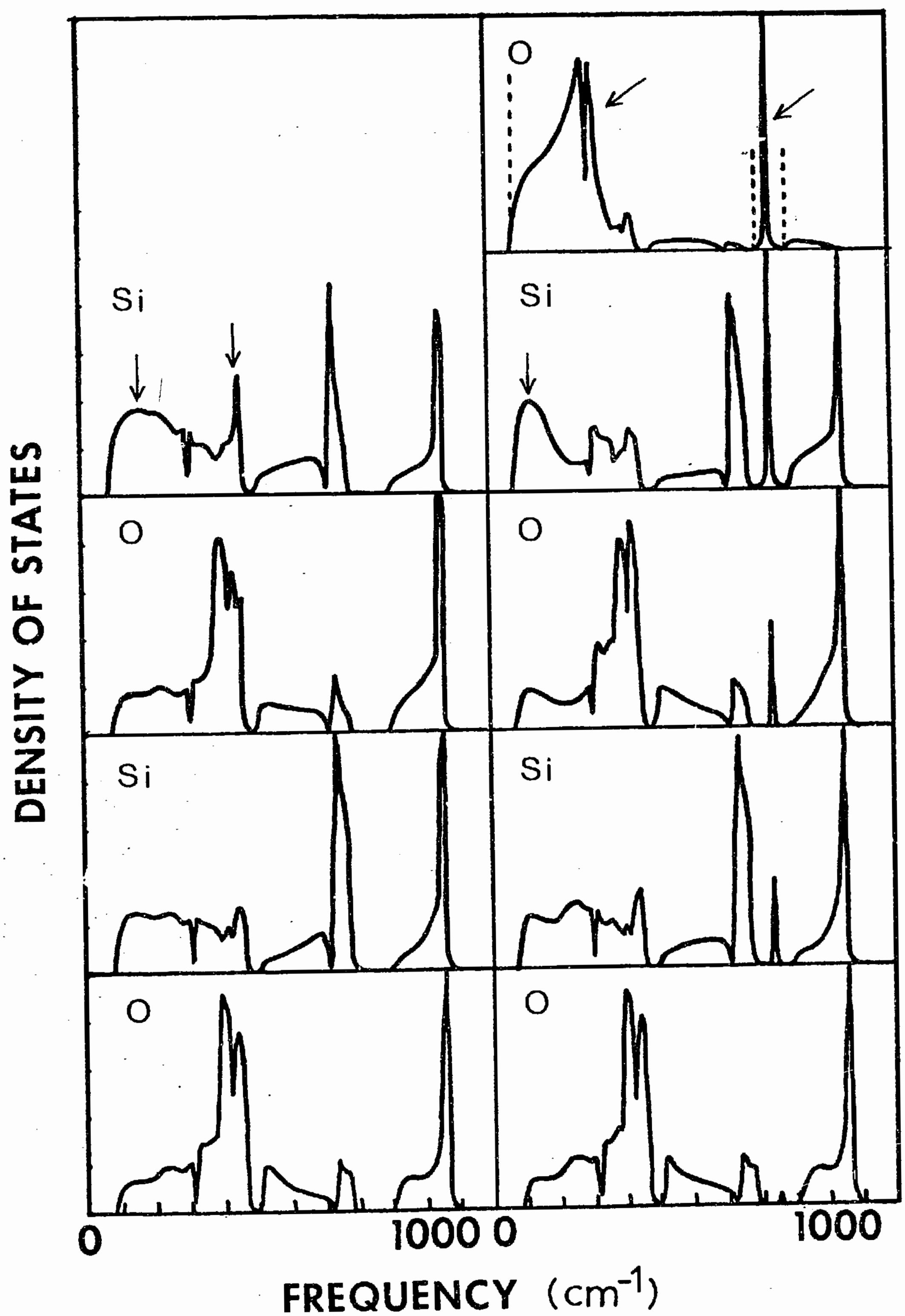
O
Si
Si
O
O
Si
Si
O
O
DENSITY OF STATES
0
1000
0
1000
FREQUENCY (cm^{-1})

slower. The feature at 450 cm^{-1} is a genuine surface state which involves primarily vibration of the surface silicon atom. Surface relaxation increases the frequency of this state and causes it to be more distinct, particularly if it falls outside the bulk bands. Both of these effects disappear by the fourth layer into the bulk.

Near the oxygen-terminated surface we see three effects. Again, there is the buildup of states near 200 cm^{-1} associated with acoustic-like surface vibrations. In addition, there is a sharp surface state near 850 cm^{-1} associated with bond-stretching motion of the surface oxygen atom and a band peaking at 300 cm^{-1} associated with a wagging motion of this atom. Again, the surface effects are by-and-large gone by the fourth atomic layer.

In Fig. 15 we have broken the surface local densities of states down into components parallel and perpendicular to the surface, in order to show the extent to which the surface states are directed. We find that the surface state at 450 cm^{-1} is a motion of the surface silicon atom normal to the surface. The stretching and wagging peaks of the oxygen-termined surface are appropriately normal and parallel to the surface respectively, with a small amount of mixing due to the asymmetry of the SiO_4 unit caused by the silicon neighbors. The low-frequency surface states are in both kinds of surface fairly isotropic. It is interesting that the wagging state at 300 cm^{-1} involves <u>reduced</u> motion of the silicon atom immediately below the surface oxygen atom, an effect which is partially responsible for the large infrared activity of the state.

Figure 15: Local densities of states versus frequency for silicon-terminated (top frame) and oxygen-terminated (bottom frames) surfaces broken down into components perpendicular to (left) and parallel to (right) the surface.

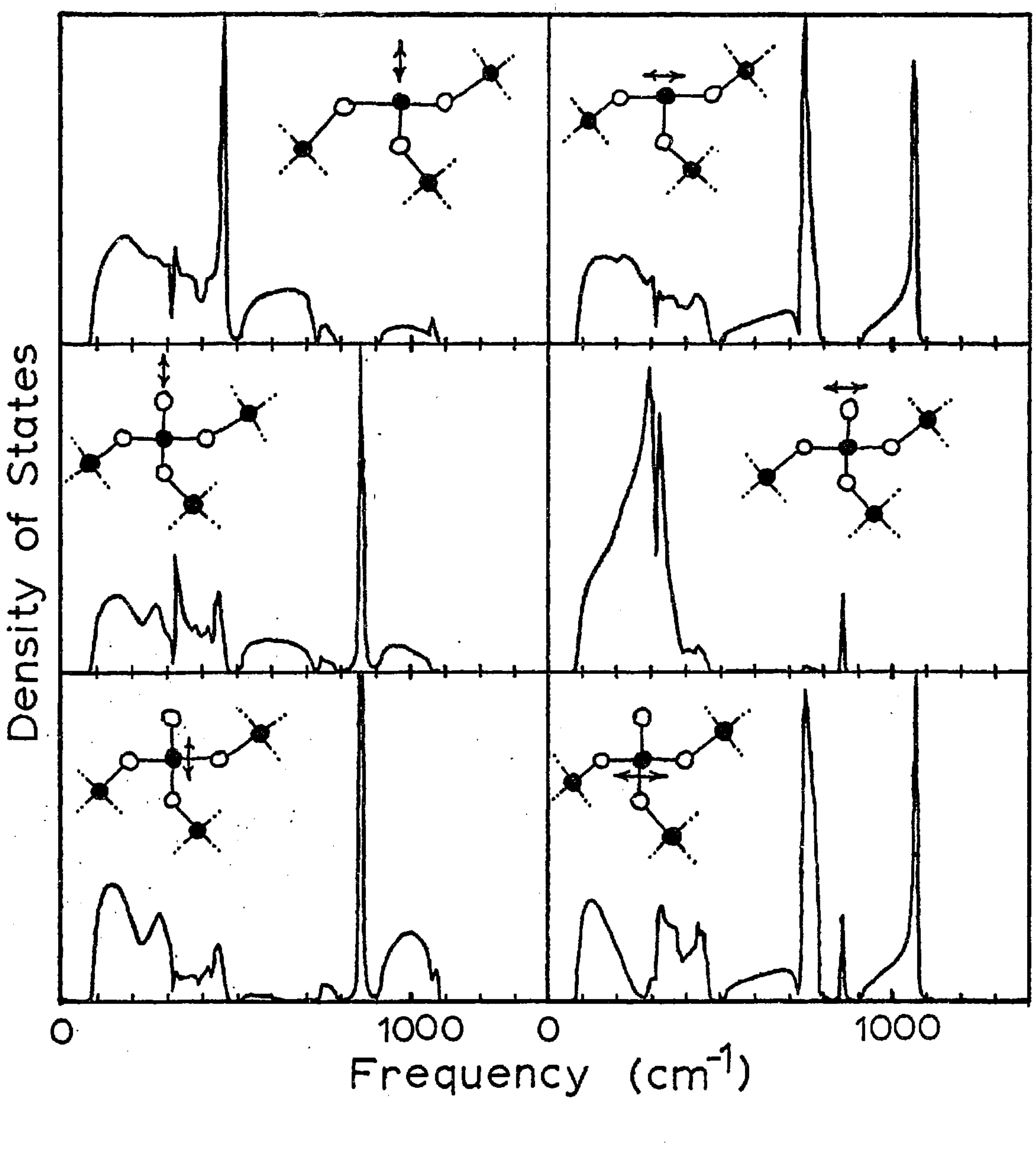
Density of States
0
1000
0
1000
Frequency (cm^{-1})

When the surface atoms are allowed to relax, we find generally that the surface states do not change substantially in character, but tend to increase in frequency. The effect of relaxing the Si-O bond at any oxygen-terminated surface is shown in Fig. 16. As the Si-O force constants at the surface are increased, the very low frequency local densities of states remain relatively unchanged, as do the bulk-like features, while the stretching and wagging features move steadily upward.

One other atomic configuration which might occur in actual silica surfaces is that of two oxygen atoms dangling into the vacuum. In Fig. 17, we show the first two local densities of states associated with such a surface. Both the stretching and wagging peaks split slightly into doublets, the stretching more so than the wagging because it couples more strongly to the silicon atom immediately below. However, the most pronounced effect is the introduction of a sharp surface state at about 100 cm^{-1} which corresponds to motion of the surface SiO_2 unit as a whole against the rest of the substrate.

Some of the changes induced by the presence of the surface in the theory have been observed in experiment.[17,18] In Fig. 18 we show Raman and infrared reflectivity measurements performed by Murray et al.[18] on samples of porous Vycor glass. Porous Vycor is a sponge-like form of amorphous silicon dioxide containing 28% voids roughly 40 Å in diameter. This material has surface-to-volume ratio sufficiently large that these measurements are sensitive to the surface phonons. The features in these spectra which are characteristic of the porous material we have marked with arrows. Those marked with b have been

Figure 16: Local densities of states versus frequency for oxygen-terminated surface with successively stronger relaxations. The surface oxygen local density of states is on the left, and that of the silicon atom below it is on the right. The Si-O force constants are multiplied respectively by 1.0 (top), 1.25 (middle) and 1.45 (bottom).

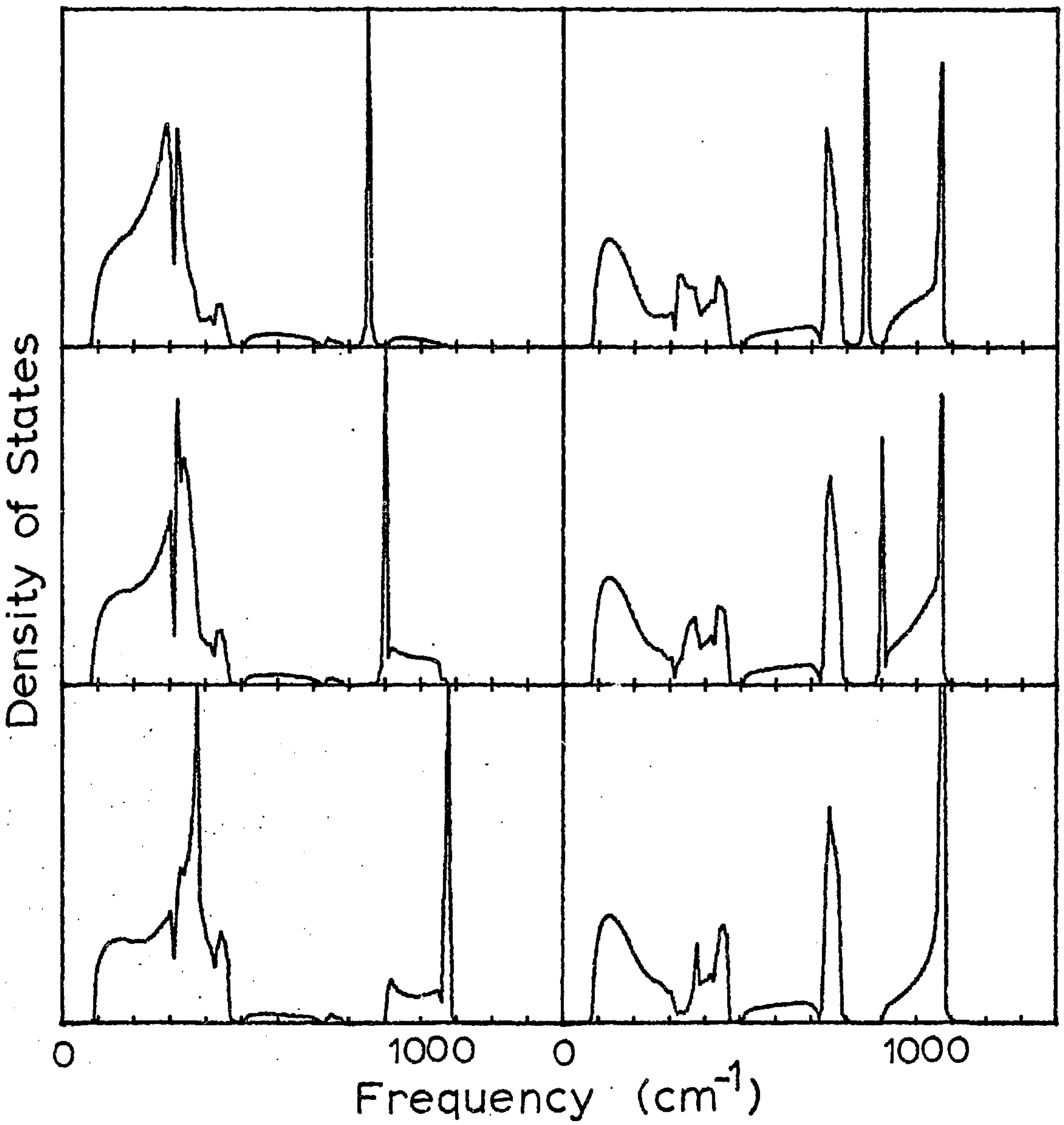
Density of States
0
1000
0
1000
Frequency (cm^{-1})

Figure 17: Comparison of surface terminated with two oxygen atoms with one terminated with only one oxygen atom.

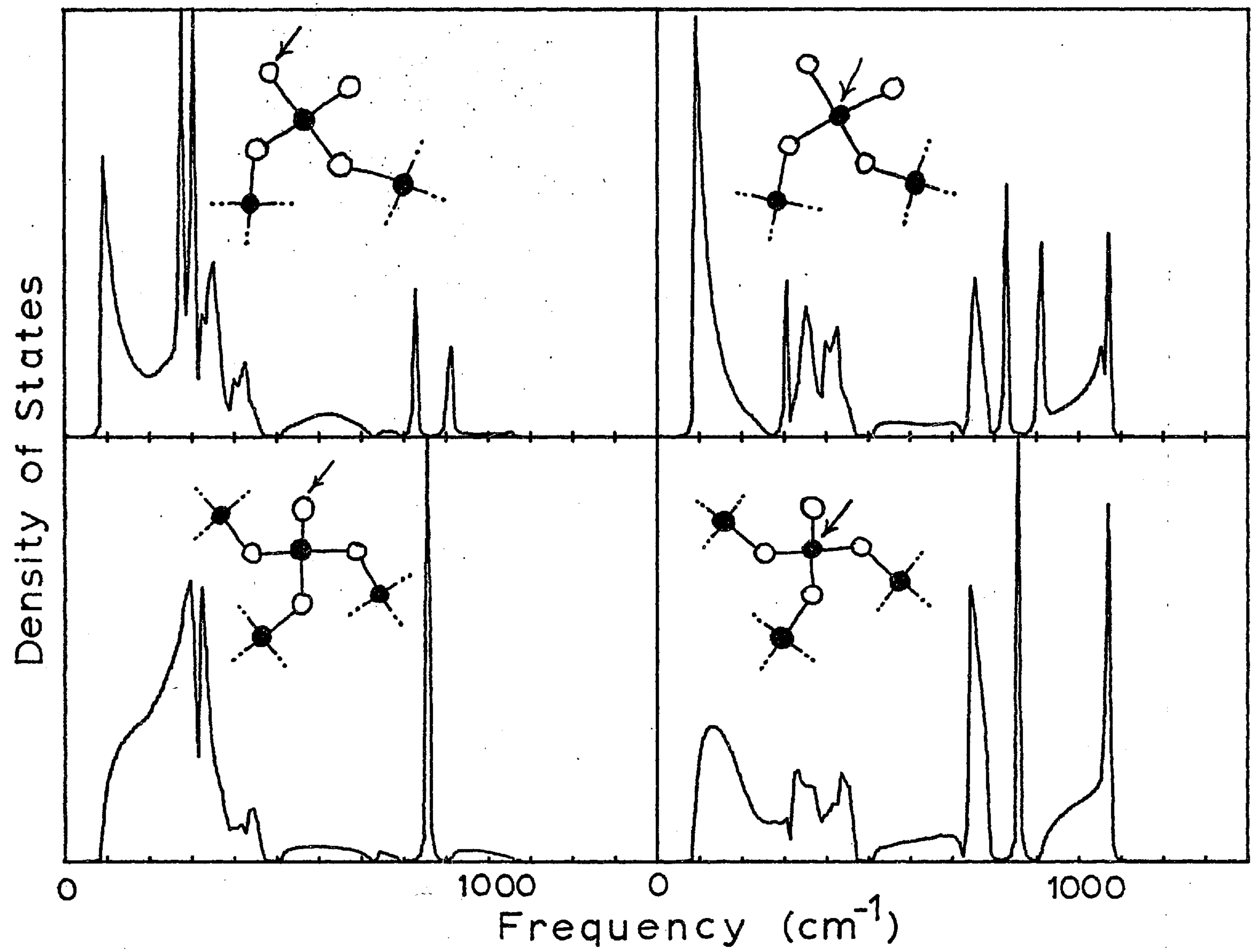

Density of States
0
1000
0
1000
Frequency (cm^{-1})

Figure 18: Experimental infrared and Raman spectra of porous Vycor glass (solid lines) and bulk fused silica (dashed lines). The surface-induced features marked b are due to the presence of Boron impurities, those marked s are due to surface phonons, and the one marked d to a defect mode.

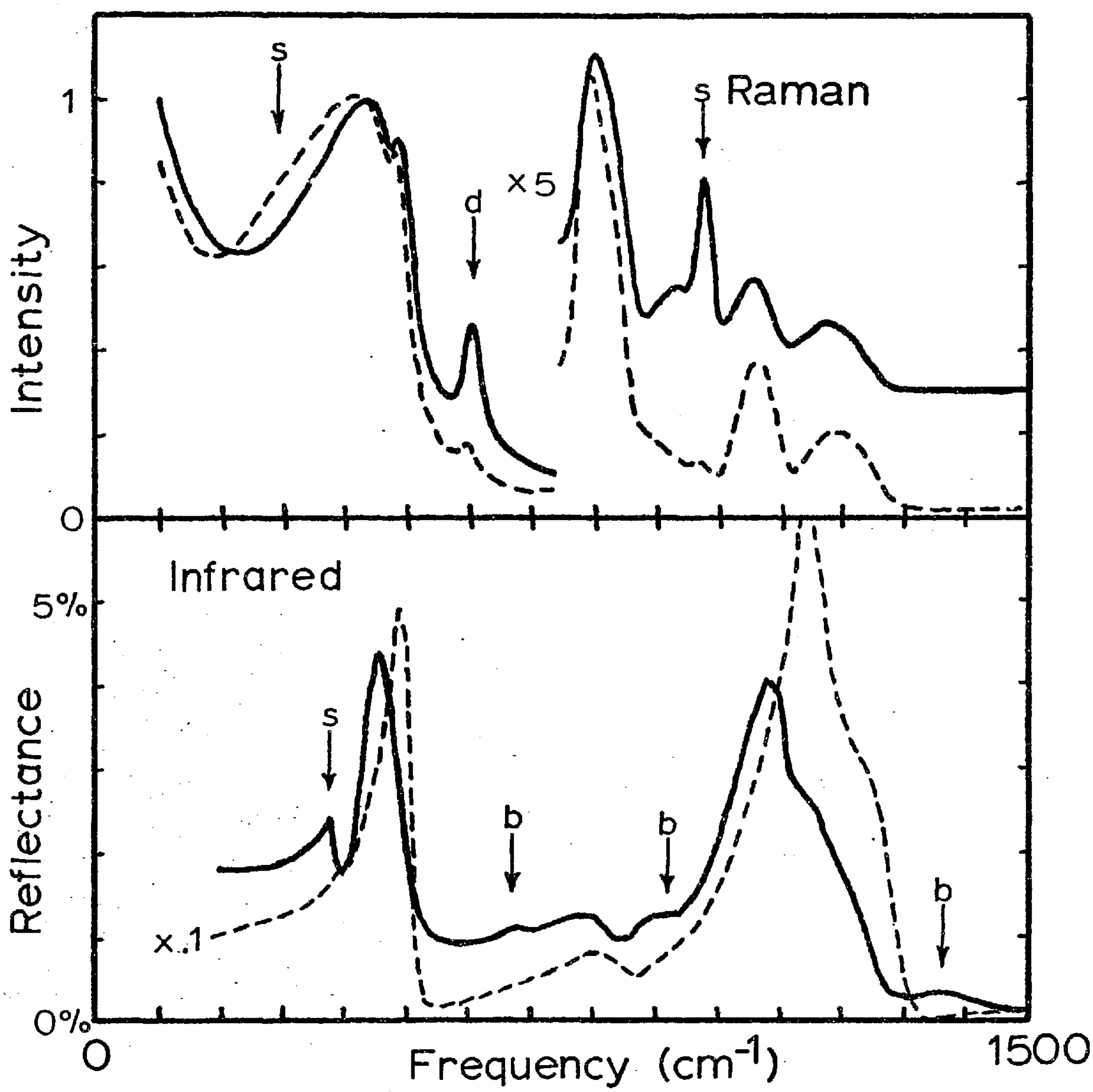
s
1
s Raman
×5
d
Intensity
0
Infrared
5%
s
b
b
b
Reflectance
x.1
0%
0
Frequency (cm^{-1})
1500

identified conclusively as being due to boron impurities in Vycor.[18,23] Those marked s are due to surface phonons characteristic of a simple oxygen-terminated surface. The one marked d has properties consistent with what one would expect for a silicon-terminated surface state. We identify the peak at 980 cm^{-1} in the Raman spectrum as the oxygen-stretching vibration, the peak at 380 cm^{-1} in the infrared as the oxygen-wagging vibration, and the buildup of Raman intensity below 100 cm^{-1} at the expense of intensity at 250 cm^{-1} as a signature of the acoustic-like surface states. All of the features in the theory appear at slightly higher frequencies in the experiment because of the increase of the interatomic forces at the surface caused by relaxation.

The peak at 980 cm^{-1} has been thought for some time[22] to be the stretching vibration of an hydroxyl group bound to a silicon atom. The other identifications, however, are new ones based in part on calculations we have performed to determine the theoretical intensities of the peaks. The model we have constructed explains why the stretching peak is visible only in the Raman effect, why the wagging peak is visible only in the infrared and why the acoustic-like surface states alter the Raman spectrum the way they do. None of these effects can be explained in terms of symmetry, and only can be explained trivially in terms of the bonding arrangement.

Using the procedures detailed in Chapter 1, we have calculated approximate infrared and Raman spectra for both a silicon-terminated and an oxygen-terminated surface. These are compared with identical calculations performed for the bulk in Fig. 19. As with

Figure 19: Approximate Raman (top) and infrared (bottom) spectra calculated for an oxygen-terminated (left) and a silicon-terminated (right) surface. The dotted lines refer to the same calculation performed for a 5-atom cluster in the bulk. Arrows indicate surface-induced features.

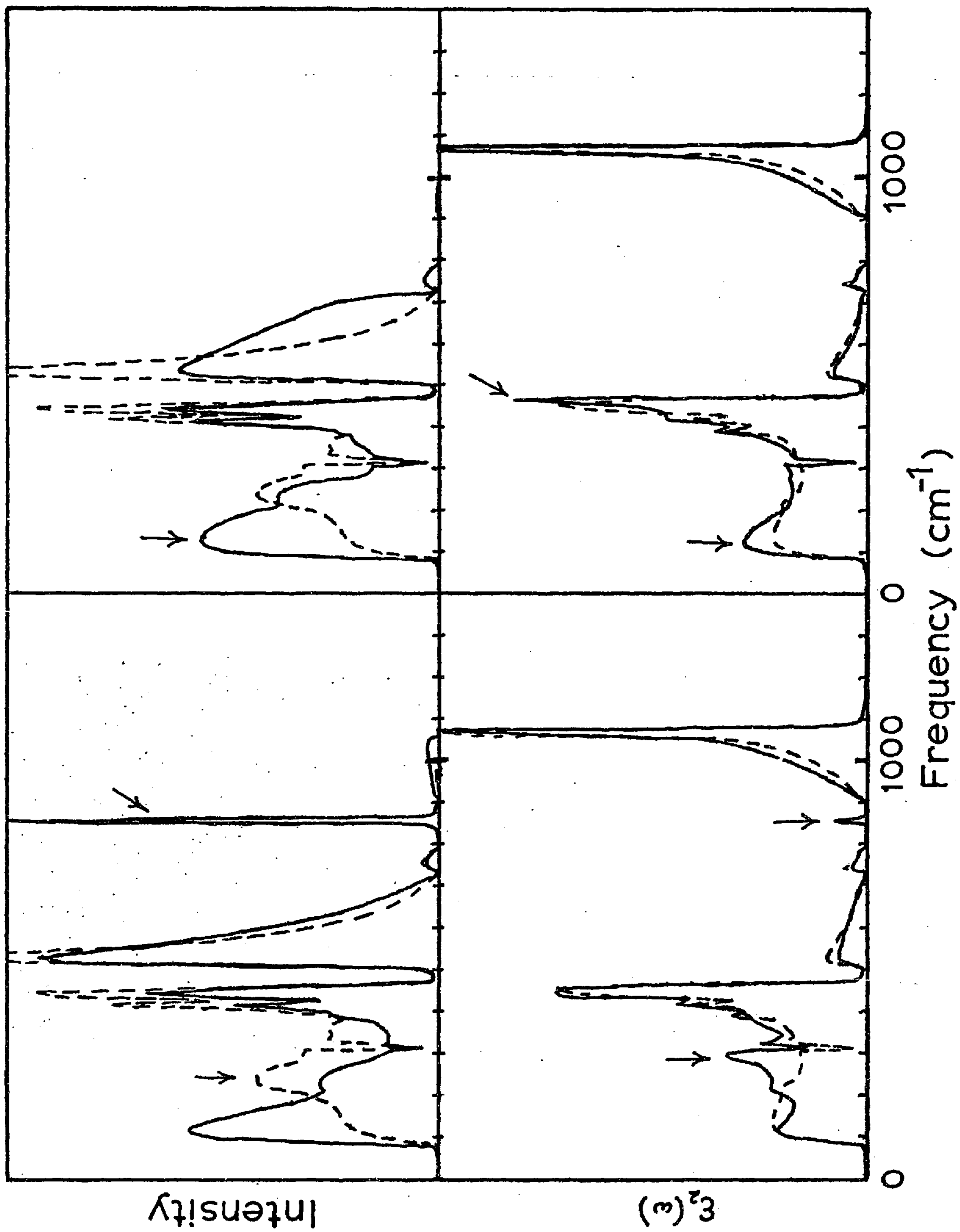
Intensity
$\varepsilon_2(\omega)$
0
1000
0
1000
Frequency (cm^{-1})

the bulk, we restrict the sums (25) and (27) to a small cluster of atoms at the surface, the size of which is limited by the extent to which the Bethe lattice structure approximates that of the actual solid. Because the surface states are confined to the first few atomic layers, we have found it suitable to restrict the sums to an SiO_4 unit, except in the case of the silicon-terminated surface, where an SiO_3 unit was used. Each spectrum has been renormalized by the number of atoms in the cluster, so that its integral, weighted by ω, is one.

In the theoretical Raman spectra, we see that both kinds of surface tend to increase the very low frequency signal associated with the acoustic-like vibrations. The oxygen-stretching peak is pronounced in the spectrum of the oxygen-terminated surface, while the wagging peak is not. This is easily understood from the point of view that only the stretching vibration compresses the bond. However, the wagging peak is additionally suppressed by the tendency of the silicon atom immediately below it to sit still at 300 cm^{-1}. The surface state at 450 cm^{-1} in the silicon-terminated surface is <u>not</u> enhanced in the Raman effect. For this reason we believe that silicon-terminated surfaces do not produce the peak labelled d in the experimental Raman spectrum. However, we believe the two are intimately related. Since the surface site is identical in our model with a broken-bond defect, the Raman calculation indicates that a silicon atom with a dangling bond is probably not the cause of the peak, as has been proposed.[24] If two such defects are bonded together to form a Si-Si defect, however, there arises a defect state near the proper frequency which <u>derives</u> from this surface state. The Raman scattering from this defect could be quite large if the polarizability derivative of the Si-Si bond were sufficiently large, and the state would be invisible in the infrared because of symmetry.

In the theoretical infrared spectrum, we see a strong enhancement of the oxygen-wagging vibration and a complementary reduction of the stretching peak. If the surface oxygen atom were considered by itself, both of these vibrations would be infrared-active. The cooperative motion of the substrate atoms, however, in conjunction with the particular effective charge tensors used, causes the stretching peak to be suppressed. The silicon-terminated surface has little effect on the infrared spectrum. There is a slight enhancement of ε_2 near the surface state at 450 cm^{-1}, but the enhancement is probably too small to be observed in experiment. The enhancement of the low-frequency surface states in the infrared is again a cluster effect.

2.4. Chlorine Chemisorption

Since we have found the model to be completely consistent with existing experimental information about silicon dioxide surfaces, we may use it to investigate the effects of chemical impurities on the surface. In Fig. 20 we show the result of bonding a chlorine atom onto a silicon-terminated surface, the situation which is thought[25] to prevail when porous glass is chlorinated. The force constants connecting the Chlorine atom to the surface silicon atom are taken to be

Figure 20: Local densities of states versus frequency for a chlorinated silica surface starting from the surface atom (top) and proceeding layer-by-layer down into the bulk.

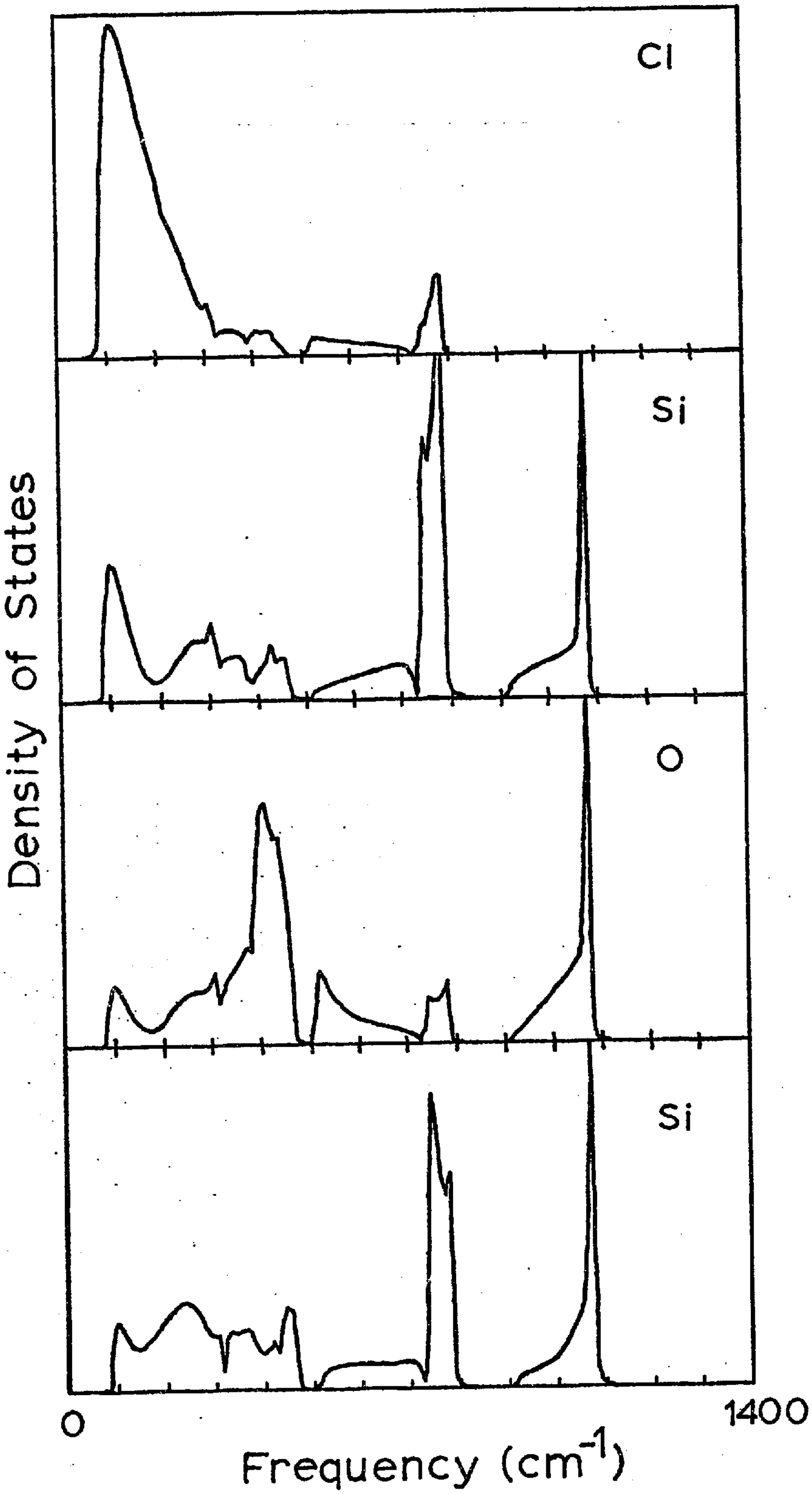
Cl
Si
O
Si
Density of States
0
1400
Frequency (cm^{-1})

the same as those connecting oxygen to silicon. The force constants are a little too large, the bending constant more so than the stretching constant, but the amount is not significant, especially in light of relaxation effects. As with an oxygen-terminated surface, we see stretching and wagging states of the surface atom. However, because of the greater mass of the Chlorine atom, the mixing of these states into the bulk bands is very pronounced. The wagging vibration is now found to have merged into the acoustic-like bands and to be no longer distinguishable from them. The stretching vibration moves downward only as far as the top of the silicon-like bands at 750 cm^{-1}, and becomes very silicon-like. This calculation indicates that the adsorbate rather than the substrate, is tending to remain stationary. The stretching vibration is no longer an adsorbate motion but one of the silicon atom underneath it. This explains why the vibration is stuck at the top of the silicon-like bands at 750 cm^{-1}. Increase of the adsorbate mass cannot move the stretching vibration below these bands. Of course, if the bending is weakened, this state will soften and eventually become the 450 cm^{-1} surface state of the silicon-terminated surface. However, we believe a fully Chlorinated surface should show up in Vycor glass as an augmentation of the 800 cm^{-1} bulk band in the Raman effect, perhaps a similar effect in the infrared, and a complete disappearance of the 980 cm^{-1} and 380 cm^{-1} hydroxyl-induced surface states.

2.5. Summary

We have presented a theory of surface phonons in amorphous silicon dioxide based on the use of the Bethe lattice as a model for the structure of the amorphous material. The theory treats the surface as an isolated atomic site which is bonded to the Bethe lattice everywhere the site ordinarily bonds to the substrate. The theory is motivated by the observed tendency in bonded solids for the two-dimensional nature of the surface to be less imporant, in most respects, than the bonding arrangement near the surface and the infinity of the substrate. We have constructed our model using a simple nearest-neighbor Hamiltonian containing two parameters which are fit to the bulk. We have used it successfully to interpret and clarify infrared and Raman scattering experiments performed on samples of porous Vycor glass. We have also predicted the effects on the Raman and infrared spectra of chlorinating the glass.

The most important accomplishment of the theory is the demonstration that the potentially complicated surface of an amorphous solid can be understood almost completely in terms of the bonding on and near a surface site. We have isolated the various effects of the substrate, identified the most important one, namely the substrate's infinity, and found a way of including it in the model so that the important <u>local</u> effects can be identified. Since the tendency of the surface states to be localized at the surface is a property of all bonded solids, cyrstal and amorphous, the theory and the simplifications inherent in it are also applicable to crystal surfaces. Accordingly, the methods discussed in this paper can be applied to an enormous variety of materials. We feel that the approach holds great promise for clarifying some of the fundamental problems of surface physics.

CHAPTER III

BULK ELECTRONIC STRUCTURES OF CRYSTALLINE AND AMORPHOUS SiO_2

In this chapter, we shall be concerned with the electronic properties of bulk amorphous SiO_2. The goal of this chapter is to pave the way towards an understanding of disorder, defects, surfaces and interfaces in SiO_2 using the cluster-Bethe-lattice technique. Despite the fact that crystalline forms of SiO_2 have been studied extensively[26-37] in recent years, disordered SiO_2 systems have not received adequate theoretical attention because of their extreme complexity. As was demonstrated in the previous two chapters, however, the cluster-Bethe-lattice method is an excellent approach for calculating excitations of these structurally indeterminate, infinite, non-periodic systems realistically.

An important step in the application of the cluster-Bethe-lattice method is the development of a realistic tight-binding description of the bulk. In this chapter, we therefore concentrate on developing a tight-binding Hamiltonian for α-quartz and using it to extrapolate to the most fundamental disordered system, the bulk amorphous material. In doing so, we develop a picture of SiO_2 which stresses the importance of the local atomic environment, and in which features of the electronic structure universal among all allotropes of SiO_2 are identified. We go beyond previous local descriptions in that we explain the widths and shapes of the major bands as well as their centers of mass. This enables us to obtain a quantitative understanding of the formation of the fundamental gap in SiO_2, and necessitates a new picture of bonding in SiO_2 in which oxygen 2s states play a crucial role. It also enables us to understand quantitatively the local symmetries of the states at the valence and conduction band edges, and thus shed light on the nature of the optical absorbtion edge. In addition to discussing the similarities between the crystalline and amorphous phases, we also discuss differences, in particular those resulting from topological and bond-angle disorder in the glass.

The plan of the chapter is as follows. In the first section, we discuss the solution of the electronic Bethe lattice. In the second section, we discuss bonding in SiO_2, starting with the bond-orbital[27] picture, which serves as a useful guide in constructing other types of localized description of the electronic states. In the fourth section, we compare the results for α-quartz and its Bethe lattice counterpart. In the fifth section, we discuss: (i) the relation between the shapes of the major bands, (ii) the symmetries of the states about the silicon centers, (iii) the disallowed nature of the first optical transitions, and (iv) the role of the various tight-binding parameters in shaping the density of states. In the sixth section, we discuss the ionicity of SiO_2 in the context of the formation of the fundamental gap, and the significance to the formation of the gap of the oxygen 2s wave function admixture in the lowest conduction states. In the seventh section, we discuss the effects of topological and bond-angle disorder in the glass. We conclude with a summary.

3.1. The Electronic Bethe Lattice

We shall illustrate the Bethe lattice formalism with an idealized form of SiO_2 in which each atom possesses only one s state. If the silicon and oxygen wavefunctions are denoted ψ_{Si} and ψ_O, then the simplified Hamiltonian is summarized as

$$\langle\psi_{Si}|H|\psi_{Si}\rangle = \varepsilon_{Si} \tag{45}$$

$$\langle\psi_O|H|\psi_O\rangle = \varepsilon_O \tag{46}$$

$$\langle\psi_{Si}|H|\psi_O\rangle = V \tag{47}$$

$$\langle\psi_O|H|\psi_O'\rangle = V' \tag{48}$$

where only nearest-neighbor interactions are nonzero.

To solve the Bethe lattice, we first renormalize away the silicon degree of freedom, effectively transforming the Hamiltonian into that of Weaire and Thorpe[38]:

$$\langle\psi_O|\tilde{H}|\psi_O\rangle = \tilde{\varepsilon}_O = \varepsilon_O + \frac{2V^2}{\varepsilon - \varepsilon_{Si}} \tag{49}$$

$$\langle\psi_O|\tilde{H}|\psi_O = \tilde{V} = V' + \frac{V^2}{\varepsilon - \varepsilon_{Si}} \tag{50}$$

This is depicted schematically in Fig. 21(a). We then confine the

Figure 21: Interaction diagram for the model Bethe lattice.

(a) With silicon degree of freedom removed, and

(b) with each oxygen orbital replaced formally with two orbitals strongly bonded together.

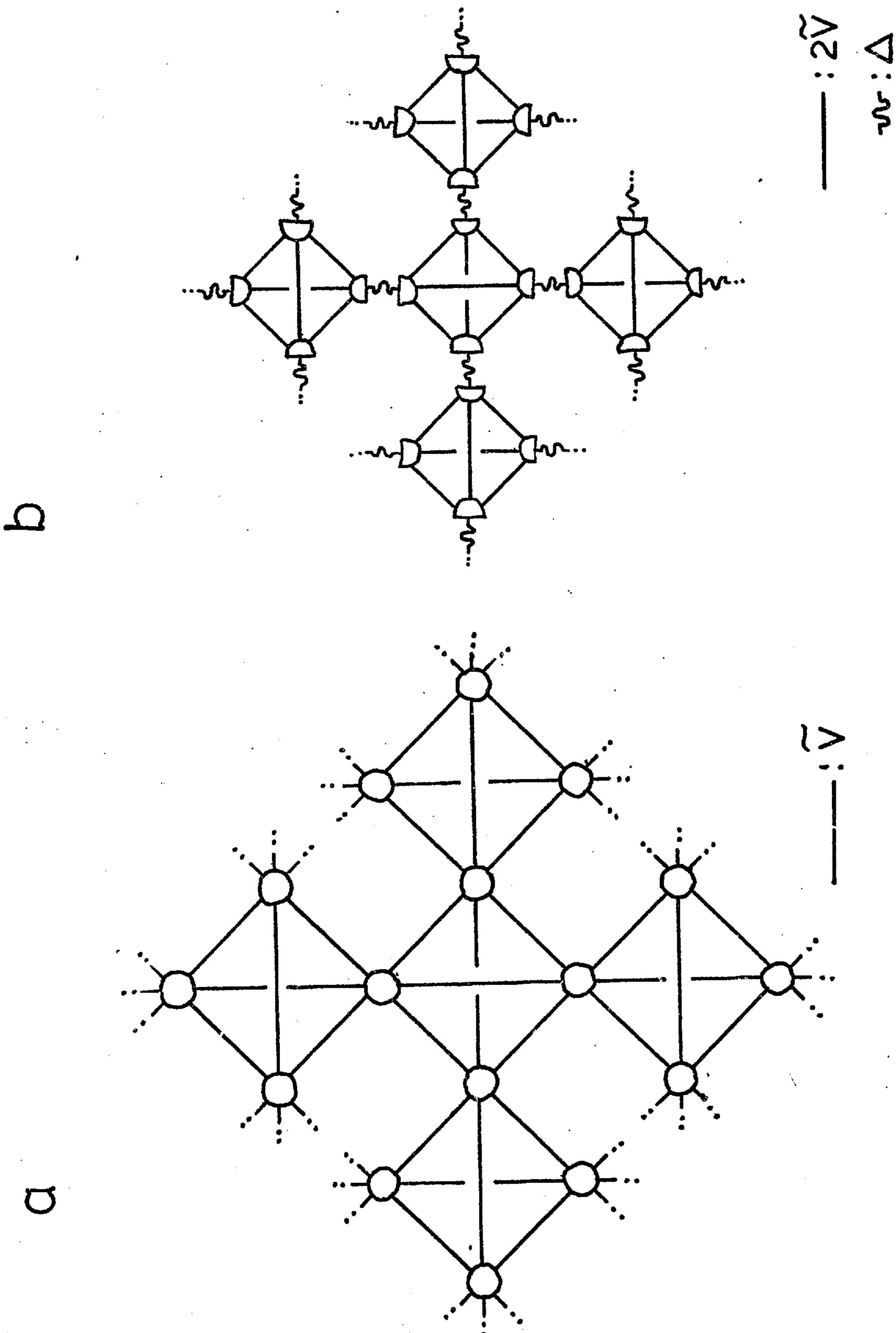

a
b
: $\tilde{V}$
: $2\tilde{V}$
: Δ

Hamiltonian to an O_4 molecule. As this has tetrahedral symmetry, the Hamiltonian is diagonalized trivially with one A_1 and three F_2 states:

$$|A_1\rangle = \frac{1}{2}\left(|\psi_1\rangle + |\psi_2\rangle + |\psi_3\rangle + |\psi_4\rangle\right) \tag{51}$$

$$|F_2\rangle = \frac{1}{2}\left(|\psi_1\rangle + |\psi_2\rangle - |\psi_3\rangle - |\psi_4\rangle\right) \tag{52}$$

$$\vdots \qquad\qquad\qquad\qquad \vdots$$

the eigenvalues of which are

$$\varepsilon_{A_1} = \tilde{\varepsilon}_o + 3\tilde{V} \tag{53}$$

and

$$\varepsilon_{F_2} = \tilde{\varepsilon}_o - \tilde{V} \quad . \tag{54}$$

The intra-molecular Green's function is thus given by

$$G = \frac{1}{\varepsilon - \varepsilon_{A_1}} |A_1\rangle\langle A_1| + \frac{1}{\varepsilon - \varepsilon_{F_2}} \sum_j |F_2^j\rangle\langle F_2^j| \tag{55}$$

Attaching the rest of the Bethe lattice is equivalent to adding an energy-dependent self-energy Z to each orbital. In the Bethe lattice, one then has for the Green's function confined to a molecule:

$$G = \frac{1}{\varepsilon - \varepsilon_{A_1} - Z} |A_1\rangle\langle A_1| + \frac{1}{\varepsilon - \varepsilon_{F_2} - Z} \sum_j |F_2^j\rangle\langle F_2^j| \tag{56}$$

The diagonal Green's function matrix element associated with an oxygen orbital is thus

$$G_{11} = \frac{1/4}{\varepsilon - \varepsilon_{A_1} - Z} + \frac{3/4}{\varepsilon - \varepsilon_{F_2} - Z} \tag{57}$$

Similar reasoning, however, may be applied to an isolated orbital. In the absence of the rest of the system, the Green's function of an orbital is

$$G_{11} = \frac{1}{\varepsilon - \tilde{\varepsilon}_0} \tag{58}$$

In the presence of the rest of the system, one has

$$G_{11} = \frac{1}{\varepsilon - \tilde{\varepsilon}_0 - 2Z} \tag{59}$$

The self-energy, Z, is thus determined by the condition

$$\frac{1}{\varepsilon - \tilde{\varepsilon}_0 - 2Z} = \frac{\frac{1}{4}}{\varepsilon - \varepsilon_{A_1} - 2Z} + \frac{\frac{3}{4}}{\varepsilon - \varepsilon_{F_2} - Z} \; . \tag{60}$$

Equation (60) may be solved iteratively or as a polynomial. The Bethe lattice density of states is then given by

$$\rho(E) = -\frac{1}{\pi}\,\mathrm{Im}\left(\frac{1}{\varepsilon - \varepsilon_0 - 2Z}\right) \; . \tag{61}$$

The significance of the eigenvalues appearing in the denominators of equation (60) may be easily understood in terms of the unbonded Weaire-Thorpe system, shown in Fig. 21(b). This Bethe lattice, which is a system of interacting O_4 molecules, is equivalent to the one on the left in the limit of large Δ. Up to a self-energy shift of $-\Delta$ counteracting the shift due to bonding, the A_1 and F_2 eigenvalues of a molecule are

$$\varepsilon'_{A_1} = 2\varepsilon_{A_1} - \tilde{\varepsilon}_0 \tag{62}$$

$$\varepsilon'_{F_2} = 2\varepsilon_{F_2} - \tilde{\varepsilon}_0 \; . \tag{63}$$

Substituting

$$Z = \frac{\varepsilon - \varepsilon_0}{2} + \frac{\delta}{2} \tag{64}$$

into equation (60) we obtain

$$-\frac{1}{2\delta} = \frac{\frac{1}{4}}{\varepsilon - \varepsilon'_{A_1} - \delta} + \frac{\frac{3}{4}}{\varepsilon - \varepsilon'_{F_2} - \delta} \; . \tag{65}$$

Thus, the parameters of the system influence its density of states only through the eigenvalues of the isolated O_4 molecule. This may be shown by explicit solution of equation (65) to delimit the band edges.

When a more realistic Hamiltonian is substituted for the simplified one, the analysis in the foregoing section remains basically unchanged but for the substitution of matrices for scalars. An equivalent method of solution is outlined in Appendix B.

3.2. Bonding in SiO_2

It was shown originally by Pantelides and Harrison[27] that the electronic structure of SiO_2 could be understood simply in terms of the electronic levels of a small bonding unit containing an oxygen atom and one sp^3 hybrid from each adjacent silicon atom. Their picture is illustrated in the upper half of figure 22. The three 2p orbitals on the oxygen interact with the hybrids to form five bond-orbitals. The oxygen p state perpendicular to the bonding plane becomes the lone-pair bond-orbital at the O_{2p} level. The remaining nonbonding oxygen p interacts with the symmetric combination of hybrids to form the weak-bonding and weak-antibonding bond-orbitals. As this interaction reduces to zero when the Si-O-Si angle is increased to 180°, the amount of mixing is fairly small. The oxygen p pointing along the bond interacts with the antisymmetric combination of hybrids to form the strong-bonding and strong-antibonding bond-orbitals. The six electrons available for bonding then fill the system up to the lone-pairs, which thus form the upper valence bands. The gap lies between the lone-pair and weak-antibonding energies, which is approximately the difference between the oxygen 2p and silicon hybrid levels.

If the interaction between adjacent hybrids on the same silicon, as well as those between nearest-neighbor oxygen atoms, are

Figure 22: Bond-orbital picture of band formation in SiO_2. Silicon hybrids and oxygen 2p states interact (top) to form five bond-orbitals, each of which subsequently broadens (bottom) into a band of characteristic shape. The width of this band scales with the nearest-neighbor interaction, $\tilde{V}$.

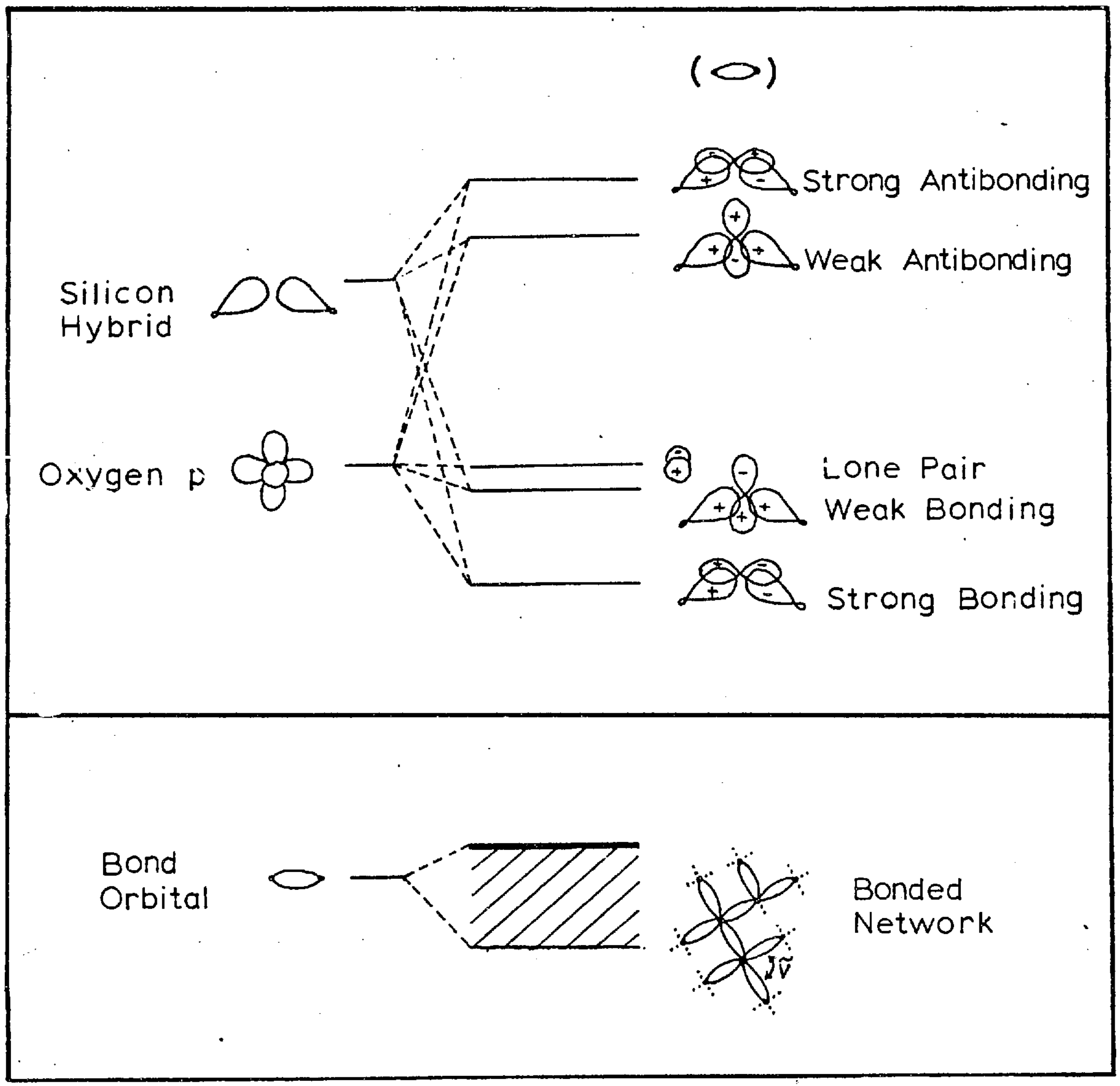

Silicon Hybrid
Oxygen p
Strong Antibonding
Weak Antibonding
Lone Pair
Weak Bonding
Strong Bonding
Bond Orbital
Bonded Network

sufficiently weak, bond-orbitals will interact effectively only with others of the same species. This is illustrated in the lower half of figure 22. To an excellent approximation, bond-orbitals interact only when they are adjacent, and always with the same interaction $\tilde{V}$. Thus the Hamiltonian which describes the broadening of a bond-orbital into a band is always the same, up to the magnitude of $\tilde{V}$, which determines the band's width. By inspection, assuming no odd-fold rings of bonds, the completely bonding state is lowered by $6\tilde{V}$, while the antibonding state is raised by $-2\tilde{V}$. This delimits the band. As the center of mass is unshifted, the antibonding states must be always more dense than the bonding states.

In the section on the bending nature of the gap, we shall criticize the bond-orbital picture just described on the grounds that it excludes oxygen 2s states. We remark at this point that inclusion of oxygen s states does not alter the picture qualitatively. Even if bonding between these states and silicon hybrids is important, by symmetry only the weak-antibonding bond-orbital will acquire significant oxygen s character. In principal, the weak-bonding state is also affected, but in practice the amount of silicon character in it is too small. The primary effect, therefore, of including oxygen 2s - silicon hybrid interactions is to push the oxygen s and weak-antibonding levels apart while mixing their characters slightly. This has been noted previously by Yndurain.[39]

3.3. Densities of States

Experimentally,[26,37,40-43] the electronic structures of crystalline and amorphous SiO_2 are known to be very similar. In figure 23, we show X-ray photoemission spectra[40] of the crystal and the glass, in which this similarity is quite pronounced. In each case, one sees two distinct bands, one composed of both weak-bonding and lone-pair states (0-5 eV) and another which is strong-bonding (6-11 eV). The widths of these bands are the same in both materials, as are their overall shapes. There is structure in the strong-bonding band of α-quartz near 9 eV which is absent in amorphous silica, but the peak at 6 eV is invariant. The lone-pair-like band tends to lose some fine structure and peak up slightly in the center as the material is made amorphous. Overall, however, the differences between these two spectra are subtle.

In figure 24, we show theoretical densities of states for α-quartz and the Bethe lattice calculated using an empirical tight-binding Hamiltonian fit to the self-consistent pseudopotential band structure of α-quartz[28] and to experiment[40]. In each case one sees four distinct bands: the oxygen s states (-22 to -19 eV), the strong-bonding states (-11 to -6 eV), the lone pair-like band (-5 to 0 eV), and the weak-antibonding conduction states (10 eV and above). There is structure in the center of the strong-bonding band of α-quartz near 9 eV which is absent in the Bethe lattice, but the spike near -6 eV is invariant. This effect is also seen in the oxygen s and lower conduction bands. There is virtually no change in

Figure 23: X-ray photoemission spectra of α-quartz (top) and amorphous silica (bottom) taken from Reference 40. The solid curves are smoothed versions of the data, shown in dots.

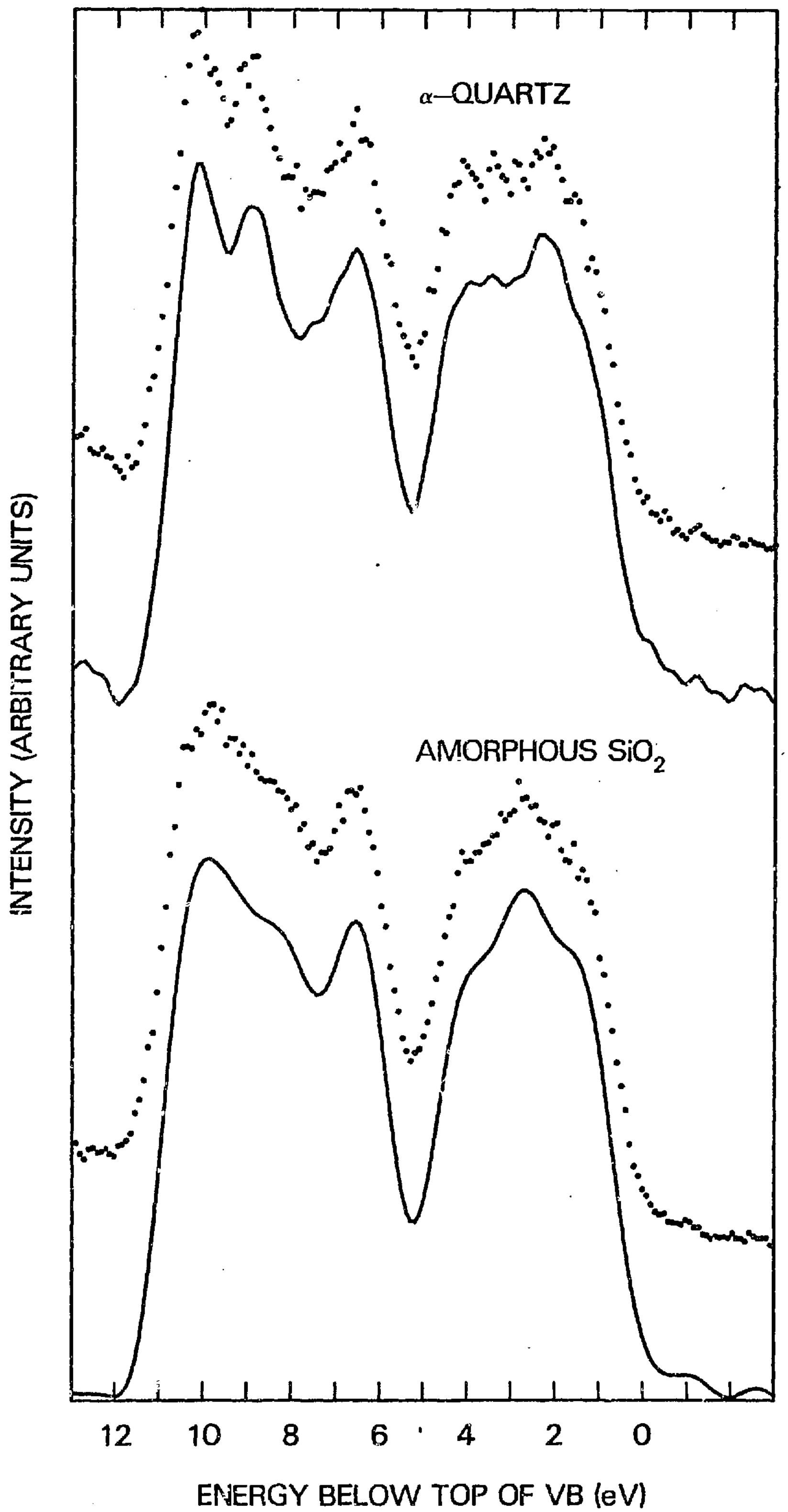
α–QUARTZ
AMORPHOUS SiO_2
INTENSITY (ARBITRARY UNITS)
12 10 8 6 4 2 0
ENERGY BELOW TOP OF VB (eV)

Figure 24: Densities of states of α-quartz and the Bethe lattice calculated using the Hamiltonian listed in Table I.

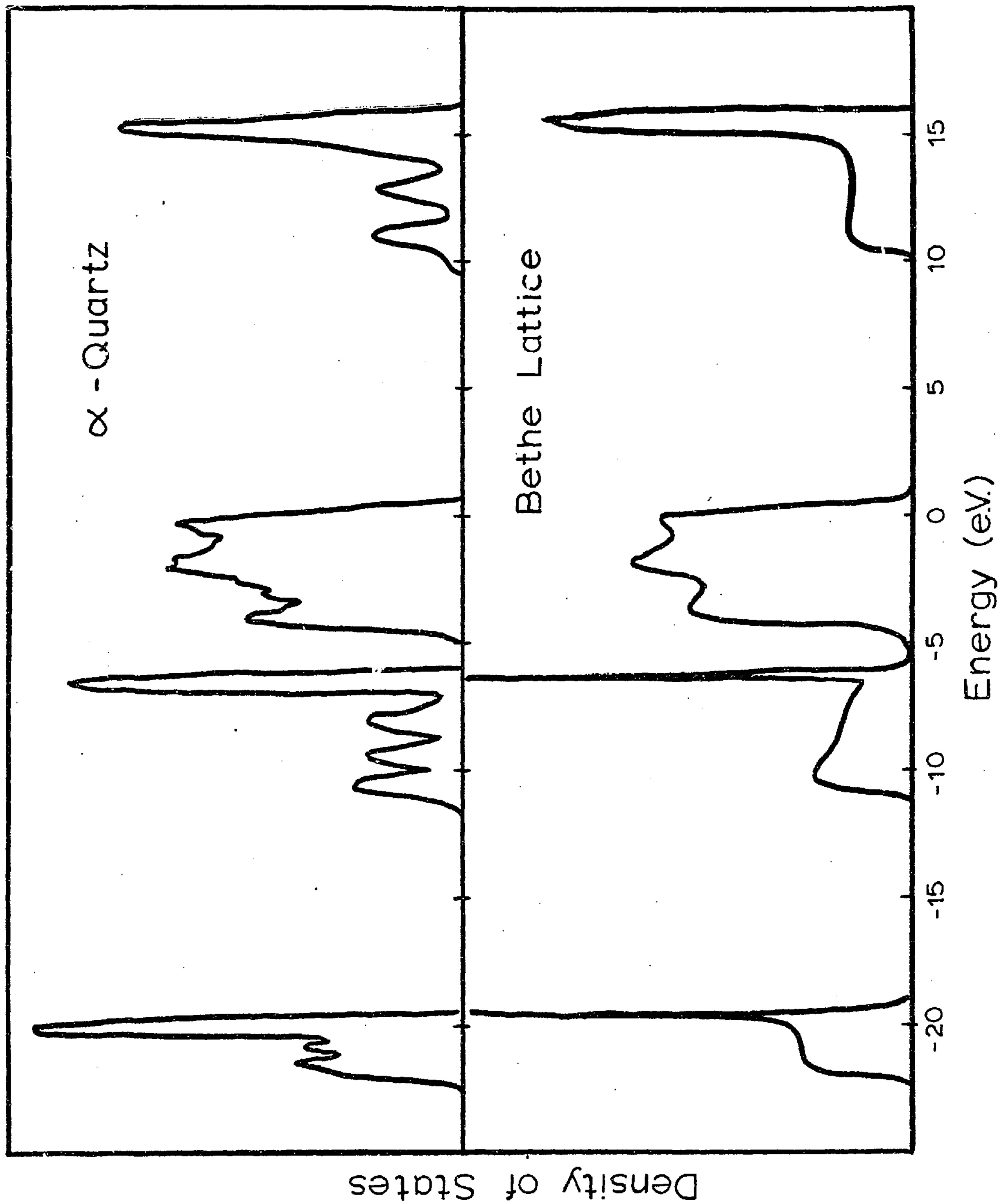
α -Quartz
Bethe Lattice
Density of States
Energy (eV.)
-20
-15
-10
-5
0
5
10
15

the lone-pair-like band when the Bethe lattice is substituted for α-quartz.

The calculated band structure of α-quartz along the principal symmetry directions of the Brillouin zone is shown in figure 25. As the pseudopotential[28] calculation gives the wrong splitting between the oxygen s and strong-bonding bands, this distance has been fit to X-ray emission[43] and XPS[40] data. The gap is indirect (A to Γ) and has a magnitude of 9.2 eV. The ordering of the degeneracies at symmetry points agrees with the pseudopotential except in the lone-pair-like bands. The density of bands in this region is so great that simultaneously fitting the density of states and the ordering of the degeneracies is impossible with the parameterization we have chosen. The dispersion of the remaining bands shows considerable duplication. The oxygen s, strong-bonding and lower conduction regions all contain six bands, only three of which disperse significantly. These three clearly scale between the oxygen s and lower conduction bands but have their degeneracies reversed in the strong-bonding bands. This reversal is due to the negative phase between the silicon hybrids in the bond-orbital. In each of these three regions, the remaining non-dispersive bands induce a large density of states at the upper edge of the band.

The parameters used in the tight-binding Hamiltonian are summarized in Table 1. The basis set consists of Si_{3s}, Si_{3p}, O_{2s}, and O_{2p} states only. All possible nearest-neighbor Si-O interactions are included, as are small nearest-neighbor O-O interactions. These

Figure 25: Band-structure of α-quartz calculated using the Hamiltonian listed in Table I.

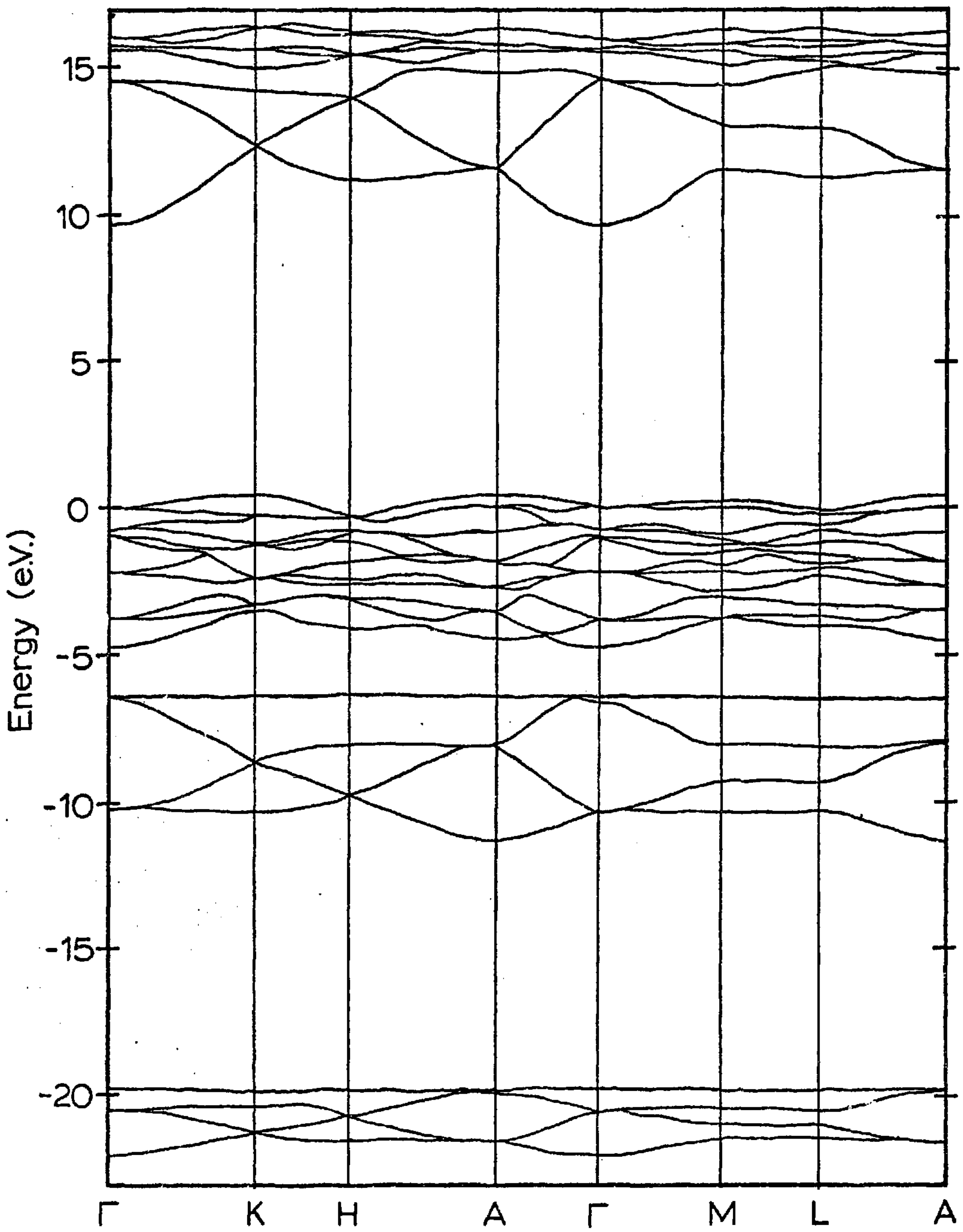

Energy (e.V.)
15
10
5
0
-5
-10
-15
-20
Γ
K
H
A
Γ
M
L
A

Table I: Tight binding parameters for SiO_2: Oxygen-oxygen parameters are defined relative to the O-Si-O bonding plane. Oxygen p orbitals in the plane may lie either along the bond or perpendicular to it. The possible in-plane interactions allowed by symmetry are parameterized by V_1^o through V_3^o.

$$\langle Si_s|H|Si_s\rangle = 4.95 \qquad \langle O_s|H|O_s\rangle = -16.4$$

$$\langle Si_p|H|Si_p\rangle = 11.2 \qquad \langle O_p|H|O_p\rangle = -1.3$$

$$\langle Si_s|H|O_s\rangle = -3.05$$

$$\langle Si_p|H|O_s\rangle = -7.0$$

$$\langle Si_s|H|O_p\rangle = -5.4$$

$$\langle Si_p|H|O_p\rangle_{\sigma} = 5.4$$

$$\langle Si_p|H|O_p\rangle_{\pi} = -1.4$$

$\langle O'|H|O\rangle$:

$$V_1^O = 0.574$$

$$V_2^O = -0.548$$

$$V_3^O = -0.75$$

$$V_4^O = 0.26$$

$$V_5^O = -0.45$$

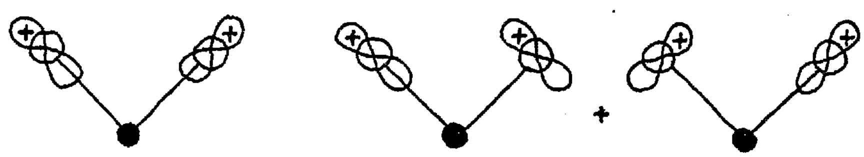

V_1^O V_2^O

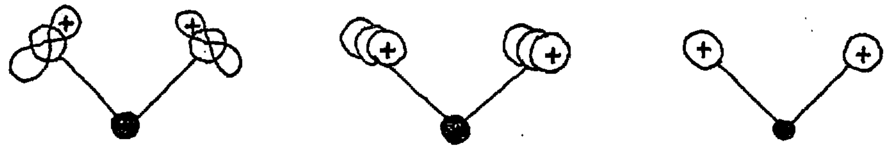

V_3^O V_4^O V_5^O

latter are described in Table 1. The criteria for determining the parameters are discussed in the next section.

3.4. Shapes of Bands

The oxygen s, strong-bonding and lower conduction bands have in common a characteristic shape in the Bethe lattice which carries over to α-quartz, up to additional superimposed structure. These bands all derive from a single bond-orbital and are thus described by the bonding part of the Weaire-Thorpe Hamiltonian.[38] The solution of the Bethe lattice using this Hamiltonian has been outlined in equations (45) through (65). If $\tilde{\varepsilon}_0$ is the energy of the bond-orbital and $\tilde{V}$ is the interaction between two bond-orbitals in the same tetrahedron, then one may substitute

$$\varepsilon'_{A_1} = \tilde{\varepsilon}_0 + 6\tilde{V} \tag{66}$$

$$\varepsilon'_{F_2} = \tilde{\varepsilon}_0 - 2\tilde{V} \tag{67}$$

into equation (65) to obtain the density of states. The symmetry of the states about the silicon centers is reflected in the local densities of states, the density of states weighted by the square of the amplitude of each state on an A_1 or F_2 combination of bond-orbitals. These are given by

$$\rho_{A_1}(\varepsilon) = -\frac{2}{\pi}\,\mathrm{Im}\left(\frac{1}{\varepsilon - \varepsilon'_{A_1} - \delta}\right) \tag{68}$$

$$\rho_{F_2}(\varepsilon) = -\frac{2}{\pi}\,\mathrm{Im}\left(\frac{1}{\varepsilon - \varepsilon'_{F_2} - \delta}\right) . \tag{69}$$

We have

$$\rho(\varepsilon) = \frac{1}{4}\,\rho_{A_1}(\varepsilon) + \frac{3}{4}\,\rho_{F_2}(\varepsilon) \tag{70}$$

In figure 26, we show the solutions to these equations for $\varepsilon_0 = 0$ and $V = -1$. The characteristic asymmetry seen in these three bands is accurately reproduced. The states at the bonding edge may be seen to have pure A_1 character, while the antibonding states are pure F_2. X-ray emission spectroscopy,[43] which probes the local densities of states, verifies this A_1 - F_2 asymmetry for both the oxygen s and strong-bonding bands: The lower edges of both are enhanced in the Si $L_{2,3}$ spectrum, while the upper edges are enhanced in the Si K_β.

It is clear from figure 24 that the three-peak structure of the lone-pair-like band also results from local symmetries which are preserved in the Bethe lattice. This can be understood in terms of a model similar to that used to describe the strong-bonding band. The width of the lone-pair-like band, which is due almost entirely to the oxygen-oxygen interactions, is much greater than the splitting between the lone-pair and weak-bonding bond-orbitals. It is appropriate, therefore, to treat this splitting as a perturbation to the system in which the Si-O-Si angle is 180°. This approximate

Figure 26: Solutions of equations (68) - (70), representing the density of states and orbital symmetries of an idealized bond-orbital-derived band.

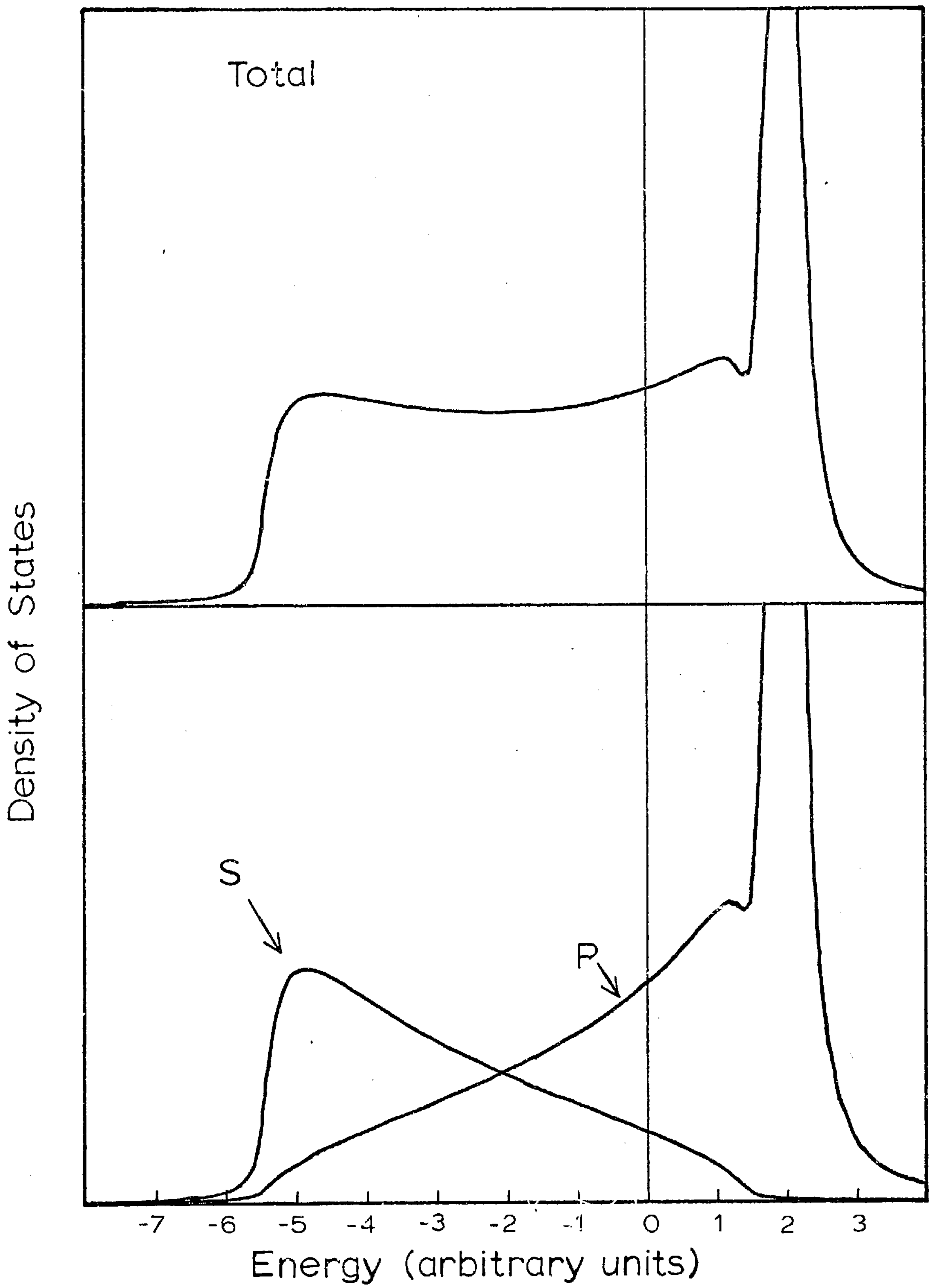
Total
S
P
Density of States
-7 -6 -5 -4 -3 -2 -1 0 1 2 3
Energy (arbitrary units)

system may be further idealized by formally removing all unnecessary orbitals: all those except the oxygen p states perpendicular to the bond. The model thus formed may be solved by analogy with equations (45) through (65). Each oxygen orbital is split into two, and one half assigned to each adjacent O_4 molecule. The transformed Hamiltonian, confined to a molecule, then splits the molecule into energy eigenstates, the eigenvalues of which appear in the denominators of equation (65). In this case, however, there are eight degrees of freedom in the molecule and three energy eigenvalues: a doubly-degenerate E state, a triply-degenerate F_2 state, and a triply-degenerate F_1 state. The analog of equation (65) for the lone-pair-like band is thus

$$-\frac{1}{2\delta} = \frac{2/8}{\varepsilon - \varepsilon_E' - \delta} + \frac{3/8}{\varepsilon - \varepsilon_{F_2}' - \delta} + \frac{3/8}{\varepsilon - \varepsilon_{F_1}' - \delta} \quad . \qquad (71)$$

In figure 27 we show the solution to equation (71) together with the E, F_1 and F_2 local densities of states. The eigenvalues are those resulting from the oxygen-oxygen interactions listed in Table 1, with the O_{2p} energy set to zero. The shape is very similar to that seen in figure 24, up to excessive strength near 2 eV and the lack of a discernable peak at -2 eV. Both of these disparities result from the absence of the Si-O-Si bend. These differences notwithstanding, the calculation shows clearly that the three-peak structure results from the integrity of the SiO_4 tetrahedra.

The oxygen-oxygen interactions have been fit to order the

Figure 27: Solution of equation (71), representing the density of states and orbital symmetries of an idealized lone-pair-like band.

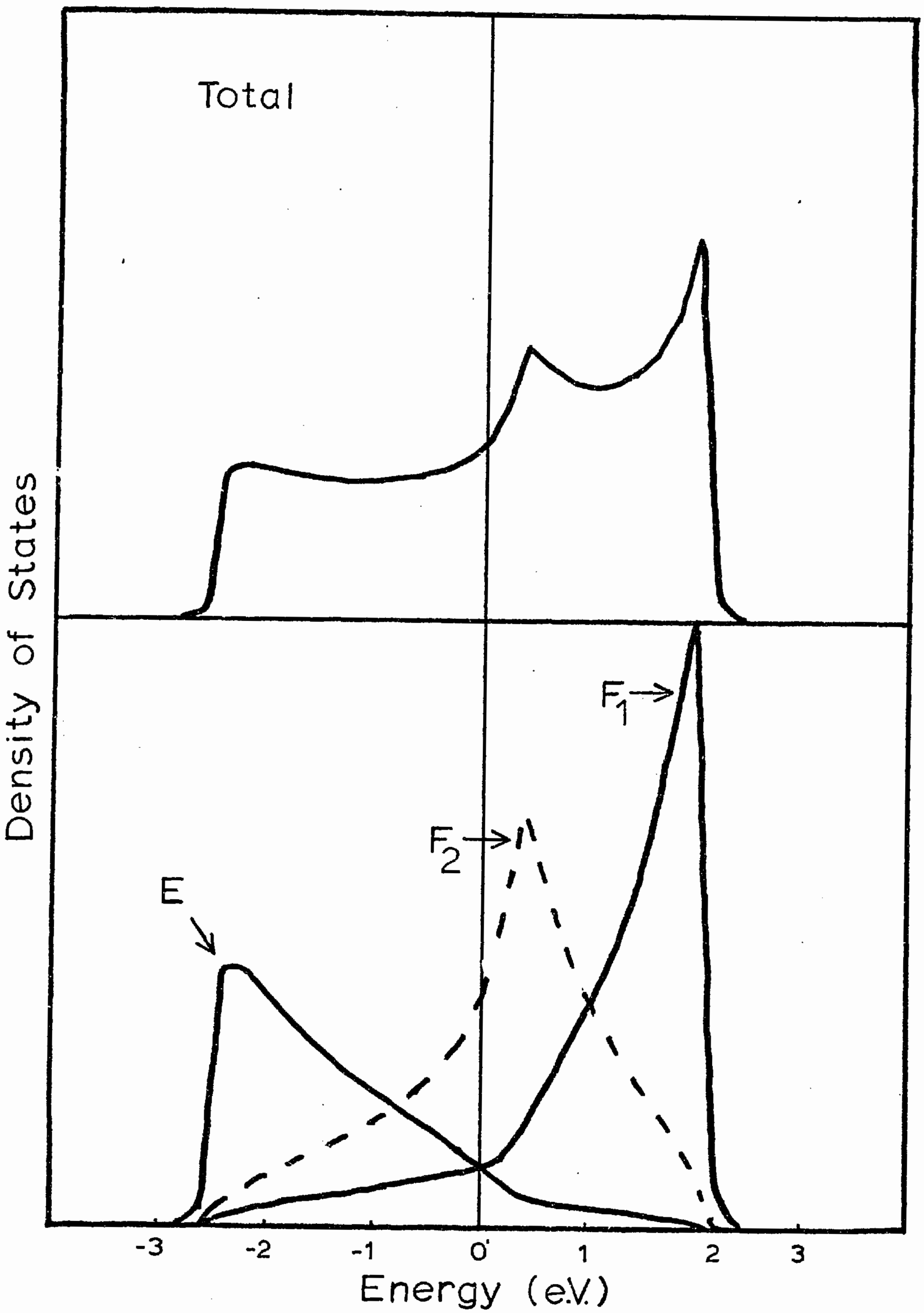
Total
Density of States
F1
F2
E
-3
-2
-1
0
1
2
3
Energy (e.V.)

eigenvalues in the manner

$$\varepsilon_E < \varepsilon_{F_2} < \varepsilon_{F_1} \tag{72}$$

as this is the ordering found in two less empirical calculations performed for the SiO_4 molecule.[29,34] We emphasize, however, that this ordering is also consistent with the pseudopotential results.[28] The pseudopotential density of states in this region is asymmetric, the low-energy side being smaller. This would indicate that the eigenvalue with the smallest degeneracy is the most deeply bound. In addition, the first direct optical transitions in the pseudopotential calculation appear to be dipole-forbidden, despite the lack of any obvious symmetry of α-quartz which should prevent them. As the lowest conduction states have s-like symmetry about the silicon centers, a reasonable explanation for this selection rule is that the states at the valence band maximum have F_1 symmetry. The orbital densities of states in the lower half of figure 27 show this to be the case with the ordering we have chosen. The F_2 state is p-like about the silicon centers, while the F_1 and E states together form a d-like manifold. Based on this interpretation, we predict that the first direct transition will be forbidden in any allotrope of SiO_2 in which the SiO_4 tetrahedra remain intact.

The model calculations discussed in this section demonstrate that parameterizing the density of states of SiO_2 effectively reduces to parameterizing a set of eleven eigenvalues, which lie at the major band edges and at peaks in the density of states. These include the A_1 and F_2 eigenvalues of the oxygen s, strong-bonding, weak-antibonding and strong-antibonding bands as well as the E, F_1 and F_2 eigenvalues of the lone-pair-like band. They may be obtained as eigenvalues of five small matrices having tight-binding parameters as elements. These are listed in Table 2. Although the table is strictly valid only when the Si-O-Si angle is 180°, it is generally helpful in showing the approximate functions of the various parameters. For example, the π interaction, which is not included in the bond-orbital picture at all, may be seen from Table 2 to couple silicon p states to the F_2 combination of lone-pair-like orbitals. It primarily causes the latter to interact virtually with itself and with the p-like spike of the strong-bonding band. This results in an apparent shift of its energy and a shifting and severe broadening of the spike. Table 2 also shows that the oxygen-oxygen parameter V_2^O has a similar effect. The fact that this spike is fairly sharp in the pseudopotential results indicates that either these parameters are small or their effects cancel.

All of the necessary eigenvalues but two may be obtained from the pseudopotential density of states or from experiment. The remaining two fall somewhere in the upper conduction bands beyond 15 eV, where both the pseudopotential and tight-binding calculations are unreliable. For want of a better value, we have set them both to roughly 17 eV. As the pseudopotential results show that the peak at 15 eV is not weak-antibonding in character, we have made it strong-antibonding. This is not completely correct either, however, and thus

Table II: Six small matrices, the eigenvalues of which determine peaks and band edges in the Bethe lattice density of states.

$$2A_1: \quad \begin{bmatrix} \langle O_s|H|O_s\rangle + 6V_5^0 & \sqrt{8}\langle O_s|H|Si_s\rangle \\ \sqrt{8}\langle Si_s|H|O_s\rangle & \langle Si_s|H|Si_s\rangle \end{bmatrix}$$

$$2A_1: \quad \begin{bmatrix} \langle O_p|H|O_p\rangle + 6V_1^0 & \sqrt{8}\langle O_p|H|Si_s\rangle \\ \sqrt{8}\langle Si_s|H|O_p\rangle & \langle Si_s|H|Si_s\rangle \end{bmatrix}$$

$$2F_2: \quad \begin{bmatrix} \langle O_s|H|O_s\rangle - 2V_5^0 & \sqrt{\frac{8}{3}}\langle O_s|H|Si_p\rangle \\ \sqrt{\frac{8}{3}}\langle Si_p|H|O_s\rangle & \langle Si_p|H|Si_p\rangle \end{bmatrix}$$

$$3F_2: \quad \begin{bmatrix} \langle O_p|H|O_p\rangle - 2V_1^0 & 4V_2^0 & \sqrt{\frac{8}{3}}\langle O_p|H|Si_p\rangle_\sigma \\ 4V_2^0 & \langle O_p|H|O_p\rangle + V_3^0 + 3V_4^0 & \sqrt{\frac{16}{3}}\langle O_p|H|Si_p\rangle_\pi \\ \sqrt{\frac{8}{3}}\langle Si_p|H|O_p\rangle_\sigma & \sqrt{\frac{16}{3}}\langle Si_p|H|O_p\rangle_\pi & \langle Si_p|H|Si_p\rangle \end{bmatrix}$$

$$1F_1: \quad \begin{bmatrix} \langle O_p|H|O_p\rangle - 3V_3^0 - V_4^0 \end{bmatrix}$$

$$1E: \quad \begin{bmatrix} \langle O_p|H|O_p\rangle + 3V_3^0 - 3V_4^0 \end{bmatrix}$$

the character of our conduction bands is probably unreliable above 14 eV. With the eigenvalues established in this manner, we have 11 constraints on the Hamiltonian and 14 parameters. To constrain the parametrization completely, we set the orbital self-energies to their atomic values, but allow the silicon levels to shift together relative to the oxygen levels. We find that in order to fit the density of states, particularly to open up the gap, the silicon levels must be shifted upward between 4.5 and 7 eV, depending on what one takes for the atomic levels.

3.5. The Bonding Nature of the Gap

One of the oldest controversies about SiO_2 is whether it is ionic or covalent. In the sense of charge transfer, there is no controvery: the amount of charge on an oxygen atom is usually estimated to be -1, placing SiO_2 easily in the category of ionic materials. In the sense of the gap, however, the issue is far from resolved. In a classical ionic materials, such as NaCl, the electronic levels of the neutral anion and cation are very different, so that qualitatively, as the atoms are brought together to form the solid, relatively little bonding occurs, and the size of the gap reflects primarily the disparity in the atomic levels. In a classical covalent material, such as silicon, the anion and cation levels are so similar (equal) that the size of the gap reflects primarily the strength of the bonding interaction. Which of these pictures is more appropriate for describing SiO_2 bears heavily on the question of inhomogenities and defects. If one breaks a bond in a covalent material, for example, the gap region will be severly perturbed, and the result will be a dangling-bond state in the gap. In an ionic material, on the other hand, the perturbation is small and there will be no state in the gap.

The charge densicies produced by the pseudopotential calculation show that the lowest conduction states of α-quartz have considerable oxygen s character. This is usually interpreted as oxygen 3s, the implicit understanding being that there is an accidental degeneracy of these states with the excited oxygen 3s resonance, which thus mixes in without significantly altering the energies. There are two strong arguments in favor of this picture:

a) Assuming that the O_{2p} level lies at the center of the lone-pair-like band, the O_{3s} state lies at roughly this energy.

b) The O_{2s} states and lower conduction bands are separated by 30 eV, an excessively large range over which to find significant oxygen 2s character.

Despite these arguments, however, we believe that the significant oxygen character is not 3s but 2s, and that is presence is crucial to the formation of the gap in SiO_2. The reasons are the following:

a) The atomic silicon 3s and oxygen 2p levels are approximately equal. Unless bonding of silicon s states with oxygen 2s is introduced, the gap can be opened only by raising the silicon levels between 7 and 9 eV. This is very unphysical, in light of the enormous charge transfer in

SiO_2. We have, in fact, been able to take matrix elements of atomic wavefunctions across the pseudopotential[44] and find, not surprisingly, that the silicon 3s level lies slightly below the oxygen 2p.

b) The pseudowavefunction of the lowest conduction state is antibonding.[44] The negative phase between silicon and oxygen amplitudes appears to be necessary in order to have orthogonality to the oxygen s bands.

c) The size of the interaction needed to open the gap, the amount of oxygen s character this places in the conduction bands, and the amount of silicon character mixed into the oxygen s bands are all reasonable.

This last statement may be shown to be true by constructing a reasonable tight-binding model which gives charge densities similar to those of the pseudopotential. For this purpose, we have pseudized Herman-Skillman[45] wavefunctions by fitting to two gaussians outside the core (distances in a.u.):

$$\psi_S \propto \exp(-0.180r^2) \tag{73}$$

$$\psi_O \propto \exp(-0.514r^2) \tag{74}$$

With the Si-O-Si angle set to 180°, one obtains the two-level problem for the energies and wavefunctions of the lowest conduction band lowest oxygen s state indicated in the first matrix in Table 2. In

Table 3, we list an alternate set of parameters in which the Si_{3s} and O_{2p} levels are reordered, but which gives the same energies as the parameters in Table 1. This is made possible by the inclusion of a small nearest-neighbor overlap. Using the amplitudes produced by these parameters, we make bonding and antibonding combinations of the wavefunctions (73) and (74), square to produce charge densities, and compare these with the pseudopotential results[28] in Figure 28. The spacing between contours is unform within a frame, but cannot be compared between frames. Figure 28 shows that the charge densities of both the oxygen s and lower conduction bands are consistent with the idea that the gap in SiO_2 is completely covalent. Despite the fact that the oxygen s states contain 12% silicon character, they look free of silicon because the silicon orbitals are so much more diffuse than the oxygen orbitals. The antibonding state is also in excellent agreement with pseudopotential. It contains less oxygen character than it should, however, which seems to indicate that oxygen 3s is participating in the state as well.

We have been able to construct an entire Hamiltonian based on atomic levels which produces densities of states virtually identical to those in Figure 24. We have not listed its parameters, however, because including the non-orthogonality causes the Hamiltonian to be severely overparameterized. It is clear, however, that such nonorthogonal Hamiltonians are closer to the truth as regards the silicon dangling bond states than is the one listed in Table 1.

Table III: Partial listing of a Hamiltonian including nearest-neighbor overlaps which produces the same density of states as the one listed in Table I. These are the parameters pertinent to Figure 28.

$$\langle O_p|H|O_p\rangle = -1.3 \qquad \langle Si_s|H|Si_s\rangle = -4.28$$

$$\langle O_s|H|O_s\rangle = -16.88$$

$$\langle Si_s|H|O_s\rangle = -5.31 \qquad \langle Si_s|O_s\rangle = 0.14$$

$$V_5^o = -0.45$$

Figure 28: Comparison between pseudopotential charge densities and those calculated using the Hamiltonian listed in Table III and the model wavefunctions (73) and (74). The dot in each frame is a silicon atom and the circles are oxygen atoms.

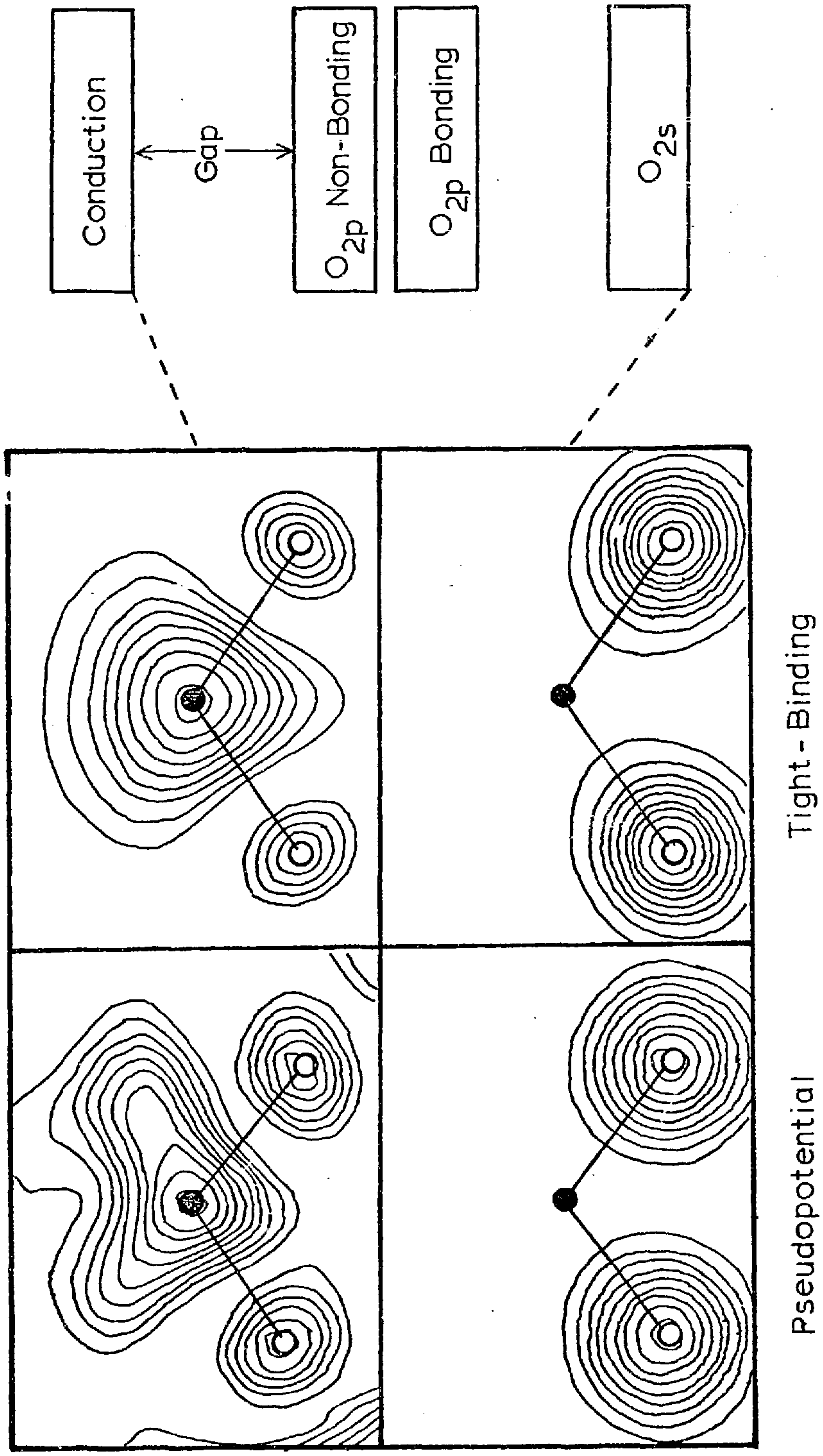
Conduction
Gap
O_{2p} Non-Bonding
O_{2p} Bonding
O_{2s}
Tight-Binding
Pseudopotential

3.6. Disorder

The major differences between the densities of states of crystalline and amorphous silicon have been attributed conclusively[46] to differences in topology. As was discussed in chapter 1, the topological randomness of the disordered system tends to be modeled well by the topological neutrality of the Bethe lattice, so that one can assess the effects of disorder by comparing the crystal and Bethe lattice densities of states. Amorphous silicon is described approximately by the same Hamiltonian[38] which was discussed in section 3.1. Thus, the differences one sees in Figure 24 between the crystal and Bethe lattice strong-bonding bands are exactly analogous to the differences between crystalline and amorphous silicon. The three-peak structure seen in this band in α-quartz has been shown by Thorpe[47] to be due to the presence of six- and eight-bold rings of bonds. In silicon, one has only six-fold rings, and this reduces the number of peaks to two.[46] Nevertheless, the disappearance of this structure when the material is made amorphous, which is evident in Figure 23, is the same phenomenon in both materials, and thus provides additional evidence that the bonding picture of SiO_2 is the correct one. While this structure has not yet been resolved in either the oxygen s or lower conduction bands, it should also be found to disappear in these bands when the solid is made amorphous.

While bond-lengths remain fairly constant in the amorphous material, bond-angle fluctuations, particularly of the Si-O-Si angle, are known[48] to be prevalent. An obvious question to ask is whether these fluctuations are the cause of the disparity in the lone-pair-like bands between the upper and lower halves of Figure 23. To the extent a nearest-neighbor description is accurate, this is not the case. The effect of opening and closing the Si-O-Si angle, for example, may be assessed by comparing the lone-pair-like region in Figure 24 with the top of Figure 27. Qualitatively, changing this angle robs states from one edge of this band and transports them to the other, without changing the band's width or putting states in the center. This is caused by a change in the splitting between the weak-bonding and lone-pair bond-orbitals. In addition, distorting the SiO_4 tetrahedron tends to increase the mean-square splitting of the lone-pair orbitals, and thus the width of the band. As the tight-binding density of states looks more like the amorphous XPS[40] than that of the crystal, a likely explanation is that these effects are caused by distant-neighbor interactions which are disrupted in the glass.

The region of the density of states which should be severely affected by bond-angle disorder is the conduction band edge. When the Si-O-Si angle is 180°, the weak-antibonding bond-orbital, which forms the bottom of the conduction band, contains no oxygen p character. As this angle is bent, progressively more oxygen p is incorporated into the state, resulting in upward motion of this state by 2 eV upon reaching the nominal α-quartz angle of 144°. The magnitude of this effect is determined by the strength of the bonding interaction, which can be determined fairly unambiguously from the splitting between the strong-bonding and lone-pair-like bands. Pantelides and Harrison[27] have shown that the interaction of this state with the oxygen p states should scale as $\cos\left(\frac{\theta}{2}\right)$. Thus the fluctuations of about ±10° seen in this angle in amorphous SiO_2[28] should result in roughly 0.5 eV band tailing at the conduction band edge. We cannot, however, describe the localization, if any, of these states at this time.

3.7. Summary

In this chapter, we have developed a picture of the electronic states of SiO_2 in which periodicity plays no role. Using the Bethe lattice as a structural model for the material, we have been able to attribute quantitatively a number of its properties to the integrity of the local atomic environment, particularly the SiO_4 tetrahedron, in its structure. The most significant of these are the overall shapes of the bands and the dipole selection rule forbidding the first optical transitions. We have also shown that SiO_2 has a classically covalent gap, the great size of which is directly attributable to the presence of oxygen 2s character in the lower conduction bands. As regards disorder, we have made two major points: (a) the major differences between the densities of states of crystalline and amorphous SiO_2 have analogs in silicon, and (b) there should unquestionably be considerable band-tailing from the conduction bands in the glass.

CHAPTER IV

ELECTRONIC STATES OF THE Si-SiO_2 INTERFACE

MOS technology is made possible, to a large extent, by the ability of a layer of silicon dioxide to stabilize a silicon surface, and to eliminate the surface states from it without introducing a large density of interface states in or near the silicon gap. Unfortunately, this elimination is not perfect. There typically remains a residual density of interface states between 10^{11} and 10^{12} per cm^2.[49] These remaining states impeded the operation of the device, and it is therefore of great interest to understand their chemical origin. In this chapter, we introduce a new theory of Si-SiO_2 interfaces we have developed which can shed some light on this problem.

The great disparity between the lattice constants of Si and SiO_2 necessarily causes the interface region between them to be highly disordered; this, in turn, causes the theoretical problem to be extremely difficult. In particular we expect to find regions in the interface in which the bonding is ideal, regions where the bonds are distorted slightly, and regions where bonds are actually broken, and all three types of regions must be included in any realistic theory. Clearly, it would be of great advantage to somehow isolate these regions and study them separately. The method we have used to study the bulk, the cluster-Bethe-lattice method, is ideally suited to this task.

4.1. Ideal Interfaces

The behavior of the interface when it is ideal can be understood very simply in terms of what happens to a silicon surface when it is oxidized. In Fig. 29, we compare local densities of states near a silicon surface when it is bare (left) and after an oxygen atom has been bonded to the surface (right). As one comes up from the interior towards the bare surface, one sees a sharp surface state growing in the middle of the silicon gap and deriving from the dangling sp^3 hybrid orbital at the surface. This contrasts sharply with the behavior when the surface is oxidized. Now as one approaches the surface, one finds no surface in or near the gap, but four oxygen-derived surface states away from the gap. These include the oxygen s level (-28 eV), the oxygen non-bonding p level (-13 eV) and a bonding (-16 eV) and antibonding (5 eV) pair formed by the interaction of an oxygen p state with the dangling hybrid at the surface. Similar features have been seen in ultraviolet photoemission spectra of oxidized silicon surfaces.[50] Now, as the oxide is allowed to thicken, these four surface states broaden and shift slightly to become the three major valence bands and the conduction band of the oxide.

In Fig. 30, we show local densities of states calculated for several atoms in and near an ideal interface. The energy difference between the silicon valence band maximum and the oxide conduction band minimum has been fit to experiment.[51] On the oxygen atom deepest in the oxide we see the three major valence bands and the conduction

Figure 29: Local densities of states versus energy for bare Si surface (left) and for the same surface with an oxygen atom attached (right).

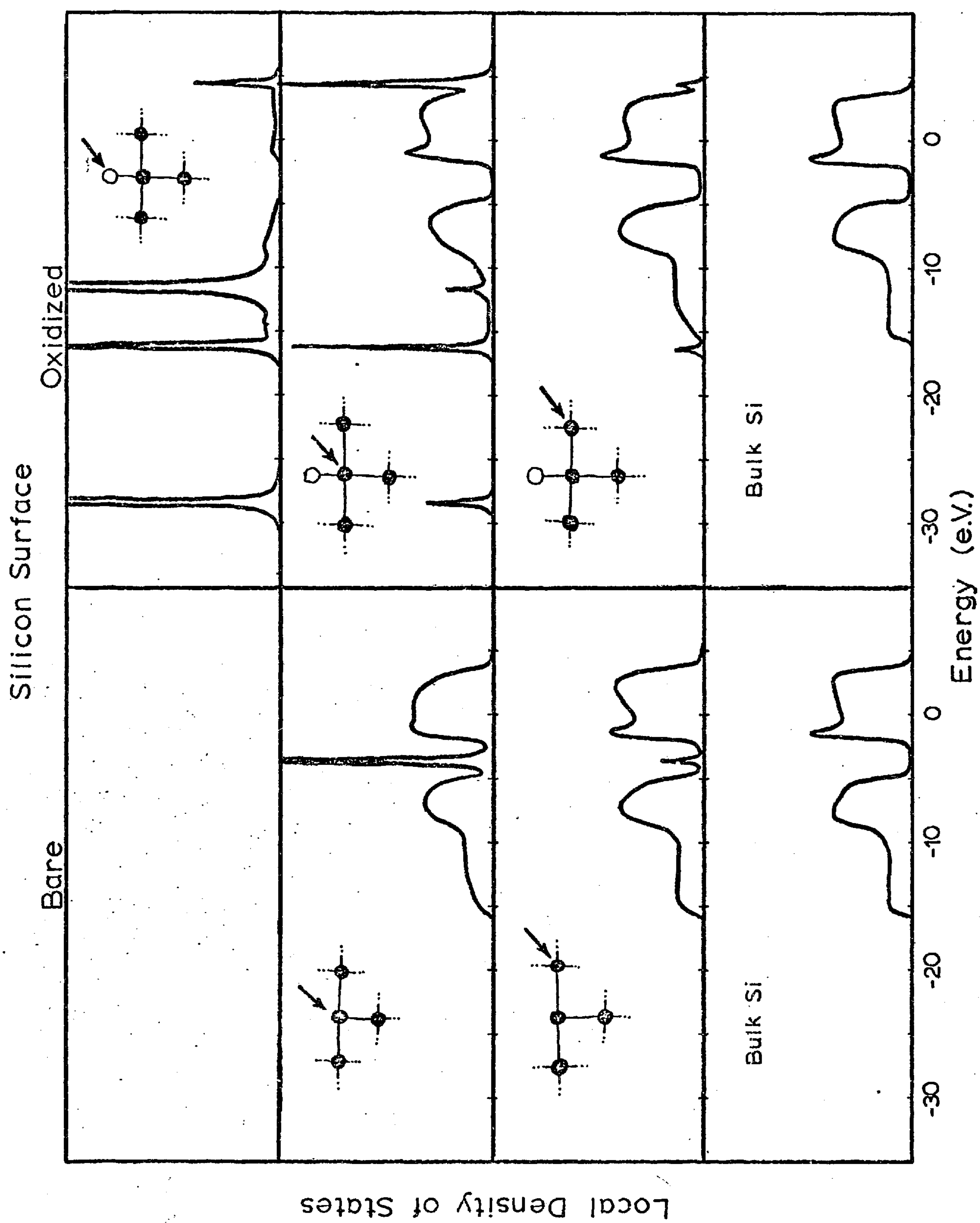
Silicon Surface
Bare
Oxidized
Bulk Si
Bulk Si
-30
-20
-10
0
-30
-20
-10
0
Energy (e.V.)
Local Density of States

Figure 30: Local densities of states versus energy for an ideal interface, starting at the top with an oxygen atom, and proceeding layer-by-layer through the interface and down into the silicon.

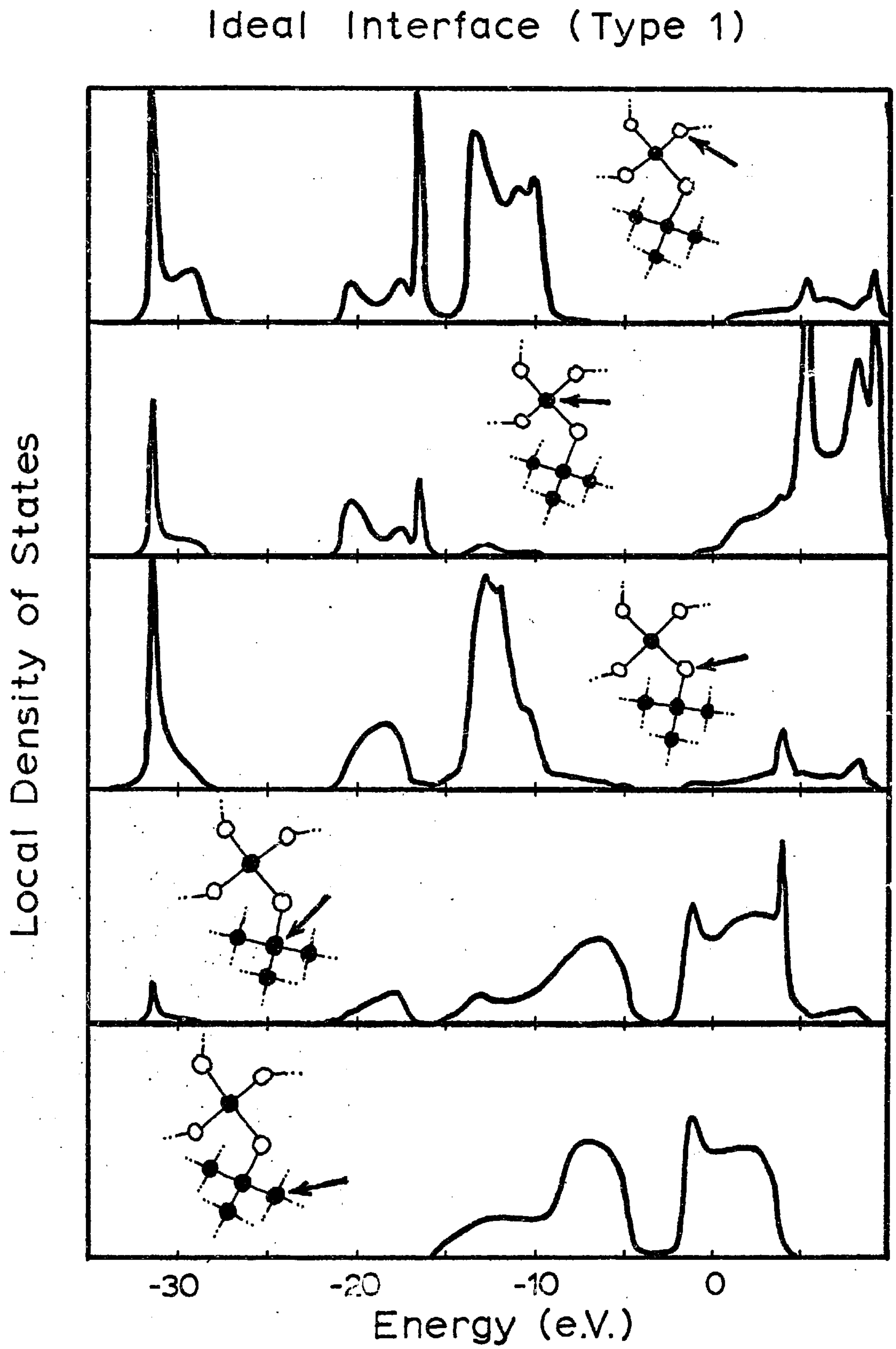
Ideal Interface (Type 1)
Local Density of States
-30
-20
-10
0
Energy (e.V.)

band just mentioned. Again, as we approach the interface from the silicon side, we see no interface state growing in or near the silicon gap. There are, however, interface resonances, in particular one at -18 eV and one at -14 eV. These can be understood simply in terms of the bond-orbital approach of Pantelides and Harrison[27] in that they derive from the incomplete (3-fold) coordination of the strong-bonding and weak-bonding bond-orbitals contained in the isolated Si-O-Si unit at the interface. However, the most important result in Fig. 30 is that there are no interface states near the silicon gap.

4.2. Disordered and Defective Interfaces

Given that an ideal interface is free of states near the gap, the observed states must be caused by deviations from ideal behavior - by disorder in the interface or by bonding defects.

In Fig. 31, we investigate explicitly the effects of distorting the Si-O-Si angle at the interface. The left column is the ideal interface with this angle closed down by 30° from its nominal value of 140°; the right column is the ideal interface with the angle opened by 30°. Concentrating on the region near the silicon gap, we see that very little happens at the valence band edge as the angle is opened. Something very important happens at the conduction band edge, however. The small tail near the conduction band edge in the upper panels grows as the angle is increased, indicating that opening the angle pulls states down out of the conduction band and places them on silicon atoms in the

Figure 31: Local densities of states versus energy for an interface with the same bonding configuration, but with the Si-O-Si angle at the center distorted by -30° (left) and +30° (right).

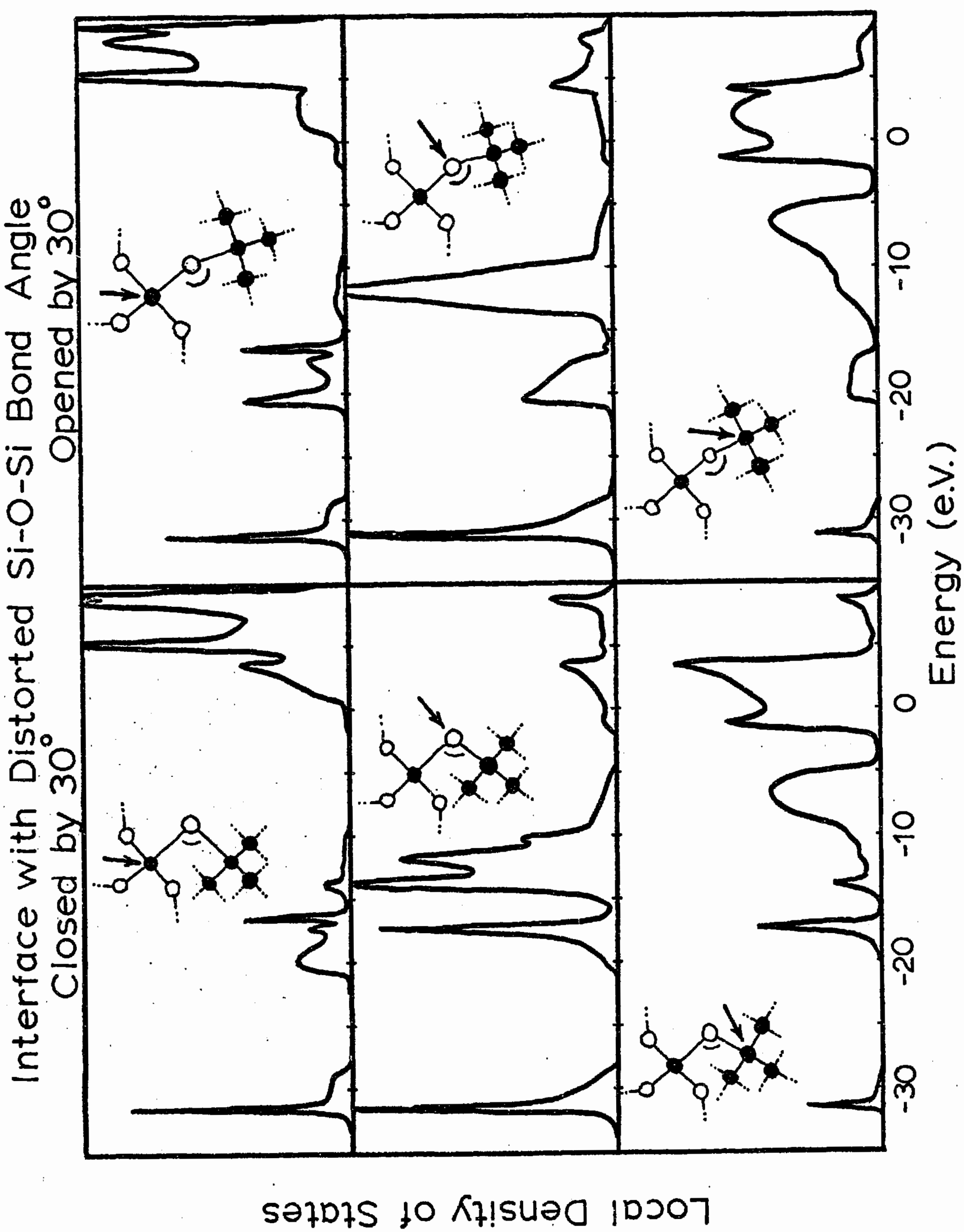
Interface with Distorted Si-O-Si Bond Angle
Closed by 30°
Opened by 30°
Local Density of States
Energy (e.V.)
-30
-20
-10
0

oxide. The effect is small because only one angle is distorted. In a real interface, many angles can be opened, causing the state to grow and eventually pop out into the gap. Therefore, we expect that distortions of the Si-O-Si angle near the interface will cause a tail of localized states near the conduction band edge. This pulling down of states occurs because the region is becoming more like β-Cristobalite, which has a smaller gap than α-quartz, given the same Hamiltonian. Opening the angle also causes states to shift away from the gap at -16 eV. This is because the bonding interaction is increasing (moving the strong-bonding states near -18 eV downward) while the weak-bonding bands (near -14 eV) are moving upward to become degenerate with the lone-pair bands at 180°. However, the most important result in Fig. 31 is that distortion of this angle can generate a tail of states near the silicon conduction band edge but <u>not</u> near the valence band edge.

Another bond-angle distortion one might investigate is that of the O-Si-O angle in the oxide. This would tend to make a tail of states near the oxide valence band edge, since the upper part of the valence band is lone-pair-like and sensitive to nearest-neighbor oxygen-oxygen interactions. However, this kind of bond-angle disorder is much less prevalent in vitreous silica[48] and it is not of immediate interest since it does not effect the silicon gap. One might also have bond-angle disorder in the silicon. We know, however, from studies[52] performed on bulk silicon that this kind of disorder generates a tail of states near the valence band edge due to dehybridization, and a much weaker tail of states near the conduction band edge due to fluctuations in the second-neighbor distance. Therefore, we have established that bond-angle disorder tends to generate states near both band edges, those near the valence band being localized in the silicon, those near the conduction band being localized in the oxide.

Localized states can also be generated by bonding defects. There are two major types of bonding defect one might find in the interface region: those deriving from dangling oxygen bonds and those deriving from dangling silicon bonds. The former tend to generate localized states near the oxide valence band edge because they are non-bonding p-like. They are thus not relevant to the problem of interface states in the silicon gap. Dangling silicon bonds, on the other hand, tend to generate state in and near the silicon gap.

In Fig. 32, we show the ideal interface discussed earlier, but with a missing atom on the silicon side. The local densities of states of the various atoms are practically identical with those of the ideal interface, except in and around the dangling-bond defect. There, we see a sharp interface state, highly localized and situated in the middle of the silicon gap at the same energy where the dangling-bond surface state appeared on the bare silicon surface. This state also derives from the dangling sp^3 hybrid at the defect site and is so localized that it is essentially the same state as appears at the silicon surface. From Fig. 32, therefore,

Figure 32: Local densities of states versus energy for an interface region containing a dangling Si bond on the silicon side of the interface.

Interface with Dangling Silicon Bond

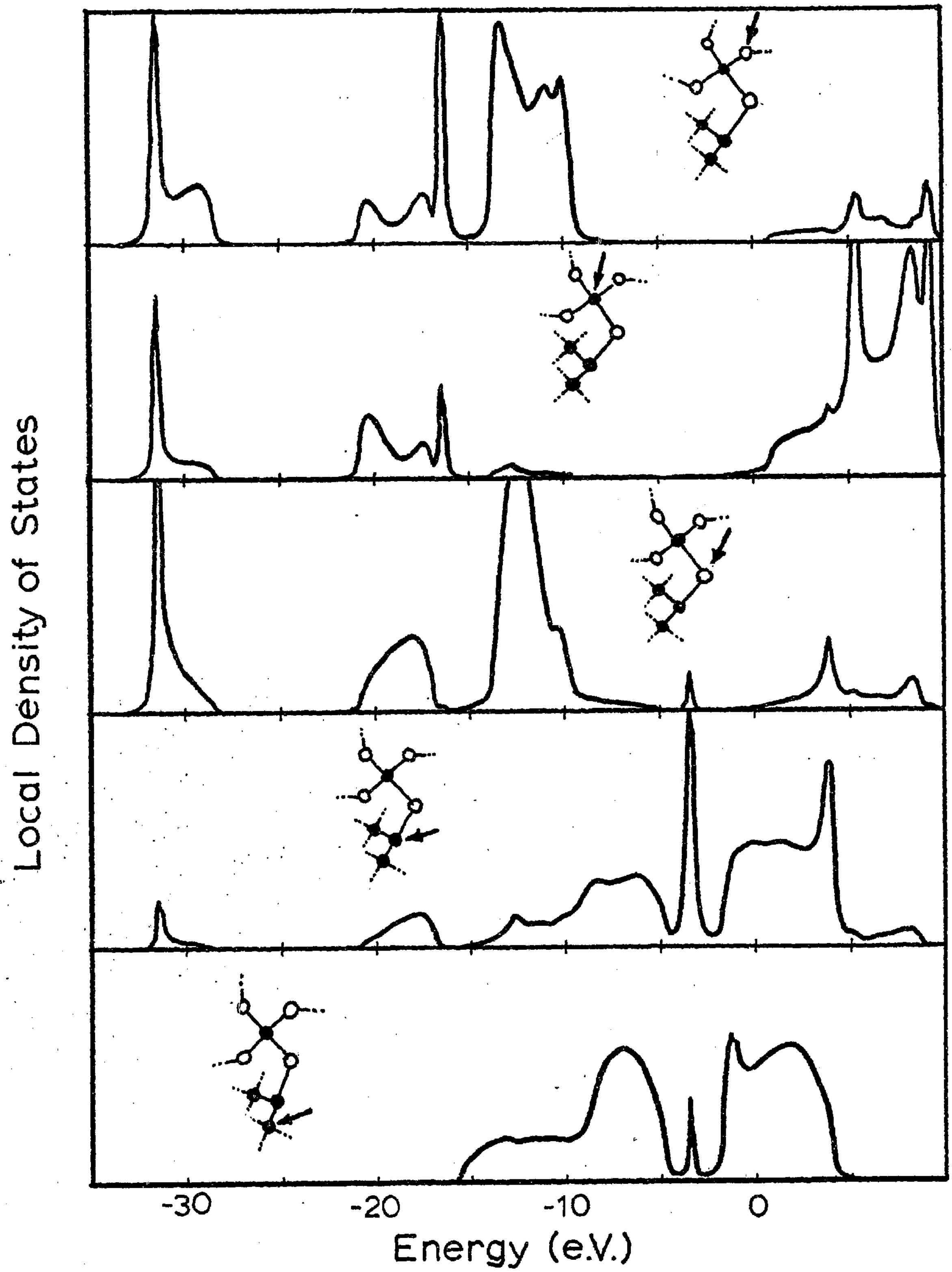

we conclude that dangling bonds on the silicon side of the interface can generate localized states deep in the gap. A sharp interface state similar to this one has been observed experimentally.[53]

4.3. Summary

In this chapter, we have established the following:

1. If the interface is ideal (containing no broken or distorted bonds), there are no interface states in or near the silicon gap.
2. Bond-angle disorder in the oxide tends to generate a tail of states near the silicon conduction band edge, but not near the valence band edge.
3. The only bonding defect which causes a sharp state deep in the silicon gap is a dangling Si bond.

REFERENCES

1. Joannopoulos, J.D. and F. Yndurain, Phys. Rev. B10, 5164 (1974).

2. Domb, C., Adv. Phys. 9, 145 (1960).

3. Edgerton and Hardin, Catal. Rev. Sci. Eng. 11(1), 71 (1975).

4. Born, M., Ann. Phys. (Leipz), 44, 605 (1914).

5. Bell, R.J., N.F. Bird and P. Dean, J. Phys. C1, 299 (1968).

6. Thorpe, M.F., Proc. I.A.P. Conf. on Structure and Excitations of Amorphous Solids, Williamsburg, 31, 251 (1976).

7. Leadbetter, A.J. and M.W. Stringfellow, Neutron Inelastic Scattering, Proc. Grenoble Conf. (IAEA), Vienna, p. 501 (1972). (see also ref. 12)

8. Galeener and Lucovsky, Phys. Rev. Lett. 37, 1471 (1976).

9. Hertzberg, G., Infrared and Raman Spectra, Van Nostrand, New York (1945).

10. Gaskell, P.H. and D.W. Johnson, J. Non-Cryst. Solids, 20, 171 (1976).

11. Sen, P. and M.F. Thorpe, Phys. Rev. B, in press.

12. Willis, B.T.M., Chemical Applications of Thermal Neutron Scattering, Oxford University Press, London, p. 26 (1973).

13. Kleinman, D.A. and W.G. Spitzer, Phys. Rev. 125, 16 (1962).

14. Shuker, R. and R.W. Gammon, Phys. Rev. Lett. 25, 222 (1970).

15. Keating, P.N., Phys. Rev. 145, 637 (1966).

16. Ibach, H., K. Horn, R. Dorn and H. Lüth, Surf. Sci. 38, 433 (1973).

17. Buechler, E. and J. Turkevich, J. Phys. Chem. 76, 2325 (1972).

18. Laughlin, R.B., J.D. Joannopoulos, C.A. Murray, K.A. Hartnett and T.J. Greytak, Phys. Rev. Lett. 40, 461 (1978).

19. Joannopoulos, J.D. and M.L. Cohen, Solid State Physics 31, 71 (1976).

20. Joannopoulos, J.D., Phys. Rev. B16, 2764 (1977).

21. Joannopoulos, J.D. and R.B. Laughlin, Proceedings of the 13th International Conference on the Physics of Semiconductors, Rome (1976), p. 196.

22. Stolen, R.H. and G.E. Walfren, J. Chem. Phys. 64, 2623 (1976).

23. Wong, J., AIP Conf. Proc. 31, 237 (1976).

24. Bates, J.B., R.W. Hendricks and L.B. Shaffer, J. Chem. Phys. 61, 4163 (1974).

25. Hair, M.L., Infrared Spectroscopy in Surface Chemistry, Marcel Dekker, New York (1967).

26. For extensive references to theoretical and experimental work, see the review articles by A.R. Ruff, J. Non-Crystal. Solids 13, 37 (1973/74); Griscom, D.L., J. Non-Crystal. Solids 24, 155 (1977).

27. Pantelides, S.T. and W.A. Harrison, Phys. Rev. B13, 2667 (1976).

28. Chelikowsky, J.R. and M. Schluter, Phys. Rev. B15, 4020 (1977); Schluter, M. and J.R. Chelikowsky, Solid State Comm. 21, 381 (1977).

29. Yip, K.L. and W.B. Fowler, Phys. Rev. B10, 1400 (1974).

30. Schneider, P.M. and W.B. Fowler, Phys. Rev. Lett. 36, 425 (1976).

31. Calabrese, E. and W.B. Fowler, Phys. Rev. B18, 2888 (1978).

32. Ciraci, S. and I.P. Batra, Phys. Rev. B15, 4923 (1977).

33. Bennett, J.A. and L.M. Roth, Phys. Rev. B4, 2686 (1971); J. Phys. Chem. Solids 32, 1251 (1971).

34. Tossell, J.A., D.J. Vaughan and K.H. Johnson, Chem. Phys. Lett 20, 329 (1973).

35. Gilbert, T.L., W.J. Stevens, H. Schrenk, M. Yoshimine and P.S. Bagus, Phys. Rev. B8, 5977 (1973).

36. Mott, N.F., Adv. Phys. 26, 363, (1977).

37. Many useful references may be found in The Physics of SiO_2 and its Interfaces, S.T. Pantelides, ed. (Pergamon Press, New York, 1978).

38. Thorpe, M.F. and D. Weaire, Phys. Rev. B4, 3518 (1971).

39. Yndurain, F., Solid State Comm., 27, 75 (1978).

40. Fischer, B., R.A. Pollak, T.H. DiStefano and W.D. Grobman, Phys. Rev. 15, 3193 (1977).

41. Phillip, H.R., Solid State Commun. 4, 73 (1966); J. Phys. Chem. Solid 32, 1935 (1971).

42. Loh, E., Solid State Commun. 2, 269 (1964).

43. Klein, G., and H.U. Chun, Phys. Status Solid B49, 167 (1972).

44. Schlüter, M., private communication.

45. Herman, F. and S. Skillman, Atomic Structure Tables, (Prentice-Hall, Englewood Cliffs, N.J., 1963).

46. Joannopoulos, J.D. and M.L. Cohen, Theory of Short Range Order and Disorder in Tetrahedrally Bonded Semiconductors, Solid State Physics, Vol. 31 (1976).

47. Thorpe, M., Ref. 37, p. 116.

48. Mozzi, R.L. and B.E. Warren, J. Appl. Cryst. 2, 164 (1969).

49. Pepper, M. and N.F. Mott, Physics of Semiconductors, (Typografia Marves, Rome, 1976) p. 762.

50. Ibach, H. and J.E. Rowe, Phys. Rev. B10, 710 (1974).

51. DiStefano, T.H., J. Vac. Sci. Tech. 13, 856 (1976).

52. Joannopoulos, J.D., Phys. Rev. B16, 2764 (1977).

53. Johnson, N.M., D.J. Bartelink and M. Schulz, ref. 37, p. 421.

APPENDIX A

THE SILICON DIOXIDE BETHE LATTICE

We first set up local coordinates on each silicon atom and make them identical by requiring that the coordinates of the nearest-neighbor oxygen atoms always be the same. The oxygen neighbors are positioned at the vertices of a perfect tetrahedron and numbered 1 through 4. For convenience, we introduce a 3 x 3 matrix S which rearranges the bonds according to a cyclic permutation σ. Letting D_ν denote the dynamical matrix connecting the central silicon atom and the ν^{th} oxygen atom, we have

$$S\, D_\nu S^{-1} = D_{\sigma(\nu)} \tag{A1}$$

We also introduce four orthogonal matrices M_ν which transform vectors from the four neighbor silicon coordinate systems into the central silicon coordinate system, and which contain the bond angle information. These are taken to be symmetries of crystalline silicon dioxide, and have the following properties:

1. $M_\nu = S^2\, M^{-1}_{\sigma(\nu)}$ (A2)

2. $M_1^3 = 1$ (A3)

3. $M_1 = M_2\, S^2$ (A4)

These are two symmetries of the crystal which send a silicon atom to its neighbor. The first rule expresses the arbitrary selection of one of these which attaches a ν bond and a $\sigma(\nu)$ bond to the same oxygen atom. There is no symmetry which attaches the same bond to both sides. The bond matching convention is illustrated in figure A1. The second rule expresses the translational symmetry connecting atoms 1 and 2. These axioms are quite sufficient to generate the four transformations, and lead to a Si-O-Si angle given by

$$\cos(\theta) = -\frac{\sqrt{5}}{3} \tag{A5}$$

and a dihedral angle given by

$$\cos(\psi) = \frac{3+\sqrt{5}}{4\sqrt{2}} \tag{A6}$$

The dynamical matrix connecting the silicon atom with itself is constrained by translational invariance of the total Hamiltonian to be

$$A = -\sum_{\nu} D_{\nu} \tag{A7}$$

and the matrix B_{ν} connecting the ν^{th} oxygen atom with itself is similarly given by

$$B_{\nu} = -[D_{\nu} + M_{\nu} D_{\sigma(\nu)} M_{\nu}^{-1}] \tag{A8}$$

Figure A1: Bond-matching rules for silicon dioxide Bethe lattice.

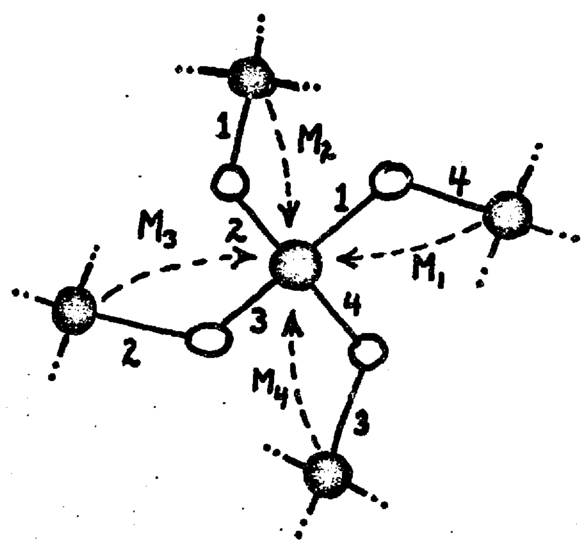
M2
M3
M1
M4
1
2
3
4

Using these dynamical matrices appropriately reduced by the silicon and oxygen masses we generate a repeating sequence of equations describing the vibrational Green's function in the frequency domain. If we let G_0 denote the 3 x 3 submatrix of the Green's function connecting a silicon atom with itself, $F_1^{\nu_1}$ the submatrix connecting the silicon atom with the ν_1 th oxygen neighbor, $G_1^{\nu_1}$ the submatrix connecting to the ν_1 th silicon neighbor, and so on, then we have

$$(\omega^2 - A)G_0 = 1 + \sum_{\nu_1} D_{\nu_1} F_1^{\nu_1} \tag{A9}$$

$$(\omega^2 - B_{\nu_1})F_1^{\nu_1} = D_{\nu_1} G_0 + M_{\nu_1} D_{\sigma(\nu_1)} G_1^{\nu_1} \tag{A10}$$

$$(\omega^2 - A)G_1^{\nu_1} = D_{\sigma(\nu_1)} M_{\nu_1}^{-1} F_1^{\nu_1} + \sum_{\nu_2 \neq \sigma(\nu_1)} D_{\nu_2} F_2^{\nu_1,\nu_2} \tag{A11}$$

$$(\omega^2 - B_{\nu_2})F_2^{\nu_1,\nu_2} = D_{\nu_2} G_1^{\nu_1} + M_{\nu_2} D_{\sigma(\nu_2)} G_2^{\nu_1,\nu_2} \tag{A12}$$

$$\vdots \qquad\qquad\qquad \vdots$$

$$\begin{aligned}(\omega^2 - A)G_n^{\nu_1,\ldots,\nu_n} &= D_{\sigma(\nu_n)} M_{\nu_n}^{-1} F_n^{\nu_1,\ldots,\nu_n} \\ &\quad + \sum_{\nu_{n+1} \neq \sigma(\nu_n)} D_{\nu_{n+1}} F_{n+1}^{\nu_1,\ldots,\nu_{n+1}} \end{aligned} \tag{A13}$$

$$\begin{aligned}(\omega^2 - B_{\nu_n})F_n^{\nu_1,\ldots,\nu_n} &= D_{\nu_n} G_{n-1}^{\nu_1,\ldots,\nu_{n-1}} \\ &\quad + M_{\nu_n} D_{\sigma(\nu_n)} G_n^{\nu_1,\ldots,\nu_{n+1}} \end{aligned} \tag{A14}$$

To solve this system we first eliminate every other equation to obtain

$$\tilde{A}\, G_n^{\nu_1,\ldots,\nu_n} = \tilde{D}^t_{\nu_n} G_{n-1}^{\nu_1,\ldots,\nu_{n-1}} + \sum_{\nu_{n+1}\neq\sigma(\nu_n)} \tilde{D}_{\nu_{n+1}} G_{n+1}^{\nu_1,\ldots,\nu_{n+1}} \tag{A15}$$

where

$$\tilde{A} = \omega^2 - A - \sum_{\nu} D_\nu[\omega^2 - B_\nu]^{-1} D_\nu \tag{A16}$$

and

$$\tilde{D}_\nu = D_\nu[\omega^2 - B_\nu]^{-1}\, M_\nu D_{\sigma(\nu)} \tag{A17}$$

A solution of the form

$$G_{n+1}^{\nu_1,\ldots,\nu_{n+1}} = \Phi_{\nu_{n+1}} G_n^{\nu_1,\ldots,\nu_n} \tag{A18}$$

is then substituted, which leads to recursion relations for the transfer matrices Φ_ν of the form form

$$\Phi_\nu = \left[\tilde{A} - \sum_{\mu\neq\sigma(\nu)} \tilde{D}_\mu \Phi_\mu\right]^{-1} \tilde{D}^t_\nu \tag{A19}$$

These equations are solved numerically by iterating the continued fraction starting from $\Phi_\nu = 0$. Once the transfer matrices are found, G_0 may be calculated using the relation

$$G_0 = \left[\tilde{A} - \sum_{\mu} \tilde{D}_\mu \Phi_\mu\right]^{-1} \tag{A20}$$

and the remainder of the Green's function constructed from G_0.

APPENDIX B

EFFECT OF SECOND-NEAREST-NEIGHBOR FORCES ON THE VIBRATIONS OF AMORPHOUS SiO_2

In Appendix A, we showed how a continued-fraction technique could be used to calculate the vibrational Green's function of a silicon-dioxide Bethe lattice constructed using a nearest-neighbor Born force law. In this Appendix, we show how a similar technique can be used when the force law involves second-nearest-neighbor interactions as well.

The inclusion of non-nearest-neighbor interactions into a Bethe lattice increases its complexity considerably by introducing rings of interactions into the Hamiltonian. For example, two oxygen atoms bonded to the same silicon atom can now interact with each other, as well as with the siicon atom to which they are bonded, to form a threefold ring. It is ordinarily the absence of rings of interactions in the Bethe lattice which facilitates its solution, rather than the absence of rings of bonds. There is no distinction between these two when only nearest-neighbor interactions are included. Even though it contains rings of interactions, however, such a system may generally be solved, provided the atoms are consolidated into larger units which interact only when they are adjacent. This procedure regularly produces an intractable numerical problem. In silicon dioxide, however, the twofold coordination of the oxygen atoms makes a solution with second-nearest-neighbor interactions practical.

In Fig. B1 we show the silicon-dioxide Bethe lattice partitioned into units which we will henceforth refer to as bubbles. Each bubble interacts only with itself and with its nearest neighbors. Interaction in this case means an atom in one unit interacting with any atom in the other one. If one now thinks of a bubble as a site with 12 degrees of freedom, then the system transforms into an ordinary tetrahedrally coordinated Bethe lattice with the exception that there are now four distinct kinds of directed sites. The four oxygen atoms in a tetrahedron are distinguisable, causing there to be four distinct kinds of bubble. The bubbles also point outward in a way that is evident in Fig. B1.

In Fig. B1 there is a central bubble with is different from all the rest. The inclusion of a central bubble is necessitated by the artificial directionality induced by the partitioning. The atoms in the central bubble are not physically distinguishable from the atoms in the periphery, and it is important to emphasize that the solution to the vibration problem is independent of the location of the central bubble. The physical system, in this case, has more symmetry than the formalism would indicate.

Since the bubbles are basically tetrahedra, we assign to them local coordinates as discussed previously. As before, we number the bond directions in a tetrahedron 1-4, and pick an outward bond-matching convention $\nu \rightarrow \sigma(\nu)$, where ν runs from 1 through 4 and σ is a cyclic permutation. We now number the four kinds of bubble by the

Figure B1: Diagram of silicon-dioxide Bethe lattice showing how it can be partitioned to remove second-nearest-neighbor interactions.

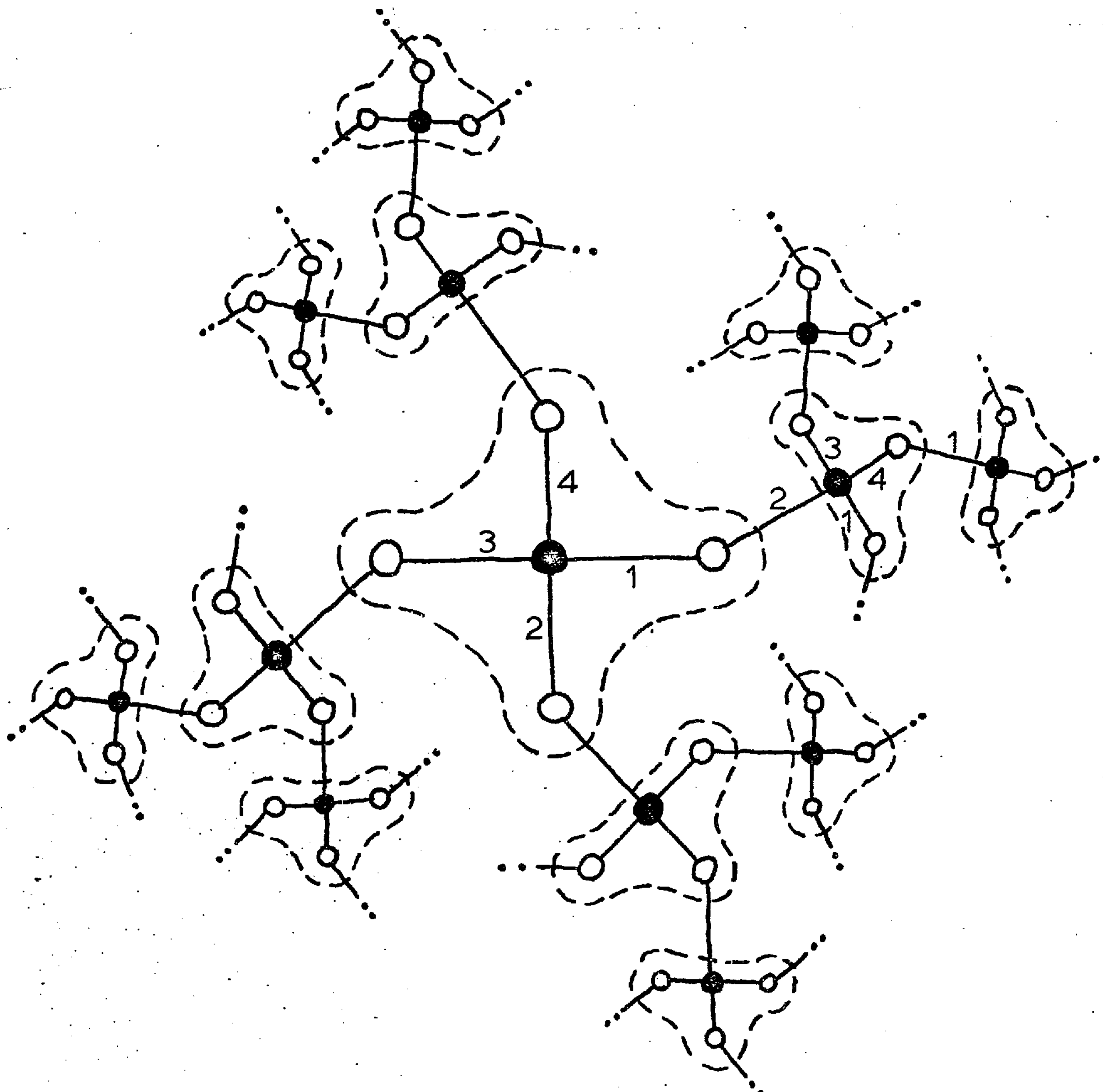

4
3
1
2
3
2
4
1
1

direction of the bond which points into them. For example, if the cyclic permutation is $1 \to 2 \to 3 \to 4 \to 1$, then a bubble which is missing a 2 oxygen atom is a 1 bubble, one that is missing a 3 oxygen atom is a 2 bubble, and so on.

Given that the displacements of the atoms in a bubble are expressed in the bubble's local coordinates, the dynamical matrix elements are well defined and can presumably be obtained. The part of the dynamical matrix connecting the central bubble with itself we denote A. The part connecting the central bubble with its nearest neighbor in the ν_1 direction we denote D_{ν_1}. The part connecting this nearest-neighbor bubble with itself we denote A_{ν_1}. The part connecting this bubble with its nearest neighbor in the ν_2 direction we denote $D_{\nu_1\nu_2}$. Since the Bethe lattice repeats from this point out, there are no more independent matrix elements. Note that ν_2 cannot be $\sigma(\nu_1)$, so that there are only twelve matrices $D_{\nu_1\nu_2}$. A is a 15 x 15 matrix, the D_ν are 15 x 12 matrices, and all the rest are 12 x 12.

As before, we index the submatrices of the vibrational Green's function by the sequence of directions $\nu_1,\nu_2,\ldots,\nu_n$ used in traveling from the central bubble to the one in question. G_0 denotes the part of the Green's function connecting the central bubble with itself. $G_1^{\nu_1}$ denotes the part connecting the central bubble to its neighbor in the ν_1 direction. $G_2^{\nu_1,\nu_2}$ denotes the part connecting to a second-nearest neighbor, and so on. G_0 is a 15 x 15 matrix, and all the rest are 12 x 15.

We now have the following sequence of equations:

$$(\omega^2 - A)G_0 = 1 + \sum_{\nu_1} D_{\nu_1} G_1^{\nu_1}, \tag{B1}$$

$$(\omega^2 - A_{\nu_1})G_1^{\nu_1} = D_{\nu_1}^t G_0 + \sum_{\nu_2 \neq \sigma(\nu_1)} D_{\nu_1\nu_2} G_2^{\nu_1,\nu_2} \tag{B2}$$

$$(\omega^2 - A_{\nu_2})G_2^{\nu_1,\nu_2} = D_{\nu_1\nu_2}^t + \sum_{\nu_3 \neq \sigma(\nu_2)} D_{\nu_2\nu_3} G_3^{\nu_1,\nu_2,\nu_3} \tag{B3}$$

$$\vdots \qquad\qquad\qquad \vdots$$

$$(\omega^2 - A_{\nu_n})G_n^{\nu_1,\dots,\nu_n} = D_{\nu_{n-1}\nu_n}^t G_{n-1}^{\nu_1,\dots,\nu_{n-1}} + \sum_{\nu_{n+1} \neq \sigma(\nu_n)} D_{\nu_n\nu_{n+1}} G_{n+1}^{\nu_1,\dots,\nu_{n+1}} \tag{B4}$$

This sequence has a solution of the form

$$G_{n+1}^{\nu_1,\dots,\nu_{n+1}} = \Phi_{\nu_{n+1}\nu_n} G_n^{\nu_1,\dots,\nu_n}, \tag{B5}$$

provided that 12 transfer matrices $\Phi_{\mu\nu}$ satisfy

$$(\omega^2 - A_\nu)\Phi_{\nu\rho} = D_{\rho\nu}^t + \sum_{\mu \neq \sigma(\nu)} D_{\nu\mu}\Phi_{\mu\nu}\Phi_{\nu\rho} \tag{B6}$$

or

$$\Phi_{\nu\rho} = \left(\omega^2 - A_\nu - \sum_{\mu \neq \sigma(\nu)} D_{\nu\mu}\Phi_{\mu\nu}\right)^{-1} D_{\nu\rho}^t . \tag{B7}$$

These equations may be solved as before by integrating the continued fraction starting at $\Phi_{\mu\nu} = 0$. Note that the quantity in parentheses depends only on ν. There are thus only four independent quantities, these corresponding physically to the Green's function of a terminated Bethe lattice restricted to the bubble at the terminus. If we let

$$F_\nu = \left(\omega^2 - A_\nu - \sum_{\mu\neq\sigma(\nu)} D_{\nu\mu}\Phi_{\mu\nu}\right)^{-1} , \tag{B8}$$

then we have

$$F_\nu = \left(\omega^2 - A_\nu - \sum_{\mu\neq\sigma(\nu)} D_{\nu\mu}F_\mu D^t_{\nu\mu}\right)^{-1} . \tag{B9}$$

For the central bubble we have

$$G = \left(\omega^2 - A - \sum_\mu D_\mu F_\mu D^t_\mu\right)^{-1} . \tag{B10}$$

In order to illustrate the validity of the method we have constructed and solve a Bethe lattice for silicon dioxide using a Keating Hamiltonian. The Keating Hamiltonian assigns a quadratic potential energy to bond-length and bond-angle distortions, rather than to bond-length and bond-directions distortions, as does the simpler Born Hamiltonian. For this reason it is rotationally invariant, and therefore more realistic than the Born Hamiltonian. For a bond length distortion Δ we have

$$\Delta U = \frac{1}{2} K_r(\Delta r)^2 , \tag{B11}$$

while for every O-Si-O angle distortion $\Delta \cos \theta$ we have

$$\Delta U = \frac{1}{2} K_s(b \; \Delta \cos \theta)^2 , \tag{B12}$$

where b is the bond length. Following Kleinman and Spitzer, we set the Si-O-Si angle distortion energy to zero as a fitted parameter. We use Kleinman and Spitzer's value for K_r, 4.32×10^5 dyn/cm, and a value for K_s of 0.27×10^5 dyn/cm. This value, slightly lower than the 0.29×10^5 dyn/cm suggested by Kleinman and Spitzer, was picked to make the frequency of the third A_1 mode of quartz agree with experiment.

In Fig. B2, we compare the density of states of the Keating Bethe lattice with that of quartz constructed using the same Hamiltonian, and with previous calculations performed using the Born Hamiltonian. The distinctions between the crystal and Bethe-lattice densities of states are again due to the presence of 12-fold rings in the crystal. The high-frequency band peaking at 1080 cm^{-1} is virtually identical to that produced by the Born Hamiltonian. These vibrations are dominated by the bond-stretching forces, which are the same in both models. The siliconlike states at 750 cm^{-1} are unchanged for the same reason. On the other hand, the low-frequency bands are broadened and shifted downwards slightly in the Keating

Figure B2: Comparison of Keating Bethe-lattice density of states against that of α-quartz constructed with the same Hamiltonian, and against similar calculations performed using a Born Hamiltonian.

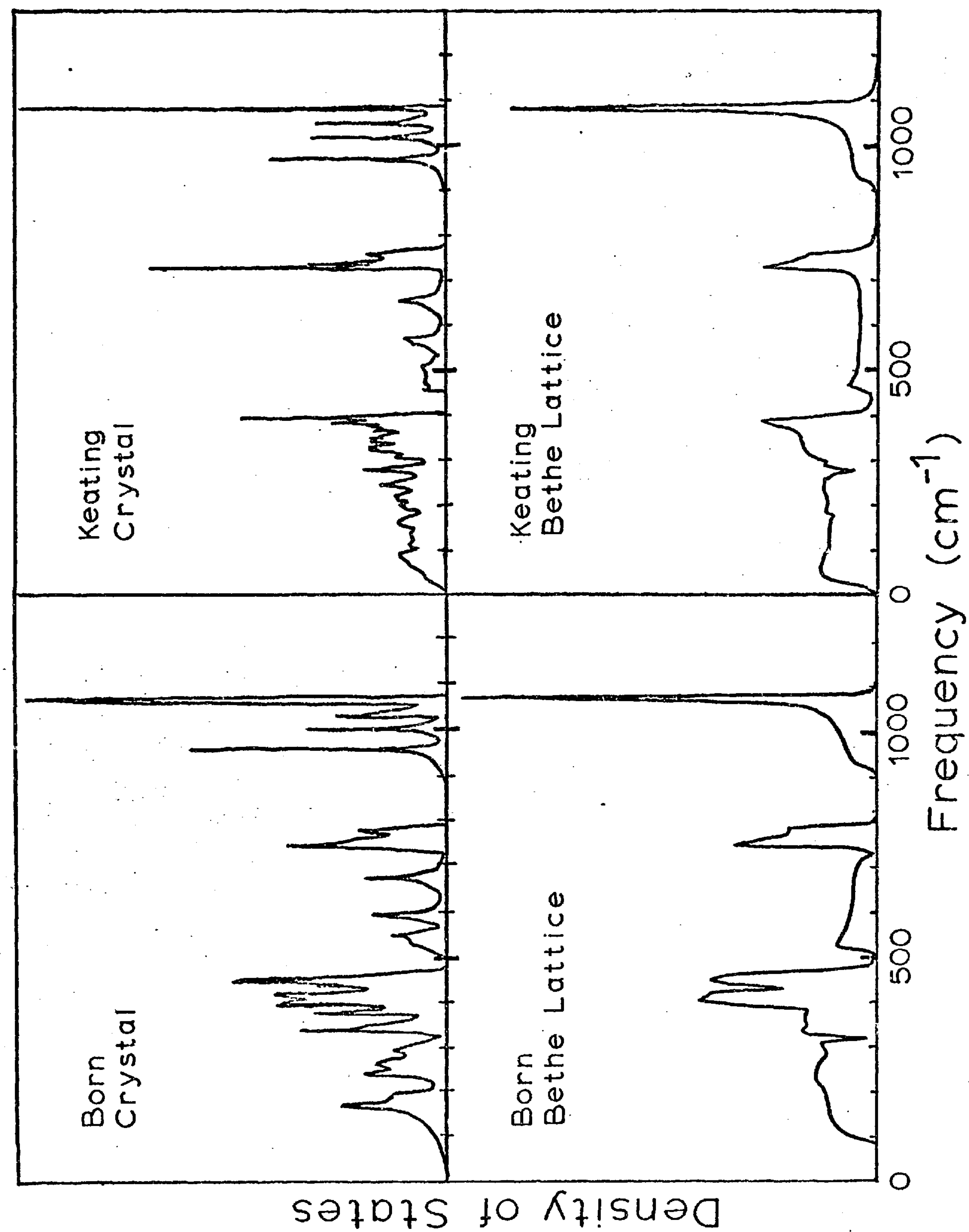

Born
Crystal
Keating
Crystal
Born
Bethe Lattice
Keating
Bethe Lattice
0
500
1000
0
500
1000
Frequency (cm^{-1})
Density of States

Bethe lattice. These bands are predominantly angle-distorting vibrations and are sensitive to changes in the angular force constants. The fact that they move downward when the Keating Hamiltonian is substituted for the Born Hamiltonian indicates that the SiO_4 units in the glass tend to be rigid at these frequencies and that the bond directions tend to vary without distorting O-Si-O angles. The Keating model agrees more closely with experiment at these frequencies.[3] Overall, however, the Keating and Born Bethe lattices are remarkably similar, and it is clear that in most respects the simpler theory is an excellent approximation to the more realistic one.